Study of generation mechanism of Pc1 pearl structure using multi-point ground-based induction magnetometers

Chae-Woo Jun

Graduate School of Science
Nagoya University

This dissertation is submitted for the degree of
Doctor of Philosophy

March 2016

Acknowledgements

This thesis was completed as part of my doctoral course at the Institute for Space-Earth Environmental Research (ISEE) in association with the Graduate School of Science of Nagoya University.

I have several people to thank for their great support. I first express my heartfelt gratitude to my supervisor, Prof. Kazuo Shiokawa for his guidance and encouragement. Drawing on his experience, I learned everything from the fundamentals of geomagnetic pulsations to auroral physics, and wave-particle interactions in the magnetosphere. As a mentor, he taught me what a good scientist ought to be and help me shape my own path, while supporting me with advice and patience while I wrote this thesis.

The work presented in this dissertation could not have been accomplished without the support and helpful comments provided by Prof. Martin Connors and Mr. Ian Schofield of Athabasca University, Canada, and Prof. Igor Poddelsky and Prof. Boris Shevtsov from the Far Eastern Branch of the Russian Academy of Sciences, Russia. I also thank Prof. Yuichi Otsuka, Prof. Nozomu Nishitani, Prof. Masafumi Hirahara, and Dr. Masaki Nishinoof the ISEE for their meaningful discussions and feedback. I am also grateful to the various members of the Applied Physics Laboratory (APL) at Johns Hopkins University for their wonderful reception during my internship in their group. Their various comments were very helpful, in particular, those from Dr. Kazue Takahashi, who was my host researcher at the APL. He gave me important advice and assessments that improved my research and provided exciting new ideas for future work. I express my appreciation to Prof. Khun-Huk Kim, my former master's degree advisor at KyungHee University, Korea, for providing the amazing opportunity to study at the ISEE, which allowed me to learn about geomagnetic pulsations with Prof. Shiokawa as the theme of my doctoral thesis.

I would like to thank my friend Claudia Martinez for sharing life at the laboratory and helping me to improve my English during this period. We spent many hours discussing our research to help each other. Special thanks are due to Mr. Kristoff Paulson, who gave me insightful advice about how to handle Van Allen Probe data. My fellow graduate students, in particular Ayumi Hashimoto, Yonezu Yusuke, and Toru Takahashi, helped me more easily adapt to Japanese culture. I am also grateful to the STEL Futsal Team for providing mem-

orable times during our weekend matches. I am thankful to K. Nishioka, M. Wakahara, M. Asakura, A. Shimura, and Y. Iwata, our division secretaries, for helping me solving various difficult problems with Japanese paperwork.

Finally, I thank my parents and brother for their loving support throughout this period, and my Korean friends for many good times, which reduced my stress enough to remain focused on my research. In particular, I express my deepest gratitude to my beloved wife and partner, Hye-Jin Shin, for her endless support and advice and for maintaining my spirits during this period. Without her support, I would never have succeeded through this tough time.

The induction magnetometer data used in this thesis is available at the magnetometer data website from the ISEE, accessible at http://stdb2.stelab.nagoya-u.ac.jp/magne/index.html. Monthly average sunspot numbers were sourced from the OMNI database, obtained from the SPDF/Goddard Space Flight Center interface at http://omniweb.gsfc.nasa.gov/. The AE indices were provided by the WDC-C2 for Geomagnetism at Kyoto University. I thank M. Sera and Y. Ikegami at the Moshiri Observatory of the Institute for Space-Earth Environmental Research, Nagoya University, the staff of the Institute of Cosmophysical Research and Radiowave Propagation (IKIR), and the Center for Science at Athabasca University. I also thank Y. Katoh, H. Hamaguchi, and Y. Yamamoto of the ISEE for their help and support in the operation of the induction magnetometers. This work was supported by KAKENHI Grants-in-Aid (numbers 16403007, 18403011, 19403010, 25247080, 20244080, and 15H05815), the Special Funds for Education and Research (Energy Transport Processes in Geospace), and the IUGONET Project from MEXT, Japan, as well as the Leadership Development Program for Space Exploration and Research from Nagoya University for Leading Graduate Schools.

Abstract

Pc1 geomagnetic pulsation is a geomagnetic oscillation at frequencies of 0.2-5 Hz observed by induction magnetometers on the ground. These waves are related to electromagnetic ion cyclotron (EMIC) waves generated in the equatorial region of the magnetosphere at L ∼4-8 due to the temperature anisotropy of energetic plasma in the radiation belts. They propagate along the magnetic field line and bounce between the Northern and Southern hemispheres. When EMIC waves reach the ionosphere, they are converted to compressional-mode waves due to interaction with ionospheric plasma. They are trapped in the F-layer of the ionosphere and propagate longitudinally and latitudinally from high to low latitudes through the ionospheric duct, and are observed as Pc1 geomagnetic pulsations. EMIC waves interact with energetic particles in the radiation belts, causing pitch angle scattering and precipitation of these particles into the ionosphere. This process is related to isolated proton aurora at subauroral latitudes. Therefore, studying the generation and propagation of EMIC/Pc1 waves is important for understanding the loss mechanism of energetic particles in the radiation belts.

Pc1 pearl structures are quasi-periodic amplitude modulations of Pc1 pulsations with a repetition period of several tens of seconds. Many studies have used ground-based and satellite observations to investigate the generation mechanisms of Pc1 pearl structures. The generation of Pc1 pearl structures can be divided into two possibilities: 1) magnetospheric and 2) ionospheric effects. Magnetospheric effects generate Pc1 pearl structures in the magnetosphere, and these structures should not change during ionospheric duct propagation. Ionospheric effects generate Pc1 pearl structures in the ionosphere, and these structures may have different shapes at different locations on the ground. Previous studies have investigated the formation of Pc1 pearl structures, but their generation mechanisms have not yet been clearly identified.

In the research presented in this thesis, we investigated the generation mechanisms of Pc1 pearl structures in the ionosphere using multi-point ground-based induction magnetometers at Athabasca (ATH) in Canada, Magadan (MGD) in Russia and Moshiri (MOS) in Japan, L ∼1.5-4.5. We investigated two Pc1 events simultaneously observed at the three stations, and we compared our observations with model calculations. Case 1 (April 8, 2010) shows that Pc1 pearl structures observed at two stations have different shapes with polarization

angle-dependence on Pc1 frequency. Case 2 (April 11, 2010) shows that they have similar Pc1 pearl structures at two stations with a constant polarization angle within Pc1 frequencies. The repetition period of the Pc1 pearl structures was ∼10 s in case 1 and ∼10 to 40 s in case 2. These periods are shorter than those expected from the bouncing wave packets model, which is a candidate for describing magnetospheric effect in the formation of Pc1 pearl structures. Using two simple model calculations under different conditions, we also investigated the possibility of beating processes in the ionosphere as a potential generation mechanism for Pc1 pearl structures. The first model assumes Pc1 waves propagated to the observation point from a latitudinally distributed source with different frequencies at different latitudes, representing beating processes in the ionosphere. The second model considers that Pc1 waves with different frequencies are mixed at a point source and propagate to the observation points, indicating Pc1 pearl structures caused by magnetospheric effects. As a result of the model calculations, the first model shows slightly different waveforms at different observation points. However, the second model shows identical waveforms among the observation points. The result of the first model is related with Case 1, which showed different Pc1 pearl structures with dependence of polarization angle on frequency at the three stations. From these results, we suggest that beating processes in the ionosphere with a spatially distributed ionospheric source can cause pearl structures during ionospheric duct propagation from high to low latitudes, with long distances from the source to the stations. In case 2, however, we cannot reliably interpret the Pc1 pearl structures with a constant polarization angle by using the beating process in the ionosphere.

We then investigated the statistical characteristics of Pc1 pearl structures observed by longitudinally (ATH and MGD) and latitudinally (MGD and MOS) separated induction magnetometers. From among six years of ground observations, from 2008 to 2013, we selected 84 Pc1 events observed simultaneously at the longitudinally separated stations (ATH and MGD) and 370 events observed at the latitudinally separated stations (MGD and MOS), all with high coherence (> 0.7) of Pc1 waveforms. We calculated the cross-correlation coefficient (similarity: r) for the Pc1 pearl structures and found that more than half of the events in both pairs had low similarity ($r < 0.7$), indicating that most Pc1 waves exhibit different pearl structures at different stations. We found that high-similarity Pc1 pearl structures ($r > 0.7$) at the longitudinally separated stations are concentrated from 6 to 15 UT when both stations are in the nighttime. The similarity of Pc1 pearl structures tends to show a negative correlation with the standard deviation of the polarization angle in both pairs. The observed repetition period of Pc1 pearl structures has a clear positive correlation with the repetition period estimated from Pc1 bandwidth by assuming beating of different frequencies. From these results, we suggest that an ionospheric beating effect could be the dominant process

for the generation of Pc1 pearl structures. Beating processes in the ionosphere with a spatially distributed ionospheric source can cause the different shapes of Pc1 pearl structures at different observation points during ionospheric duct propagation.

However, we should also consider that magnetospheric processes, such as EMIC waves modulated by long-ULF waves, could be a major contribution in the generation of Pc1 pearl structures. To identify the spatial and temporal characteristics of the generation and propagation of Pc1 pearl structures in the ionosphere and in the magnetosphere, we will investigate quasi-periodic and randomly structured EMIC/Pc1 waves using multi-point ground induction magnetometers and the Van Allen Probes.

Table of contents

List of figures

List of tables

Chapter 1

Introduction

1.1 Overview

Pc1 geomagnetic pulsation is an ultra low-frequency (ULF) pulsation at frequencies of 0.2-5 Hz. These waves are observed by induction magnetometers on the ground as a geomagnetic oscillation. *Jacobs et al.* [1964] classified these geomagnetic pulsations by frequency range, as shown in Table 1.1. *Fukunishi et al.* [1981] investigated Pc1 pulsations in the range of 0.2-2 Hz observed at the Showa station. Pc1 pulsations were classified according to their spectral spectra to eight subtypes in the Pc1 geomagnetic frequency range. Figure 1.1 shows the dependence of preferential magnetic local time for these subtypes of geomagnetic pulsations as a function of frequency with their spectral structures. For example, periodic hydromagnetic (HM) emission bursts preferably occur at the magnetic noon, and Pc 1-2 bands are frequently observed between 6 and 18 MLT. The HM emissions tend to decrease in frequency from the morning to the dusk. *Fukunishi et al.* [1981] suggested that this frequency variations of HM emissions with local time are related to L-shell variations associated with the generation regions of HM emissions in the plasmapause.

Figure 1.2 shows a schematic of the generation and propagation of electromagnetic ion cyclotron (EMIC)/Pc1 waves in the magnetosphere and ionosphere. The EMIC waves are due to the temperature anisotropy ($T_{\parallel} < T_{\perp}$) of energetic ions in the equatorial regions of the magnetosphere, and they usually have left-hand polarity. These waves propagate along

Table 1.1 Classification of geomagnetic pulsations (*Jacobs et al.*, 1964)

	Pc1	Pc2	Pc3	Pc4	Pc5
Period Range [sec]	0.2-5	5-10	10-45	45-150	150-600
Frequency Range	0.2-5 Hz	0.1-0.2 Hz	22-100 mHz	7-22 mHz	2-7 mHz

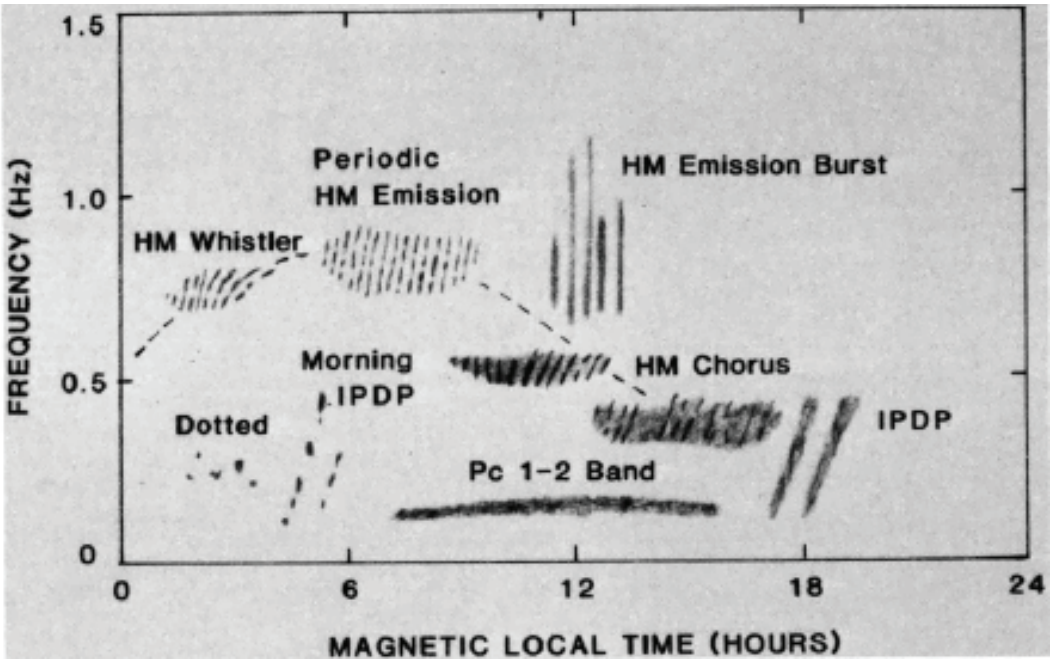

Figure 1.1 Dependence of subtypes HM emissions on magnetic local time within the Pc1 frequency range (reproduced from *Fukunishi et al.*, [1981].

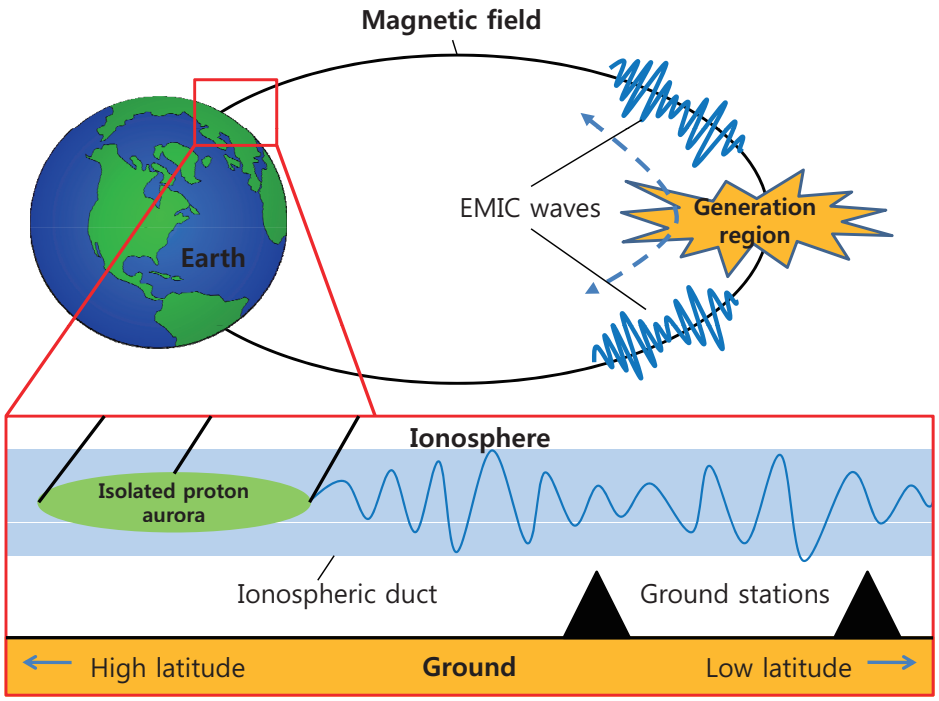

Figure 1.2 Schematic of the generation and propagation of electromagnetic ion cyclotron (EMIC)/Pc1 waves in the magnetosphere and ionosphere.

the magnetic field lines and bounce between the Northern and Southern hemispheres. When EMIC waves reach the ionosphere, they interact with ionospheric plasma and are converted to compressional-mode waves. These waves are trapped in the F-layer of the ionosphere and propagate latitudinally and longitudinally from high to low latitudes through the ionospheric duct, and are observed as Pc 1 geomagnetic pulsations on the ground at frequencies of 0.2-5 Hz.

The important features of EMIC waves are related to the loss of energetic particles in the radiation belts and precipitation into the ionosphere. When EMIC waves resonate with energetic particles in the radiation belts during bouncing motions, they cause pitch-angle scattering into the loss-cone. Particles precipitated into the ionosphere generate isolated proton aurora at sub-auroral latitudes [e.g., *Sakaguchi et al.*, 2007; *Miyoshi et al.*, 2008; *Sakaguchi et al.*, 2008].

Pc1 geomagnetic pulsations have been widely studied since the 1960s to identify their characteristics. Characteristics of Pc1 geomagnetic pulsations associated with ionospheric duct propagation have been extensively investigated, for example, for attenuation effects (0-13 dB/1,000 km) [e.g., *Althouse and Davis*, 1978; *Kim et al.*, 2010], the propagation speed (89-2,000 km/s) [e.g., *Greifinger and Greifinger*, 1968; *Manchester*, 1970; *Fraser*, 1975a; *Lysak*, 2004; *Kim et al.*, 2010], propagation direction (mainly along the magnetic meridian, but also latitudinally with higher attenuation effect) [e.g., *Kawamura et al.*, 1981], and the polarization parameters (angle and sense) obtained by multi-point magnetometer ground stations [e.g., *Nomura et al.*, 2011]. The relation with isolated proton aurora has been also investigated using all-sky images and ground magnetometer stations [e.g., *Sakaguchi et al.*, 2007; *Miyoshi et al.*, 2008; *Sakaguchi et al.*, 2008]. In statistical studies by *Fraser* [1968] and *Kuwashima et al.* [1981], Pc1 geomagnetic pulsations were more frequent during the daytime and in winter at high latitudes. A low latitudes, Pc1 geomagnetic pulsations peaked during the nighttime and in equinox months.

Pc1 pearl structures are quasi-periodic amplitude modulations of Pc1 waves with repetition periods of several tens of seconds. There are several possible generation mechanisms of Pc1 pearl structures. In particular, we can classify these mechanisms according to the regions in which Pc1 pearl structures are mainly produced, namely, magnetospheric and ionospheric effects. Magnetospheric effects are, for example, bouncing wave packets between the Northern and Southern hemispheres and EMIC waves modulated by long-period ULF waves. In these effects, Pc1 pearl structures are caused in the magnetosphere and propagate into the ionosphere. Ionospheric effects are those where Pc1 pearl structures are formed in the ionosphere, in which case the shape of the pearl structures can change during the ionospheric duct propagation.

In this introduction, Section 1.2 describes the geomagnetic environments from Earth's magnetosphere to its ionosphere. The geomagnetic environment is very important to understand the generation and propagation of EMIC/Pc1 waves. Section 1.3 describes the general equations of EMIC waves, including their growth rate, resonance conditions, and dispersion relation. Section 1.4 reviews observations of Pc1 pulsations and their characteristics. In that section, we introduce the propagation and polarization characteristics of Pc1 pulsations. Section 1.5 describes possible generation mechanisms of Pc1 pearl structures in detail.

1.2 Geomagnetic environment

This section describes the geomagnetic environments of the magnetosphere and the ionosphere, within which we are interested to investigate electromagnetic wave activities. The Earth, one of the planets in the solar system, is surrounded by a well-defined magnetic field called the Earth's magnetosphere. The Earth's magnetosphere forms a bubble around the Earth, and protects it from the dense solar winds containing many energetic particles. The magnetosphere can be approximated as a dipole magnetic field with a magnetic moment of 8.05×10^{22} Am^2. The structure of the magnetosphere is complicated, because interplanetary magnetic field (IMF) and energetic plasma particles in the solar wind interact with the Earth's magnetic field, the configuration of which is shown in Figure 1.3. On the dayside of the magnetosphere, solar wind pressure compresses the Earth's magnetic field, and reconnection between the IMF and the Earth's magnetic field occurs when the IMF has a southward component. The solar wind transports the reconnected magnetic field to the night side, creating a magnetotail that is stretched in the range from 10 to more than 200 R_E.

Energetic plasma entering the Earth's magnetosphere from the Sun is transported from the magnetotail toward the Earth contributing to the particle distribution in the inner magnetosphere. The plasmasphere has the densest (> 100 cm^2) and coldest (< 1 eV) plasma configuration in the range of 1-4 R_E. The ring current region shows as torus-like structures where the energy density of the plasma is the highest in the inner magnetosphere. The Van Allen radiation belts consist of energetic particles of electrons and ions within more than a few hundreds keV. Radiation due to these energetic particles is very harmful to life, including to human beings.

Injected energetic particles from the magnetotail are a free energy source for the generation of various types of plasma waves. During geomagnetically disturbed periods, called storm interval, many hot, energetic particles are injected into the inner magnetosphere and cause various instabilities, such as temperature anisotropy, that generate plasma waves. The generated plasma waves interact with cold and hot plasma in the inner magnetosphere, chang-

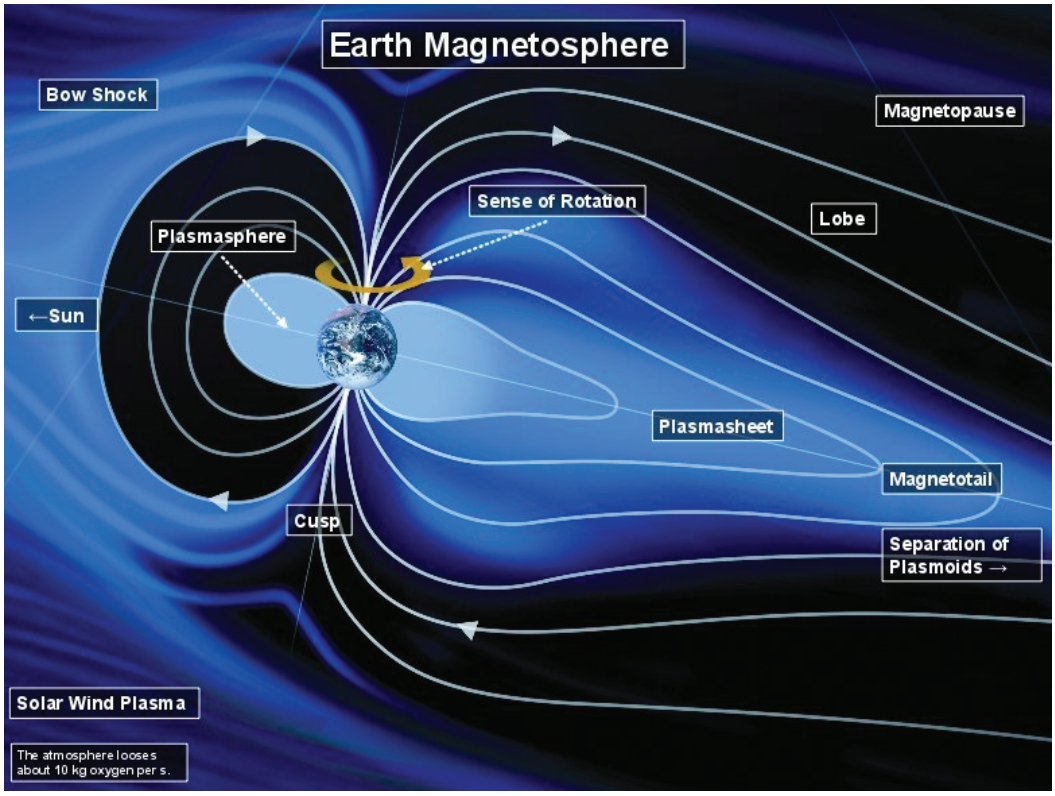

Figure 1.3 The Earth's magnetosphere, showing characteristic regions and magnetic field lines. [Source: http://www.mps.mpg.de/1969078/PPGresearch]

ing their energies and pitch angles. These interactions are called wave-particle interactions, and they cause the acceleration and loss of energetic particles. Particle scattering into the loss cone is the main process causing particle loss to the ionosphere and is an important cause of visible auroral activities. Figure 1.4 shows wave activity in the inner magnetosphere during geomagnetic storms.

The ionosphere is a region in the Earth's upper atmosphere at altitude of 60-1,000 km. It includes the thermosphere and part of the mesosphere. It is distinguished by ionized particles due to solar radiation. The ionosphere is also a boundary between the magnetosphere and the atmosphere, and plays an important part in atmospheric electricity. Figure 1.5 shows the several layers created by electron density variation in the ionosphere as a function of altitude. These layers follow daily variations. At night time, the F layer is the only layer with significant ionization; the ionization in the E and D layers is extremely low. During the day time, the D and E layers become much more ionized, and the F layer separates into two regions, the F1 and F2 layers. The F2 layer persists both day and night and is the region mainly responsible for EMIC wave refraction.

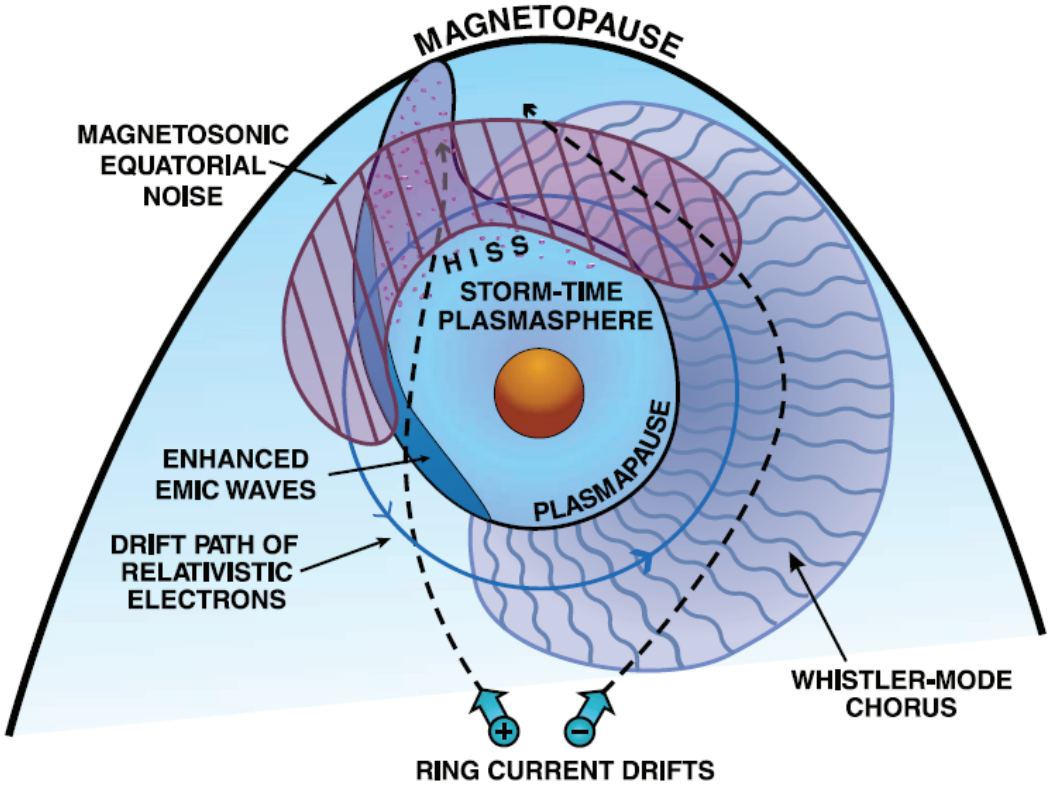

Figure 1.4 Spatial distribution of plasma waves during a geomagnetic storm in relation to the position of the plasmapause and the drift paths of ring current electrons and ions. Electrons injected into the magnetosphere excite a whistler-mode chorus on the dawn side, and the ions generate EMIC waves on the dusk side near the plasmapause reproduced from *Thorne*, [2010].

1.3 Electromagnetic ion cyclotron waves

EMIC waves are predominately left-hand polarized emissions observed at frequencies of 0.1-5 Hz near the equator region of the magnetosphere. In the presence of heavy ions He^+ and O^+ in the inner magnetosphere, EMIC waves are generally distinguished into three distinct bands: the H^+ band between ω_{He^+} and ω_{H^+}, the He^+ band between ω_{O^+} and ω_{He^+}, and the O^+ band below ω_{O^+}. EMIC wave amplitude can reach 1-10 nT during geomagnetic storms. According to THEMIS satellite observations by *Min et al.* [2010], the peak EMIC occurrence rate in space is separated with frequency band; for H^+ band EMIC waves, there is a peak occurrence in the dawn sector at 8-12 R_E, while He^+ band EMIC waves have a maximum occurrence in the dusk sector at 8-12 R_E. EMIC waves strongly interact with radiation belt electrons and ions, leading to loss of these particles into the ionosphere.

We describe the dispersion relation, resonance condition, and growth of the EMIC waves and their interaction with plasma. Figure 1.6 shows the dispersion relation of EMIC waves

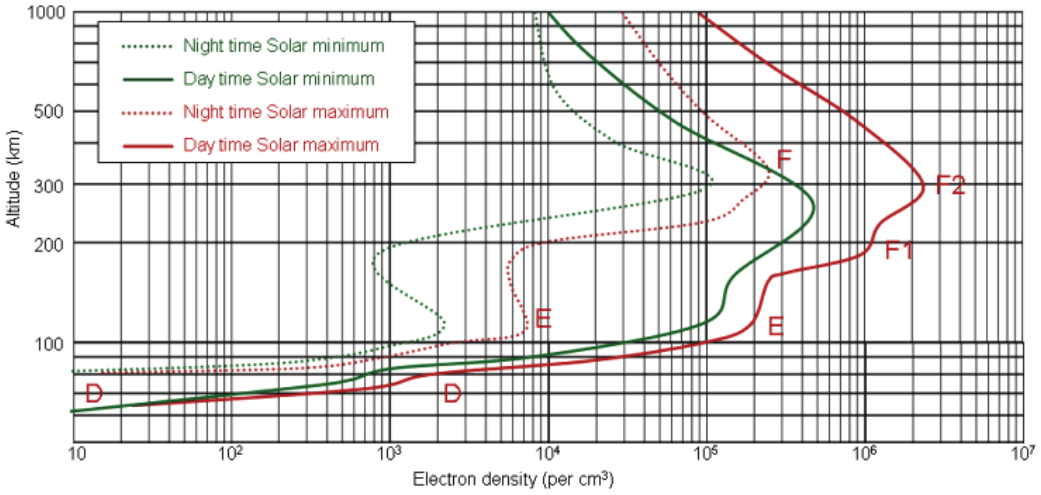

Figure 1.5 The variation of electron density as a function of altitude in the ionosphere. The green (red) lines indicate the variation of electron density during solar minimum (solar maximum). The solid lines and dashed lines denote day time and night time, respectively [Source: http://sidstation.loudet.org/ionosphere-en.xhtml].

for realistic ion compositions in the inner magnetosphere. For parallel propagation of EMIC waves, the dispersion relation including electrons and multi-ion dynamics is described in *Parks* [2004], as

$$N_{R,L}^2 = 1 - \frac{\omega_{pe}^2}{\omega(\omega \mp \Omega_e)} - \sum_s \frac{\omega_{pis}^2}{\omega(\omega \pm \Omega_{is})}, \tag{1.1}$$

where the upper and lower sign indicates the R-mode and L-mode, respectively, $\sum_s$ is a summation with respect to ions of species s, ω_{pe} and ω_{pis} are plasma frequencies of electrons and s-species ions, and Ω_e and Ω_i are gyrofrequencies of electrons and s-species ions. Field-aligned L-mode EMIC waves are confined to frequency bands below each ion gyrofrequency. Propagation along the magnetic field line within the stop-band of L-mode propagation is not allowed between the cut-off frequency and each heavy ion gyrofrequency. The relative composition of heavy ions controls the location of the cut-off frequency. EMIC waves can grow due to energy transfer from ions to waves, such as pitch-angle anisotropy, to recover from the unstable condition. This process occurs when the temperature at energetic ions in the parallel direction to the magnetic field is lower than in the perpendicular direction ($T_{\parallel} < T_{\perp}$), as called the ion cyclotron instability. During storm intervals, hot and energetic injected particles from the magnetotail develop the ring current and radiation belts in the inner magnetosphere. Ion cyclotron instability frequently occurs in such situations. The

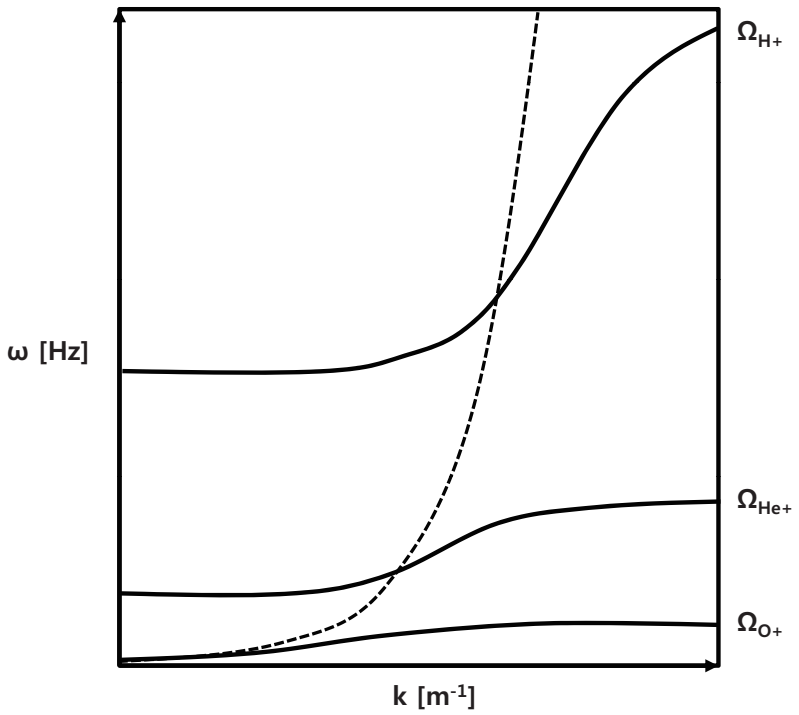

Figure 1.6 Dispersion relation of EMIC waves for parallel propagation in a plasma composed of 70% H^+, 20% He^+, and 10% O^+ species. The solid curves show the three left-handed polarized modes below the H^+, He^+ and O^+ cyclotron frequencies, respectively. The dashed curve denotes the right-handed polarized mode.

growth rate γ of EMIC waves is described as,

$$\gamma = \sqrt{\pi}\frac{N_0}{N_1}\frac{\omega_{ci}^2}{\kappa U_\parallel}\frac{(1-x)^2}{2-x}[A(\frac{1-x}{x})-1]exp[-\frac{\omega_{ci}^2(1-x)^2}{\kappa^2 U_\parallel^2}], \tag{1.2}$$

where N_0 and N_1 are the cold and hot plasma densities, respectively, ω_{ci} is the angular frequency of the ion cyclotron waves,κ is the Boltzmann constant, $x = \omega/\omega_{ci}$, $A = T_\perp/T_\parallel - 1$ is the temperature anisotropy constant, $T_\perp$ and $T_\parallel$ are the perpendicular and parallel temperatures, $U_\parallel = (2\kappa T/m_i)^{1/2}$, and m_i is the ion mass [*Fukunishi et al.*, 1983]. If the growth rate is higher than zero, EMIC waves can grow. In this equation, $T_\perp$ and $T_\parallel$ are the most important parameters controlling EMIC wave growth.

In contrast, EMIC wave energy can be transported to ions through ion cyclotron resonance. Whenever radiation belt particles can resonate with EMIC waves, the Doppler-shifted EMIC wave frequency as viewed in the reference frame of the particle is an integer multiple ($n = 0, \pm1, \pm2, ...$) of the particle gyrofrequency. The resonance condition of EMIC waves

is expressed in *Parks* [2004] as,

$$\omega - \kappa_{\parallel} v_{\parallel} = \frac{n\Omega}{\gamma}, \tag{1.3}$$

where $\gamma = (1 - (v/c)^2)^{-1/2}$ is a relativistic factor and $\kappa_{\parallel}$ and $v_{\parallel}$ are the wave propagation vector and particle velocity along the magnetic field line, respectively. This wave-particle interaction causes energy transfer from EMIC waves to particles and particle scattering.

1.4 Pc1 geomagnetic pulsations

1.4.1 Ground observations of Pc1 pulsations

EMIC waves are known to be generated at L-shells 4 to 8 in the equatorial regions of the magnetosphere due to ion cyclotron instabilities with an anisotropic energy distribution. Theoretical studies [e.g., *Horne and Thorne*, 1993] and observations [e.g., *Anderson et al.*, 1996] have suggested that EMIC waves are left-hand polarized Alfvén waves located near the generation region in the magnetosphere. They propagate by bouncing along the magnetic field lines between the Southern and Northern hemispheres. During this bouncing motion, some portions of EMIC wave energy pass through the ionospheric resonance region, allowing the waves to propagate into the ionosphere [*Fraser*, 1975a, 1975b; *Altman and Fijalkow*, 1980; *Fujita and Tamao*, 1988]. In the ionosphere, right-hand polarized compressional (fast) isotropic waves are generated through the interaction of incident EMIC waves with ionospheric plasma in the F-region. Theory and observations show that after this mode conversion from Alfvén to compressional waves, the compressional waves can be trapped in the ionospheric duct (or waveguide) centered in the F2-region (a layer of maximum electron density at an altitude of ∼400 km) with minimum Alfvén speed [e.g., *Manchester*, 1966; *Tepley and Landshoff*, 1966; *Campbell*, 1967; *Kuwashima et al.*, 1981; *Kawamura et al.*, 1981; *Kim et al.*, 2011; *Waters et al.*, 2013]. These trapped waves propagate latitudinally and longitudinally from the ionospheric source region to low latitudes. These waves are observed on the ground as Pc1 pulsations at frequencies of 0.2-5 Hz [*Jacobs et al.*, 1964]. During ionospheric duct propagation, the wave energy of Pc1 pulsations is attenuated with an attenuation ratio of 0 to 13 dB/1,000 km [*Althouse and Davis*, 1978; *Kim et al.*, 2010]. In previous studies, Pc1 pulsations were frequently observed at high latitudes during the daytime with a maximum occurrence at 1 to 2 h before sunrise during winter. On the other hand, the occurrence of Pc1 pulsations at low latitudes peaked during the nighttime about 1 h after local magnetic midnight and during equinoxes [*Fraser*, 1968; *Kuwashima et al.*, 1981].

Figure 1.7 shows typical Pc1 pulsations observed on the ground using induction magnetometers. During the day on April 8, 2010, we observed several Pc1 pulsations at Athabasca (ATH) in Canada, Magadan (MGD) in Russia, and Moshiri (MOS) in Japan, in the frequency range of 0.2-2.2 Hz. The first Pc1 burst at 03-09 UT is mainly observed at ATH, but observations at MGD and MOS were very weak, probably because of attenuation during ionospheric duct propagation. This indicates that the ionospheric source for this event should be close to ATH, as ATH was in the pre-midnight sector while MGD and MOS were in the afternoon sector. These Pc1 waves may have difficulty propagating latitudinally, due to the sudden change of electron density profile in the F layer of the ionosphere at the dusk side terminator. Conversely, MGD and MOS simultaneously observed Pc1 pulsations at 10-21 UT, but these were not seen at ATH. During this time interval, MGD and MOS were in the night time, when variation in the electron density of the ionosphere would be stable. This condition could present a well-defined ionospheric duct in the F-layer, propagating Pc1 pulsations further. At the same time, ATH was in the morning sector, over the dawn side terminator, probably making propagation of Pc1 pulsations difficult.

1.4.2 Trapped Pc1 pulsations and propagation in the ionospheric duct

Pc1 waves with left-hand polarization have a mode conversion to the compressional waves near the ionospheric source region at high latitudes. These waves propagate latitudinally from higher to lower latitude through the ionospheric duct centered by the F layer of the ionosphere [e.g., *Greifinger and Greifinger*, 1968]. Figure 1.8 shows the ionospheric duct propagation for Pc1 pulsations from high to low latitudes, as described in *Kawamura et al.* [1981]. In the F layer in the ionosphere, there is maximum electron density at an altitude of ∼400 km with minimum Alfvén speed. Pc1 waves are trapped in this layer, and these trapped waves propagate latitudinally and longitudinally from the ionospheric source region to low latitudes. From this process, Pc1 pulsations can be observed at low latitudes, even though these waves observed at high latitudes strongly connect with direct propagation of EMIC waves from the magnetosphere.

The plasma density of the ionosphere is key to Pc1 propagation from the ionospheric source at high to low latitudes. The attenuation effect in the ionospheric duct leads to a difference of Pc1 occurrence rate between high and low latitudes. The occurrence rate of Pc1 pulsations observed at high latitudes has a maximum during the daytime and up to 1 h after magnetic local noon,while observations at low latitudes are maximized during the nighttime and up to 1 h before sunrise. This is probably due to differences in ionospheric electron density profiles in the F-region. In seasonal variations of Pc1 occurrence, they reach a maximum at equinoxes at high latitudes and in the winter at low latitudes, probably due to seasonal

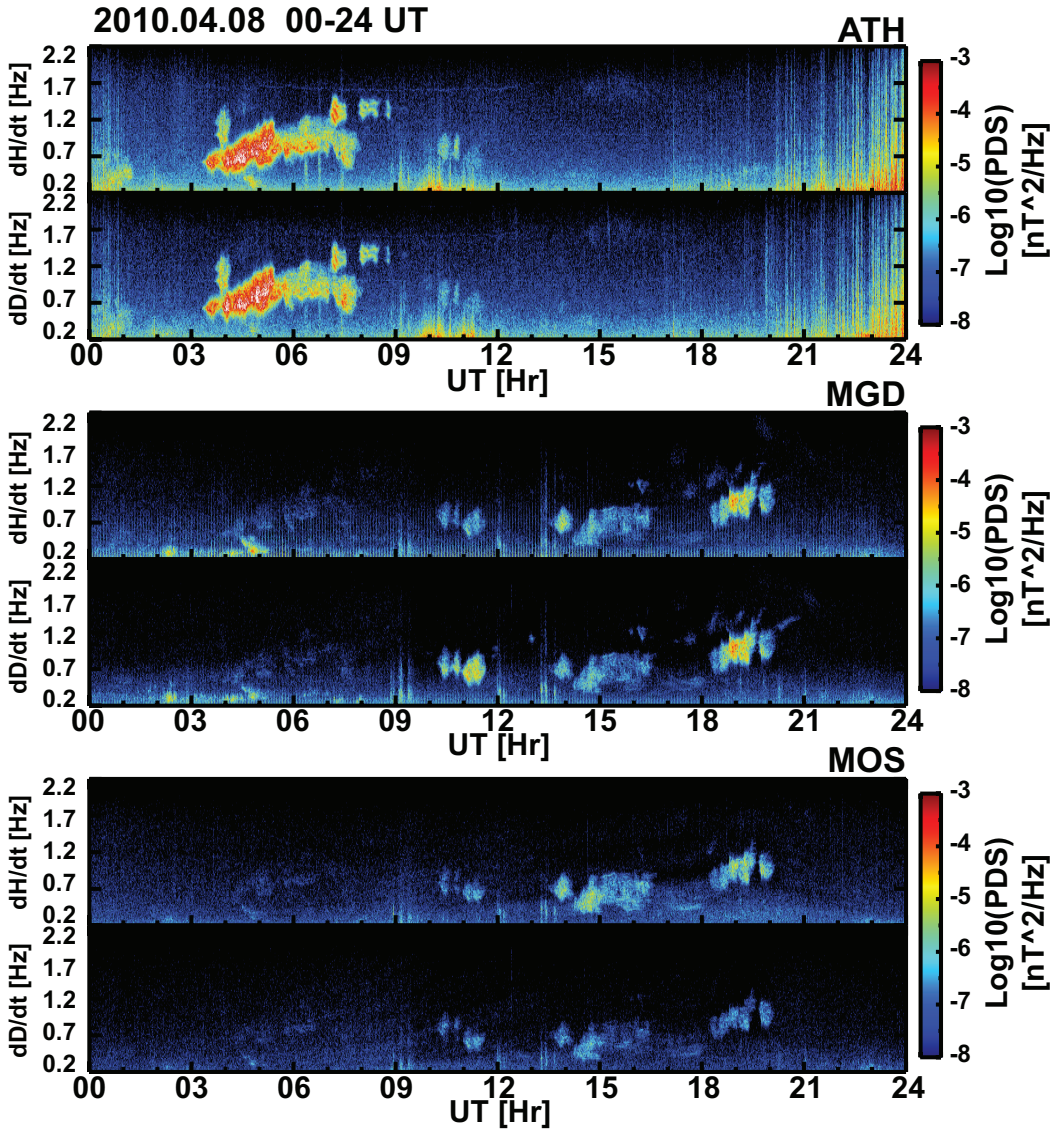

Figure 1.7 Dynamic spectra of the H and D components for the magnetic field variations observed at ATH, MGD and MOS at 00-24 UT on April 8, 2010, in the frequency range of 0.2 to 1.8 Hz.

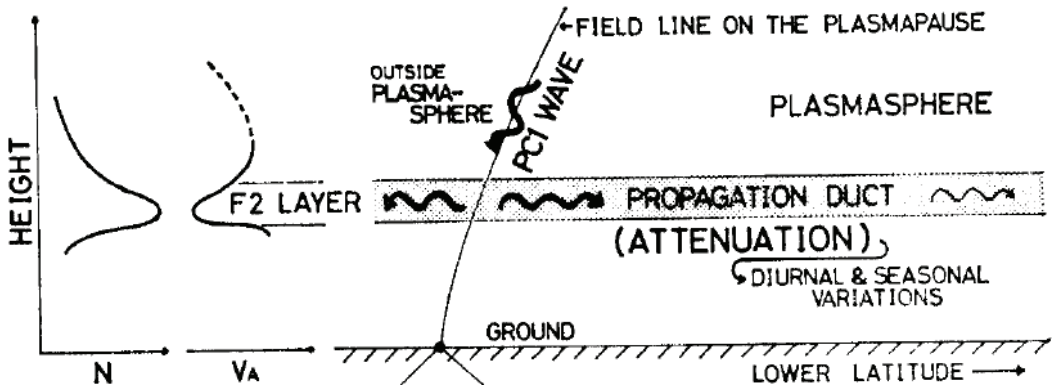

Figure 1.8 Schematic figure of ionospheric duct propagation of Pc1 pulsations reproduced from *Kawamura et al.* [1981].

differences in the attenuation of Pc1 waves during ionospheric duct propagation. The Pc1 occurrence also has an anti-correlation with sunspot number variation, which is an indicator of solar activity [*Fraser-Smith*, 1970; *Kawamura et al.*, 1985; *Park et al.*, 2013].

1.4.3 Dependence of Pc1 polarization angle on frequency

The polarization angle of Pc1 pulsations observed on the ground can provide important information on their ionospheric source region. In theoretical studies [*Greiginger*, 1972; *Fujita and Tamao*, 1988], polarization parameters (angle and sense) vary significantly with the latitudinal scale of the ionospheric source region of Pc1 waves and the distance between the source and the location of the observation.

Fujita and Tamao [1988] conducteda model calculation of the dependence of Pc1 polarization parameters on the distance and position of the Pc1 ionospheric source. The orientation of the polarization angle observed on the ground varies as a result of coupling between magnetospheric EMIC waves and ducted Pc1 waves. Near the source region, the polarization angle mainly follows magnetospheric EMIC waves,with the minor axis of the polarization angle pointed to the source region. Far from the source region, however, the major axis of the polarization angle points toward the ionospheric source region.

The polarization angle of Pc1 pulsations is useful for determining the location of the ionospheric source region of the waves. At mid-to-low latitudes, this region is generally located far from the source region, so the major axis of the polarization angle mainly points to the Pc1 ionospheric source [*Fraser*, 1976]. *Nomura et al.* [2011] found that $\sim$ 70% of Pc1 pulsations observed at low-latitude ground stations have a dependence of polarization angle on frequency. This result suggests that Pc1 pulsations have latitudinally distributed ionospheric source region.

1.4.4 Distributed ionospheric source region observed by isolated proton aurora at subauroral latitudes

Precipitation of magnetospheric ions scattered by resonance with EMIC waves in the magnetosphere causes isolated proton auroras at subauroral latitudes. From space and ground observations, *Yahnina et al.* [2000] reported that proton precipitation at subauroral latitudes has a relation with ground Pc1 pulsation activity. They also found that the frequency of Pc1 pulsations increases with decreasing proton aurora latitudes. *Sakaguchi et al.* [2008] found that the spatial distribution of isolated proton auroras has limited latitudinal and longitudinal widths of less than 230 km and 250-800 km, respectively. They also found that as isolated arcs moved equatorward (poleward), the frequency of simultaneous Pc 1 pulsations increased (decreased). In temporal variation of the isolated proton aurora, the isolated proton auroral spots, indicators of Pc1 ionospheric sources, were intermittently distributed over a 4-h MLT period in the pre-midnight sector equatorward of substorm auroral activity at auroral latitudes [*Sakaguchi et al.*, 2012]. Figure 1.9 shows a photograph of an isolated proton aurora observed at Athabasca, Canada, at subauroral latitudes. The bottom left of this figure partially shows a typical diffuse aurora, while the main photograph shows an isolated proton aurora with two separated patches.

1.5 Pc1 pearl structures

A *`Pc1 pearl structure'* is a quasi-periodic amplitude modulation of Pc1 pulsations with a repetition period of several tens of seconds [*Troitskaya and Gul'Elmi*, 1967]. Figure 1.10 shows dynamic spectra and time series of the H and D components of the magnetic field observed at ATH at 13-18 UT on February 16, 2013. In Figure 1.10(a), we can see quasi-periodic modulation of Pc1 pulsations at both components in at frequencies of 0.2-1.2 Hz. To see the magnetic field variation in detail, in Figure 1.10b we zoom in at 1415-1419 UT. We can see many amplitude modulations of Pc1 waves in this time interval with a repetition period of approximately 30 s. Theses quasi-periodic modulations in the spectral domain and amplitude modulations in the time domain are called as *`Pc1 pearl structures'*.

1.5.1 Generation of Pc1 pearl structures

There have been many studies using ground-based and satellite observations to investigate the generation mechanisms of the Pc1 pearl structures [e.g., *Perraut*, 1982; *Erlandson et al.*, 1992; *Guglielmi et al.*, 1996; *Mursula*, 1997; *Rasinkangas and Mursula*, 1998; *Mursula et al.*, 1999; *Mursula*, 2007; *Usanova et al.*, 2008; *Nomura et al.*, 2011; *Jun et al.*, 2014]. Pc1

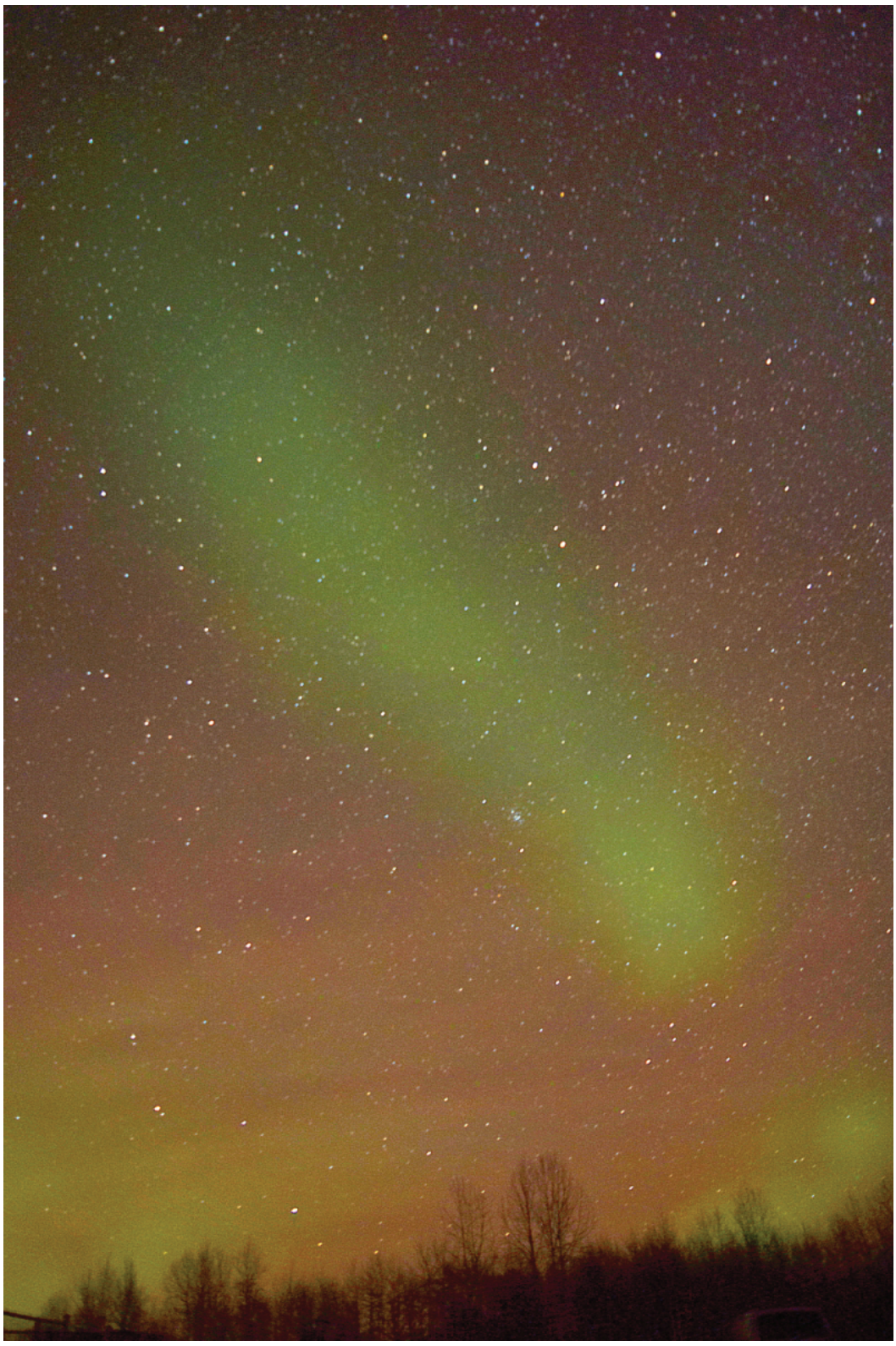

Figure 1.9 Photograph of an isolated proton auroral arc in the southeastern sky of Athabasca, Canada, on November 12, 2015 (photo: Claudia Martinez-Calderon).

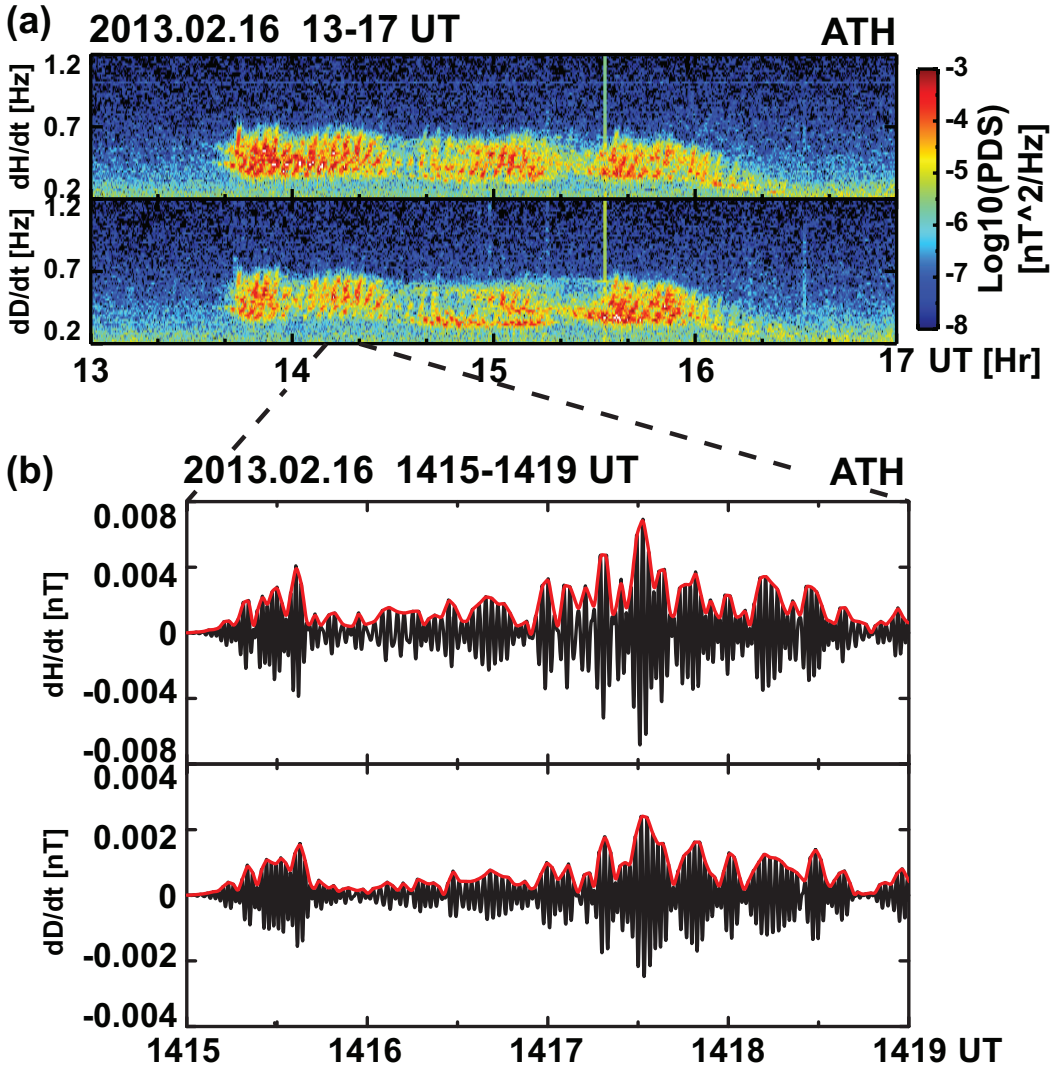

Figure 1.10 (a) Dynamic spectra of the H and D components of magnetic field variations observed at ATH at 13-18 UT and (b) band-pass filtered (0.2-1.2 Hz) Pc1 waveform of the magnetic field of the H and D components observed at ATH at 1415-1419 UT on February 16, 2013.

pearl structures can be generated by magnetospheric and ionospheric effects. Though many previous studies have investigated the formation of Pc1 pearl structures, their generation mechanisms have not been conclusively identified.

If magnetospheric effects are dominant in the creation of Pc1 pearl structures, the pearl should not be changed during ionospheric duct propagation. If ionospheric effects are dominant, however, the structures may change during ionospheric duct propagation.

1.5.2 Magnetospheric effects

One candidate for the magnetospheric effect is the bouncing wave packets model (BWP model) [e.g., *Guglielmi et al.*, 1996; *Mursula et al.*, 1999]. This model suggests that the bouncing of EMIC waves along the magnetic field lines between the Northern and Southern hemispheres cause Pc1 pearl structures. According to this model, the length of a magnetic field line associated with EMIC wave sources could be a main controller for the repetition period of Pc1 pearl structures. The Alfvén velocity in the magnetosphere depends on plasma conditions along the field line, and the traveling time of the wave packets between both hemispheres determines the bouncing periods. The repetition period of Pc1 pearl structures also depends on the length of the magnetic field lines. This period varies in a range of several tens of seconds, depending on the L-value of the EMIC generation region. However, some recent studies have suggested reconsidering whether the BWP model is appropriate for the formation of Pc1 pearl structures. For example, their repetition periods can significantly differ from the results expected from this model [e.g., *Perrant et al.*, 1982; *Paulson et al.*, 2014]. If Pc1 pearl structures are mainly caused by BWP model, the repetition period in space should be half that on the ground. However, comparing ground and satellite observations, *Perrant et al.* [1982] found that the repetition periods of Pc1 pearl structures observed in space did not have this relation. Furthermore, *Paulson et al.* [2013] observed repetition periods on the ground that were similar to those in space. Additionally, using data obtained by the Viking satellite near the plasmapause, *Erlandson et al.* [1992] found that the Poynting flux of Pc1 pearl structures was mainly directed downwards, along the magnetic field lines and into the ionosphere, contradicting the BWP model.

Another candidate magnetospheric effect for Pc1 pearl generation is the modulation of EMIC waves by long-period ULF waves (such as Pc4 or Pc5 pulsations), as suggested by *Mursula et al.* [2001] and *Mursula* [2007], who found that EMIC waves observed in space were modulated by magnetospheric Pc3 pulsations. The generation of Pc1 pulsations by ion cyclotron instability also causes amplitude modulations, such as EMIC rising tone emissions [*Omura et al.*, 2010; *Shoji and Omura*, 2013; *Nakamura et al.*, 2014]. It has also been suggested that Pc1 pearl structures can be generated by the superposition of EMIC waves

traveling in the magnetosphere with a coherence length associated with the waves' growth [*Hu and Denton*, 2009].

1.5.3 Ionospheric effects

Some studies have instead suggested beating processes in the ionosphere for the generation of Pc1 pearl structures [e.g., *Pope*, 1964; *Nomura et al.*, 2011; *Jun et al.*, 2014]. In previous studies, *Pope* [1964] suggested that Pc1 pearl structures could be generated during ionospheric duct propagation by the superposition of Pc1 waves with a broad frequency. *Nomura et al.* [2011] showed that around 70% of Pc1 pulsations observed at low-latitude ground stations have a dependence of Pc1 polarization angle on its frequency, indicating that the Pc1 ionospheric source is spatially extended from north to south. *Sakaguchi et al.* [2008] found that the isolated proton auroral spots associated with Pc1 pulsations had longitudinal extents of 250-800 km. These observations show that Pc1 pulsations observed at some ground stations could be a mixture of several waves from different ionospheric source regions. Figure 1.11 shows Pc1 pearl structures caused by beating processes in the ionosphere and their ionospheric duct propagation from source region to ground. Beating processes occur in the ionosphere when Pc1 waves with slightly different frequencies associated with a north-south extended ionospheric source region are superposed at the observation points. The propagation time differences from the extended sources to the ground stations generate different amplitude modulations at different observation points. Pc1 pearl structures may thus have different shapes at different locations on the ground due to different wave-beating conditions. This process also implies that the amplitude modulation of Pc1 pulsations might not be related to the energy transfer between energetic particles and waves. From these considerations, we should investigate similarities in Pc1 pearl structure between different stations to identify this mechanism for Pc1 pearl generation.

1.6 Purpose of this thesis

Ground induction magnetometers present the prefect opportunity to investigate the generation mechanisms of Pc1 pearl structures in the ionosphere. While Pc1 source regions in the ionosphere are located far from the ground stations, we can observe Pc1 pulsations through their ionospheric duct propagation. The Pc1 polarization angle is a key parameter to demonstrating the source distribution of waves. This information led to our idea that Pc1 pearl structures could be caused by beating processes in the ionosphere. Previous studies have tried to understand the generation mechanisms of Pc1 pearl structures using satellites and

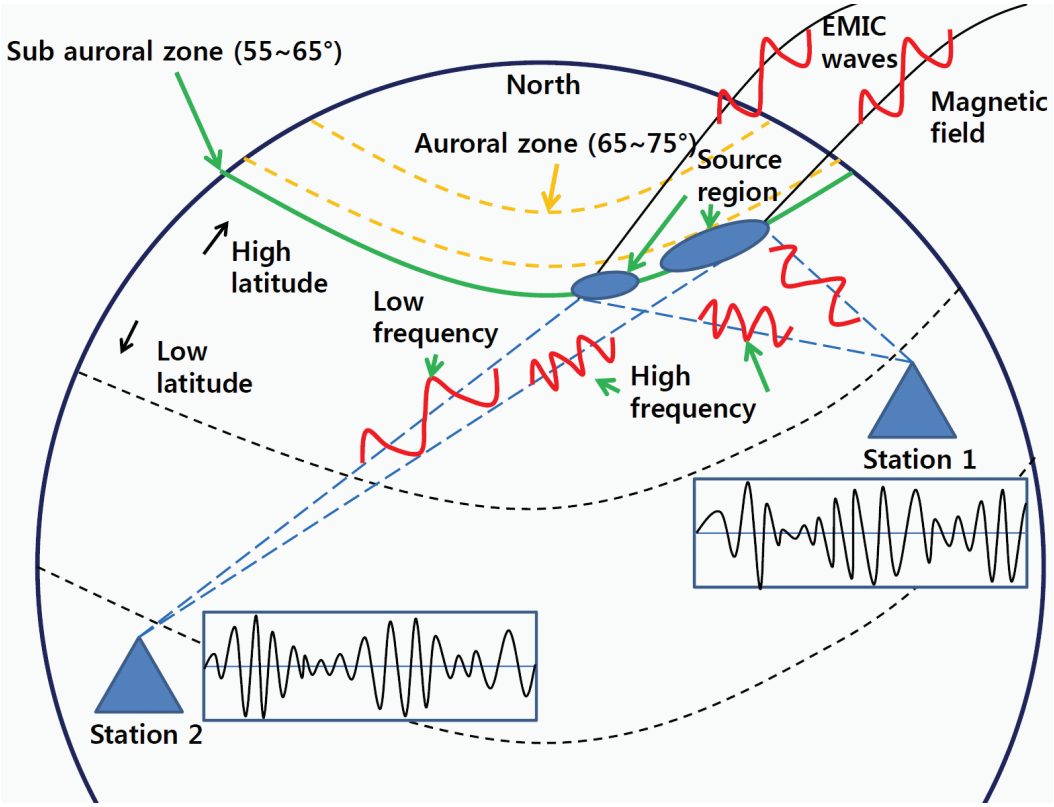

Figure 1.11 Beating processes in the ionosphere.

ground magnetometer chains, but despite many mechanisms having been suggested for the formation of Pc1 pearl structure, the dominant mechanism is not yet well understood.The purpose of this research is thus to identify the dominant generation mechanism of Pc1 pearl structures.

In Chapter 2, we introduce the instrumentation and data analysis methods used in this study. We present the characteristics of the induction magnetometers installed at Athabasca (ATH) in Canada, Magadan (MGD) in Russia, and Moshiri (MOS) in Japan. We also describe the calibration of the induction magnetometers, and how we used the data obtained these instruments. We calculate the spectral parameters (wave power, central frequency, and bandwidth) and polarization parameters (angle and sense), as well as coherence of Pc1 waveforms. For the waveform analysis, we make a band-pass filter function to reduce noise from outside the Pc1 frequencies. To identify similarity between Pc1 pearl structures at different stations, we use cross-correlation analysis based on the upper envelope of Pc1 waveforms.

In Chapter 3, we investigate the possibility of Pc1 pearl generation by beating processes in the ionosphere, using two Pc1 pulsation events simultaneously observed at three stations combined with model calculations. Case 1 presents different Pc1 pearl structure shapes at

different stations with polarization-angle dependence on Pc1 frequency. Case 2 shows similar Pc1 pearl structures at different stations with a constant polarization angle. To understand their differences, we use model calculations of Pc1 pearl structures. The first model assumes that Pc1 waves propagate from the distributed source region to the observation points with different arrival times for each frequency. The second model assumes that all Pc1 frequencies are mixed at a point source before propagating to the observation points. We then compare our ground-based observations with model calculations.

In Chapter 4, we present a statistical description of Pc1 pearl structures using multi-point ground-based induction magnetometers for a six-year period from 2008 to 2013. The purpose is to identify the dominant generation mechanism of Pc1 pearl structures in the ionosphere. We separate these into two groups, longitudinally (ATH and MGD) and latitudinally (MGD and MOS) separated stations, then classify Pc1 pulsation events into these two groups. We show the distribution of similarity for Pc1 pearl structures for both groups. We also present temporal variations (UT dependence, monthly dependence, and annual dependence) of similarity of Pc1 pearl structures. We also present Pc1 pearl similarity dependencies on geomagnetic conditions and wave properties, and discuss possible Pc1 pearl generation caused by beating processes in the ionosphere.

In Chapter 5, we summarizing the study and suggest areas for future research.

Chapter 2

Instrumentation and data analysis methods

2.1 Induction magnetometers

In this thesis, we use multi-point ground induction magnetometers installed by the Institute for Space-Earth Environmental Research, Nagoya University, at Athabasca (ATH; 54.7°N, 246.7°E, L=4.3) in Canada, Magadan (MGD; 60.1°N, 150.7°E, L=2.6) in Russia, and Moshiri (MOS; 44.4°N, 142.3°E, L=1.5) in Japan [*Shiokawa et al.*, 2010]. The stations are separated by 5,317 km between ATH and MGD and 1,880 km between MGD and MOS. Table 2.1 shows the geographic and geomagnetic coordinates, L-values, and the dates of data acquisition start of these stations. Figure 2.1 is a map showing the locations of these stations with their geographic coordinates and dipole geomagnetic latitudes, as obtained by the IGRF-11 model using an epoch time of 2010.

The induction magnetometer is a sensor that measures variations of magnetic flux in frequency ranges from several mHz to hundreds of MHz. The induction magnetometer is based on Faraday's law of induction. Temporal variation of the magnetic field intensity ($\boldsymbol{B}$)

Table 2.1 Locations and date of data acquisition start at the three stations

	glat	glon	mlat	mlon	L-value	Acquisition start
ATH	54.7	246.7	61.7	306.2	4.5	Sep. 7, 2005-
MGD	60.1	156.7	51.9	213.2	2.6	Nov. 5, 2008-
MOS	44.4	142.3	35.6	209.5	1.5	Jul. 14, 2007-

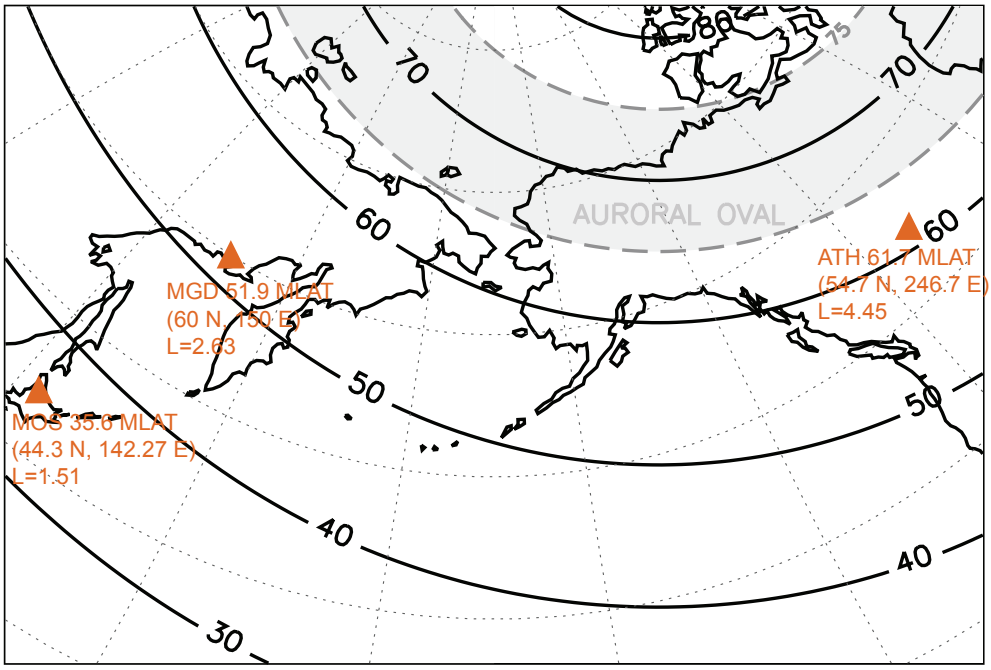

Figure 2.1 Locations of the three induction magnetometer stations: Athabasca (ATH) in Canada, Magadan (MGD) in Russia, and Moshiri (MOS) in Japan. Solid lines indicate dipole magnetic latitudes calculated using the IGRF-11 model with an epoch time of 2010. Dashed lines indicate geographic coordinates.

through the number of circuit turns (n) will induce a voltage (V) as:

$$V = -nS\frac{dB}{dt}, \tag{2.1}$$

where S is the size of the coil cross-section. The induced voltage has dependence on the magnetic permeability, which is a measure of the ability of a material to support the formation of a magnetic field within itself. The permeability constant (μ_0), also known as the magnetic constant, is a measure of the amount of resistance encountered when forming a magnetic field in a vacuum. The magnetic constant is $4\pi \times 10^7$ Hm^{-1}. The output voltage of the induction magnetometer varies in proportion to the temporal variation of the magnetic field, allowing us to compute variations in the magnetic field from the recorded voltage.

2.1.1 Data sampling

We use induction magnetometers to measure the H (horizontal), D (perpendicular), and Z (vertical) components of geomagnetic field variation. This measurement records voltage variations, which are generated by magnetic field fluctuation due to Faraday's law. Figure 2.2

shows the induction magnetometer system. For MGD and MOS, to prevent noise from the cable connecting the sensors to the main amplifier, the system has a pre-amplifier near the sensor. This amplifies signals 100 times before sending them to the main amplifier. However, the induction sensors at ATH were installed near the observation site, making a pre-amplifier unnecessary. The three sensors were installed in the geomagnetic H-, D-, and Z-directions at all stations.

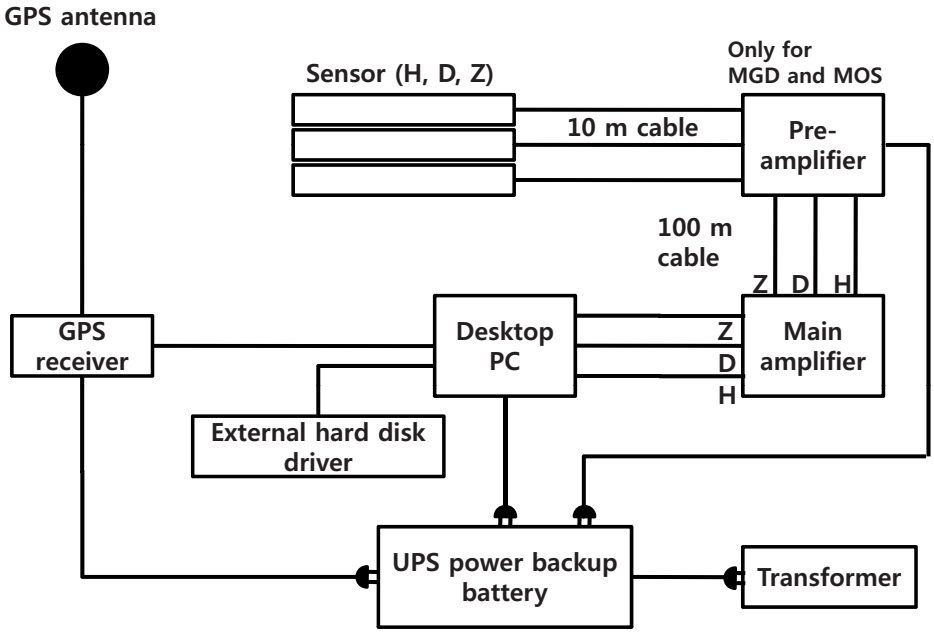

Figure 2.2 The induction magnetometer system.

Magnetic field data obtained by induction magnetometers are recorded at a sampling rate of 64 Hz. To ensure time accuracy of the data,we use a GPS clock with approximately 1 μs accuracy to correct the clock of the personal computer every 10 min with a 1 pps signal. This signal is divided into a 64 Hz signal to trigger the data sampling. The clock information generated by the personal computer is written to a data file every 4 s. The time accuracy of this GPS system is thus considered suitable for investigating Pc1 geomagnetic pulsations with frequencies of 0.2-5Hz.

2.1.2 Calibration

To obtain the sensitivity, phase difference, and polarity of induction magnetometers at 0.1-50 Hz for the three stations, we calibrated these measurements using the calibration test system shown in Figure 2.3. We used a calibration coil for this test. The length, diameter, and num-

ber of turns of the calibration coil are 2 m, 0. m, and 100 turns/m, respectively. The method of calibration for the induction magnetometers is as follows: First, we set up the induction sensor in the middle of the calibration coil. Then, the AC oscillator generates an artificial sinusoidal current with a specific frequency in the range of 0.1-50 Hz, inducing magnetic field fluctuation in the calibration coil. The induction magnetometer sensor installed in the middle of the calibration coil measures the magnetic fluctuation. The equation of magnetic field intensity for the finite coil length L (=2 m) is

$$B(T) = \frac{\mu_0 n I}{2} \cdot \frac{L}{\sqrt{(L/2)^2 + R^2}}, \tag{2.2}$$

where μ_0 is the permeability of vacuum ($\mu_0 = 1.26 \times 10^{-6}$H/m), and R is the radius of the calibration coil.

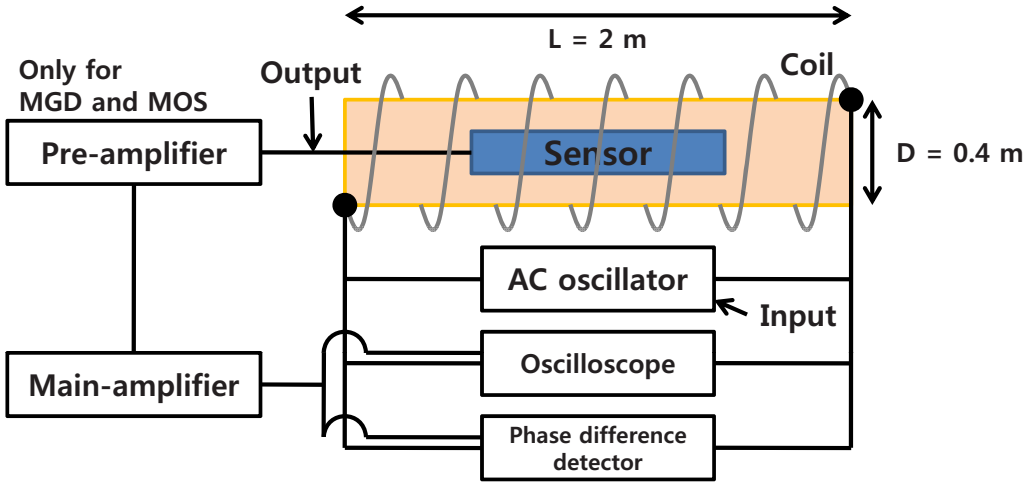

Figure 2.3 Magnetometer calibration system.

The relation between input current I (A) and magnetic field B (nT) is

$$I = \frac{B}{n\mu_0}, \tag{2.3}$$

where n is the number of turns of the coil. We set the target B value to 100 nT. Then, we can compute V from Ohm's law with a resistance R (Ω) as

$$V = IR = \frac{BR}{n\mu_0}. \tag{2.4}$$

Because of the accuracy of the AC oscillator, the actual voltage V_a in this calibration system is not exactly the expected ideal input. We therefore have to calculate the actual current I_a and the actual magnetic field intensity B_a from the measured input voltage V_a. Since I_a is

$$I_a = \frac{V_a}{R}, \tag{2.5}$$

the B_a generated in this coil is

$$B_a = n\mu_0 I_a = \frac{n\mu_0}{R}. \tag{2.6}$$

For the calibration test of the magnetometer system for Zhigansk in Russia, which have not yet installed, we use a voltage with 100 nT peak-to-peak oscillation generated by the AC oscillator into the calibration coil with $n = 100$ turns/m. We also add a resistance of 10 kΩ. Thus, the voltage obtained by Equation 2.4 is

$$V = \frac{100 \times 10^{-9} \cdot 10^4}{100 \cdot 1.26 \times 10^{-6}} = 8.116(V). \tag{2.7}$$

From Equation 2.6 using the voltage obtained above,

$$B = \frac{100 \cdot 1.26 \times 10^{-6}}{10^4} = 101(nT). \tag{2.8}$$

The magnetometer output signals are sent to the phase difference detector and the oscilloscope. We perform measurements five times and average them to determine the sensitivity and phase difference. The sensitivity (V/nT) is obtained by dividing the output voltage by the input magnetic field intensity (∼100 nT) applied on the sensor. More detailed information regarding the calibration is presented in *Shiokawa et al.* [2010].

Sensitivity and phase difference

We measured the sensitivity and phase difference of the induction magnetometer infrequency range 0.1-50 Hz. Figure 2.4 shows the sensitivity for the H, D, and Z components of the induction magnetometers at the three stations as a function of frequency. The maximum sensitivity of the induction magnetometer is 0.46 V/nT at 5.5 Hz for ATH, 0.45 V/nT at 1.8 Hz for MGD, and 13.16 V/nT at 2.7 Hz for MOS. The output voltages are proportional to frequency within the frequency range below these turnover frequencies, as expected from the characteristics of the induction magnetometer.

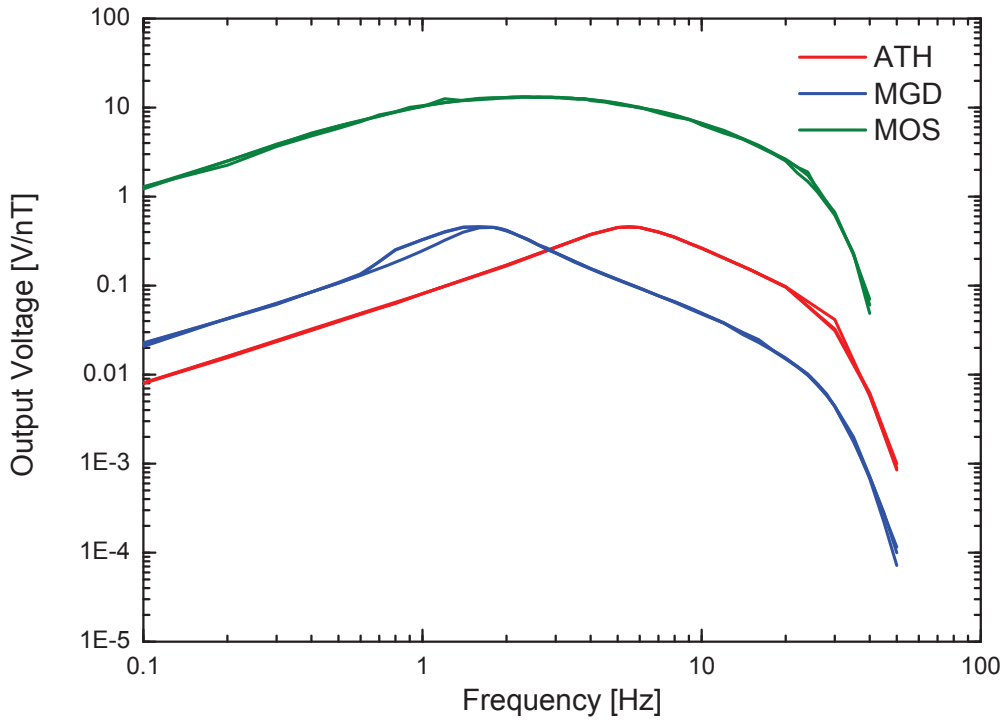

Figure 2.4 Sensitivities of the induction magnetometers at ATH (red), MGD (blue), and MOS (green). H,D, and Z components are shownin the same color and overlap.

Figure 2.5 shows the phase differences for MGD and MOS. The data for ATH is not shown in this figure because we did not measure the phase differences at ATH. The phase difference at the two stations continuously decreases with increasing frequency. These values are close to 0˚ near the turnover frequencies, indicating maximum sensitivity of the induction magnetometer.

As shown in Figures 2.4 and 2.5, the sensitivities and the phase differences of the induction magnetometer at the three stations clearly respond within Pc1 frequencies (0.2-5.0 Hz). These instruments, therefore, are enough to demonstrate the characteristics of Pc1 geomagnetic pulsations.

Polarity

We checked the polarity of the induction sensors at the three stations using a 1.5 V dry battery cell connected to the calibration coil. This battery produces a sudden increase in magnetic field intensity in the calibration coil when it is connected to the coil. If the output voltage sign from the induction sensor is positive (negative) with increasing magnetic field, the polarity of this sensor is defined as positive (negative). The polarity of the induction sensor is very important for identifying the polarization parameters of Pc1 geomagnetic pulsations and the

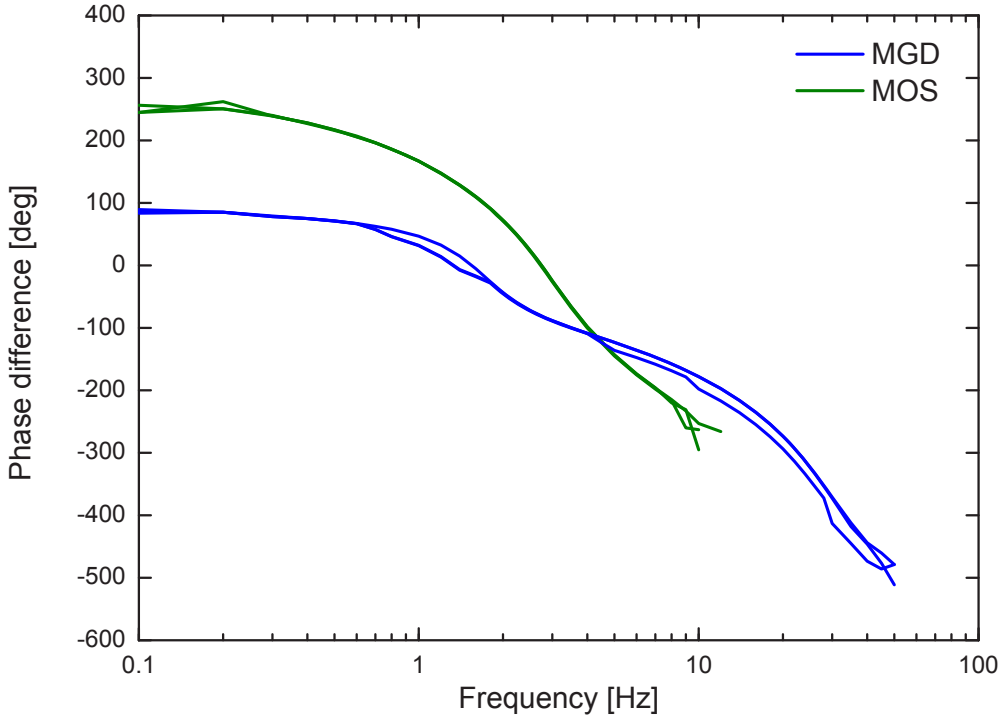

Figure 2.5 Phase differences of the induction magnetometers at MGD (blue) and MOS (green). The horizontal dashed line indicates 0˚ of phase difference. Blue and green vertical dashed lines denote the turnover frequencies at MGD and MOS, respectively.

similarity of Pc1 pearl structures between two stations. The positive polarities of the H, D, and Z components of the induction magnetometer are northward, eastward, and upward for ATH, northward, eastward, and downward for MGD, and southward, westward, and upward for MOS.

2.2 Data analysis method

This section describes our data analysis methods. We used spectral analysis, including polarization parameters and waveform analysis. We obtained the spectral parameters described by *Hino* [1977]. The polarization parameters are computed by the method of *Fowler et al.* [1967]. The waveform analysis is performed as described in these references for band-pass filtering and cross-correlation.

We follow the data process shown in Figure 2.6. This analysis considers the frequency and time domain. To obtain the polarization parameters, we first calculate a Fast Fourier transform (FFT) with a Tukey window, converting the original magnetic field data into the frequency domain. We then multiply the calibration parameter (frequency-dependent sensi-

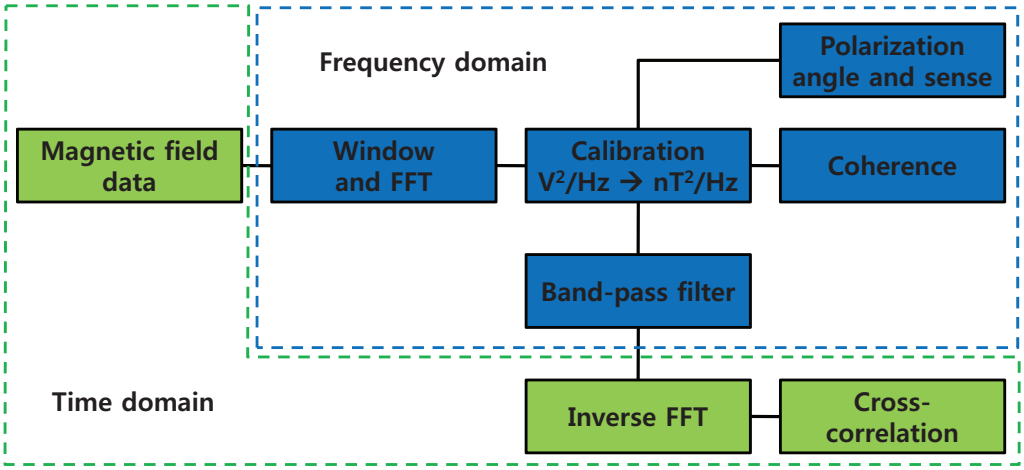

Figure 2.6 Schematic of the data analysis process.

tivity of the induction magnetometer) by the obtained power spectral density (PSD). Finally, we calculate polarization parameters (angle and sense) from the H and D components of the PSDs of a station and coherence of Pc1 waveforms between two stations. To identify similarities in Pc1 pearl structures observed at two stations, we use a cross-correlation analysis of the upper envelopes of the Pc1 waveforms. For this purpose, we compute FFT with a Tukey window and multiply the calibrated parameters, and apply a band-pass filter to extract the pure oscillation due to Pc1 waves without noise. We then convert this filtered PSD from the frequency domain to the time domain. Finally, we calculate the envelopes of the Pc1 waveforms and cross-correlation of the envelopes between two stations.

2.2.1 Window function and Fast Fourier transform

In signal processing, a window function is a mathematical function that is zero-valued outside of some chosen time interval. This function is used to reduce the error of estimated PSD on FFT analysis applied to a finite time segment. If we calculate PSD for a finite time segment without the window function, the results contain side lobes from the sudden jump of values at either edge of the time segment. Applying an appropriate window function to the time segment before applying FFT avoids this problem. We use a Tukey window function

called the tapered cosine window. In this case, the Tukey window $|W(n)|$is expressed as

$$|W(n)| = \begin{cases} sin\left(\frac{\pi}{2} \cdot \frac{n}{N/10}\right) & 0 \leq n \leq N/10 \\ 1 & N/10 \leq n \leq N - N/10 \\ sin\left(\frac{\pi}{2} \cdot \frac{N-n}{N/10}\right) & N - N/10 \leq n \leq N, \end{cases} \tag{2.9}$$

where N is total number of data points in the FFT time segment.

FFT converts a signal from its original time or space domain into the frequency domain and inverse FFT is used for conversion in the opposite direction. This analysis is widely used for many applications in engineering, science, and mathematics. The Fourier transform is expressed as

$$F(\omega) = \frac{1}{N} \sum_{t=0}^{N-1} f(t) exp[-i2\pi\omega t/N], \tag{2.10}$$

andthe inverse Fourier transform is defined as

$$f(t) = \sum_{\omega=0}^{N-1} F(\omega) exp[-i2\pi\omega t/N], \tag{2.11}$$

where $F(\omega)$ is the spectrum, $f(t)$ is the time series, ω is the frequency, N is total number of data, and i is the imaginary number. We used a FFT procedure provided in the IDL programming language. In this procedure, we first applied a Tukey window function to the original magnetic field data for each component with a time interval of 64 s (4096 data points) every 15 s. We then calculated the PSD given by the FFT in this time interval. Because we took spectral averages of four points in frequency domain, the final frequency resolution is 0.0156 Hz. This procedure is performed every 15 s.

2.2.2 Cross-spectrum and coherence

The PSD $P(\omega)$ is described by *Hino* [1977] as

$$P\left(\frac{\omega}{T}\right) = \frac{1}{T} E[X(\omega)X^*(\omega)], \tag{2.12}$$

where ω is the frequency, T is the time segment, $X(\omega)$ and $X^*(\omega)$ are the product of the conjugate vectors, and E denotes the ensemble average.

The cross-spectrum function $S_{xy}(\omega)$ is expressed as

$$S_{xy}(\omega) = \frac{2\pi}{T} E[X^*(\omega)Y(\omega)]. \tag{2.13}$$

The term $2\pi/T$ is multiplied to express $S_{xy}(\omega)$ in units of PSD.

To examine whether Pc1 waves observed in different observations have the same ionospheric source region, we calculated the coherence $C_{xy}(\omega)$ of Pc1 waveforms with the same time window of PSD. This is described in *Hino* [1977] as

$$C_{xy}(\omega)^2 = \frac{\left|S_{xy}(\omega)\right|^2}{S_{xx}(\omega)S_{yy}(\omega)}, \tag{2.14}$$

where $S_{xx}(\omega)$ and $S_{yy}(\omega)$ are the PSDs for time series $x(t)$ and $y(t)$, respectively, and $S_{xy}(\omega)$ is the cross-spectrum density. If the coherence of the Pc1 waveforms between two stations is close to one, then these signals are identical, indicating that they come from the same source. If there is no relation between the two signals, the coherence is close to zero, indicating different sources. We calculated four pairs of the Pc1 waveform coherence between stations: coherence between $\mathrm{H}_{Station1}$ and $\mathrm{H}_{Station2}$, coherence between $\mathrm{H}_{Station1}$ and $\mathrm{D}_{Station2}$, coherence between $\mathrm{D}_{Station1}$ and $\mathrm{H}_{Station2}$, and coherence between $\mathrm{D}_{Station1}$ and $\mathrm{D}_{Station2}$. We considered the highest coherence of these four pairs as the representative coherence between the two stations.

2.2.3 Polarization

To investigate the polarization characteristics of Pc1 pulsations, we use the method of polarization analysis described by *Fowler et al.* [1967]. This analysis is more useful in investigating the frequency dependence of Pc1 pulsations, because ordinary hodogram analysis can only provide an average value within a certain frequency range. This analysis provides polarization parameters such as ratio, angle, and sense between the H and D components of the magnetic field variations. The polarization ratio R between the totally polarized and non-polarized signals is

$$R = \sqrt{1 - \frac{4|J|}{(P_{xx} + P_{yy})^2}}, \tag{2.15}$$

where the coherency matrix $|J|$ is written as

$$J = \begin{pmatrix} P_{xx} & P_{xy} \\ P_{yx} & P_{yy} \end{pmatrix}, \tag{2.16}$$

where P_{xx} and P_{yy} are the PSDs for the H and D components of the magnetic field variations, respectively, and P_{xy} and P_{yx} are the cross-spectra of the two signals. This ratio varies from 0 to 1.

The polarization angle θ, which is the major axis angle between the H and D components of the magnetic field variations, is defined as

$$tan(2\theta) = \frac{-2RePxy}{P_{xx} - P_{yy}}. \tag{2.17}$$

The polarization angle is defined to be positive as measured westward from magnetic north. Finally, the polarization sense ϵ is expressed as

$$sin2\epsilon = \frac{2ImP_{xy}}{P_{xx} + P_{yy}}. \tag{2.18}$$

ϵ is negative (positive) for left-handed (right-handed) polarity of the two signals.

2.2.4 Band-pass filter

The band-pass filter allows only certain frequencies of a signal to go through, while removing those outside the predetermined parameters. This becomes useful to extract a certain target frequency range from the original signal. The band-pass filter in the frequency domain is expressed as:

$$F_{filtered}(f) = F_{original}(f) \cdot F_{filter}(f) \tag{2.19}$$

There are several band-pass filters that can be used for spectral analyses. In this thesis, we used a multiplied high-and low-pass (MHL) filter, designed by combining low- and high-pass filters. This filter gives us a flat frequency response within a selected frequency range. The functions of Low- and high-pass filter are defined as,

$$F_{Low-pass}(f) = \frac{1}{1 + \left[f/f_{low}\right]^S} \tag{2.20}$$

$$F_{High-pass}(f) = \frac{1}{1 + \left[f/f_{high}\right]^S} \tag{2.21}$$

where f_{low} and f_{high} are the lower and higher cutoff frequencies, respectively, and S is the order of the filter ($S = 20$ in this thesis). The function of MLH filter ($F_{MHL}(f)$) is expressed

by,

$$F_{MHL}(f) = F_{Low-pass}(f) \cdot F_{High-pass}(f) \tag{2.22}$$

Figure 2.7 shows the gain response curve of the MHL band-pass filter function in the frequency domain. As shown in Figure 2.7, we see a flat curve between the high and low cutoff frequencies, as well as that the half of the gain is well within the applied cutoff frequencies.

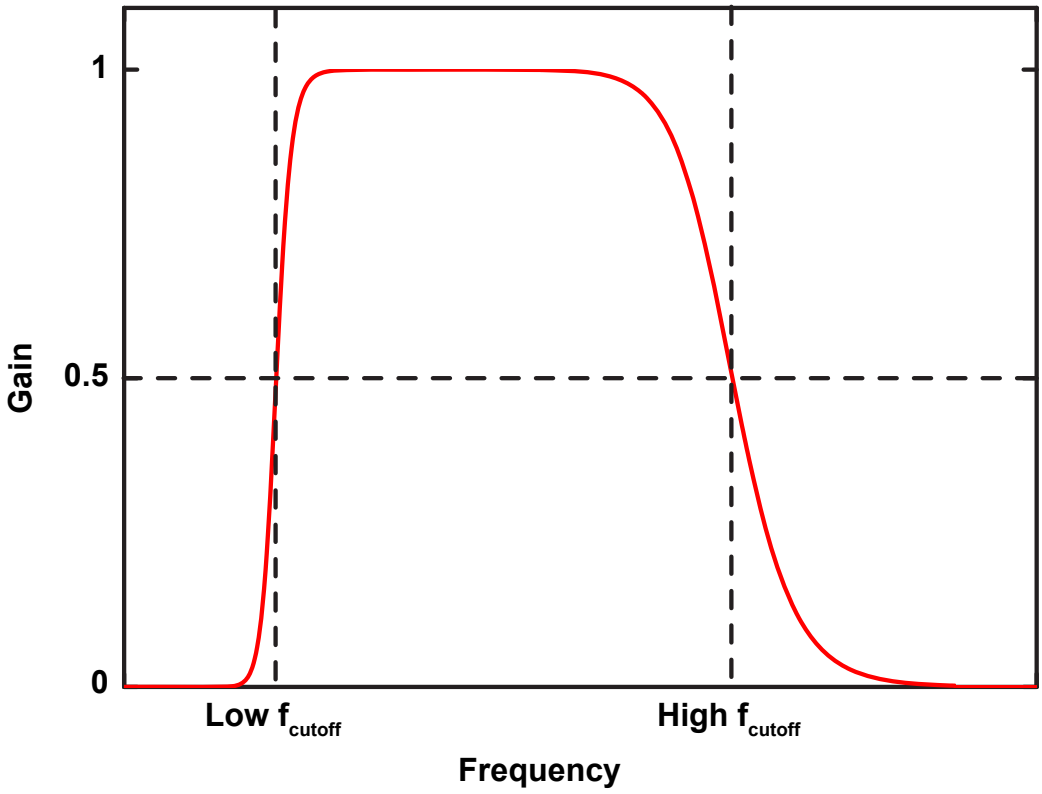

Figure 2.7 Gain curve for the MHL band-pass filter (red) as a function of frequency. The horizontal dashed line indicates the half of the gain. The vertical dashed lines indicate the required cutoff frequencies (left: low frequency, right: high frequency).

We also checked the phase difference between original and filtered signal, using artificial sinusoidal waves from 0.1 to 10 Hz. Figure 2.8 shows the result of the phase difference between original and filtered signal for the MHL filter. This filter has no phase difference between the original and the filtered signal for all the frequency ranges.

To determine the suitability of this filter for our study, we applied the MHL filter to the magnetic field data. Figure 2.9 shows the waveform of the original magnetic field data and the signal after applying the MHL filter for a case at ATH at 14:16:00-14:17:00 UT on February 16, 2013. We set up the frequency range of the band-pass filter from 0.3 to 0.8 Hz in this particular case. The original signal (upper panel in Figure 2.9) shows the oscillations

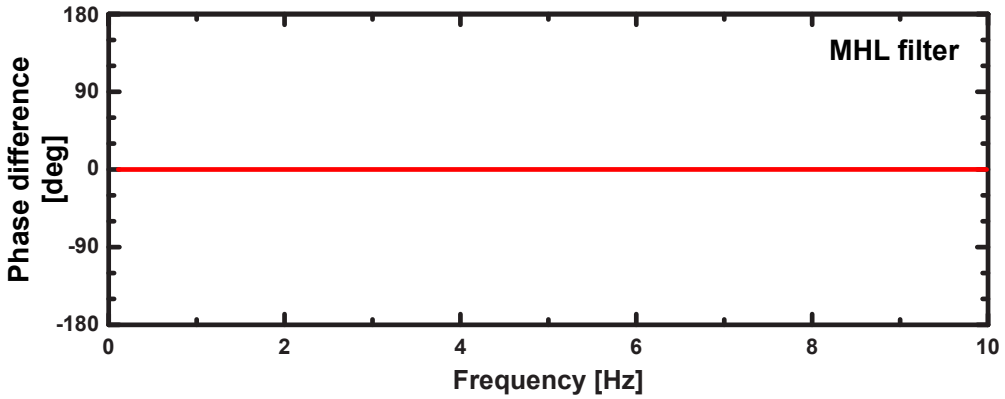

Figure 2.8 Phase difference between the original signal and filtered signal for the MHL filter with a red solid line.

of the magnetic field, as well as high frequency noises. In this case, it is difficult to define the repetition period of the waveforms which is why we applied the MHL filter in this signal as shown in the bottom panel in Figure 2.9. The filtered waveforms show clear oscillations of the magnetic field in this time interval. Therefore, the MHL filter is suitable to investigate the Pc1 waveform while removing the high-frequency noise.

2.2.5 Cross correlation

Cross-correlation analysis is useful for investigating the time delay between two signals. After calculating the cross-correlation between the two signals, the maximum coefficient time indicates the timing when the two signals are best aligned. A positive (negative) coefficient is indicates in-phase (out of phase) correlation between the two signals. The cross-correlation $r_{xy}(\Delta t)$ between the two time series x and y is described as,

$$r_{xy}(\Delta t) = \frac{\sum_{k=0}^{N-1} \left(x_k - \bar{x}\right)\left(y_{k+\Delta t} - \bar{y}\right)}{\sqrt{\left[\sum_{k=0}^{N-1} \left(x_k - \bar{x}\right)^2\right]\left[\sum_{k=0}^{N-1} \left(y_{k+\Delta t} - \bar{y}\right)^2\right]}} \tag{2.23}$$

where t is the time lag, N is the total number of data, and $\bar{x}$ and $\bar{y}$ are the averages of the two signals, respectively. In this thesis, we calculated the cross-correlation coefficient of the upper envelope of Pc1 waves to quantify the similarity of Pc1 pearl structures between two stations. For this calculation, we applied the maximum propagation time delay between two stations considering the minimum ionospheric duct propagation speed. Previous studies

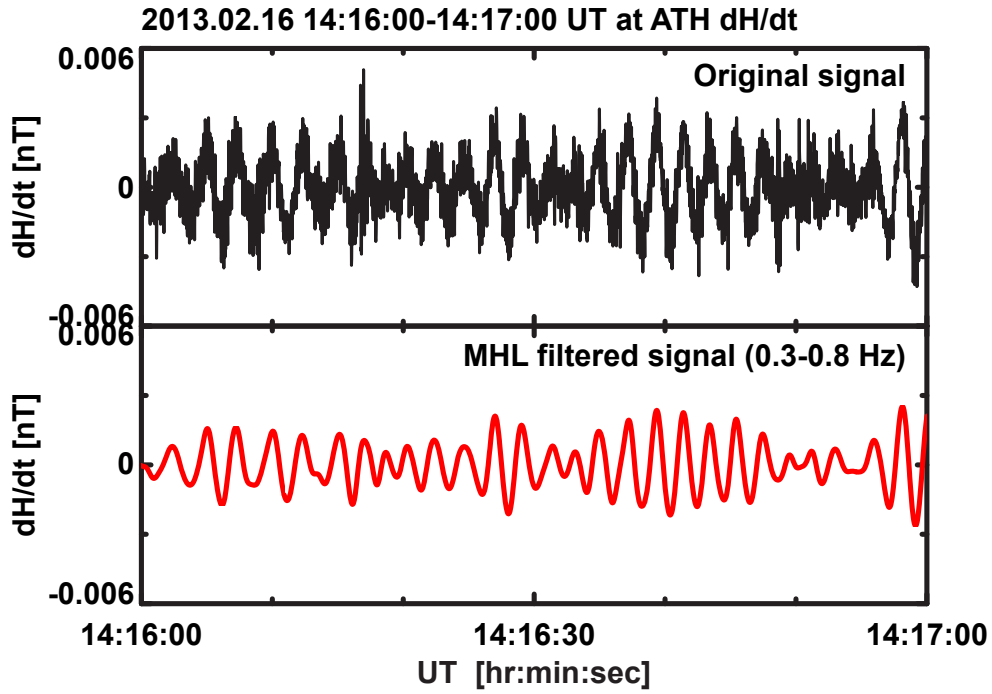

Figure 2.9 H-component Pc1 waveforms in the magnetic field variation observed at ATH at 1416:50-1417:40 UT on February 16, 2013. The black solid curve indicates the original signal. The red solid curve denotes the filtered signals applied a MLH band-pass filters.

[*Greifinger and Greifinger*, 1968; *Manchester*, 1970; *Fraser*, 1975a; *Lysak*, 2004; *Kim et al.*, 2010] have suggested that the Alfvén speed of Pc1 pulsations in the ionosphere should be between 89 to 2,000 km/s depending on ionospheric conditions. So, in this study, we chose a maximum propagation time delay of ±59.7 s at the longitudinally separated stations (ATH and MGD), and ±21.1 s at the latitudinally separated stations (MGD and MOS) using the lowest propagation speed in the ionosphere (89 km/s).

2.2.6 Physical meaning of parameters

Figure 2.10 shows a schematic of physical meanings of the coherence of Pc1 waveforms, the cross-correlation of the upper envelopes of Pc1 amplitudes and the standard deviation of Pc1 polarization angles. To examine if Pc1 waves observed at different observation points propagated from the same ionospheric source region, we calculated the coherence of Pc1 waveforms $C(\omega)$ with same time window of PSD using their waveforms, black solid curves shown in Figure 2.10a. More detailed calculation of $C(\omega)$ is written in Section 2.2.2. From all of these cases, we selected the best pair satisfying our criteria (given below) to define the frequency range.

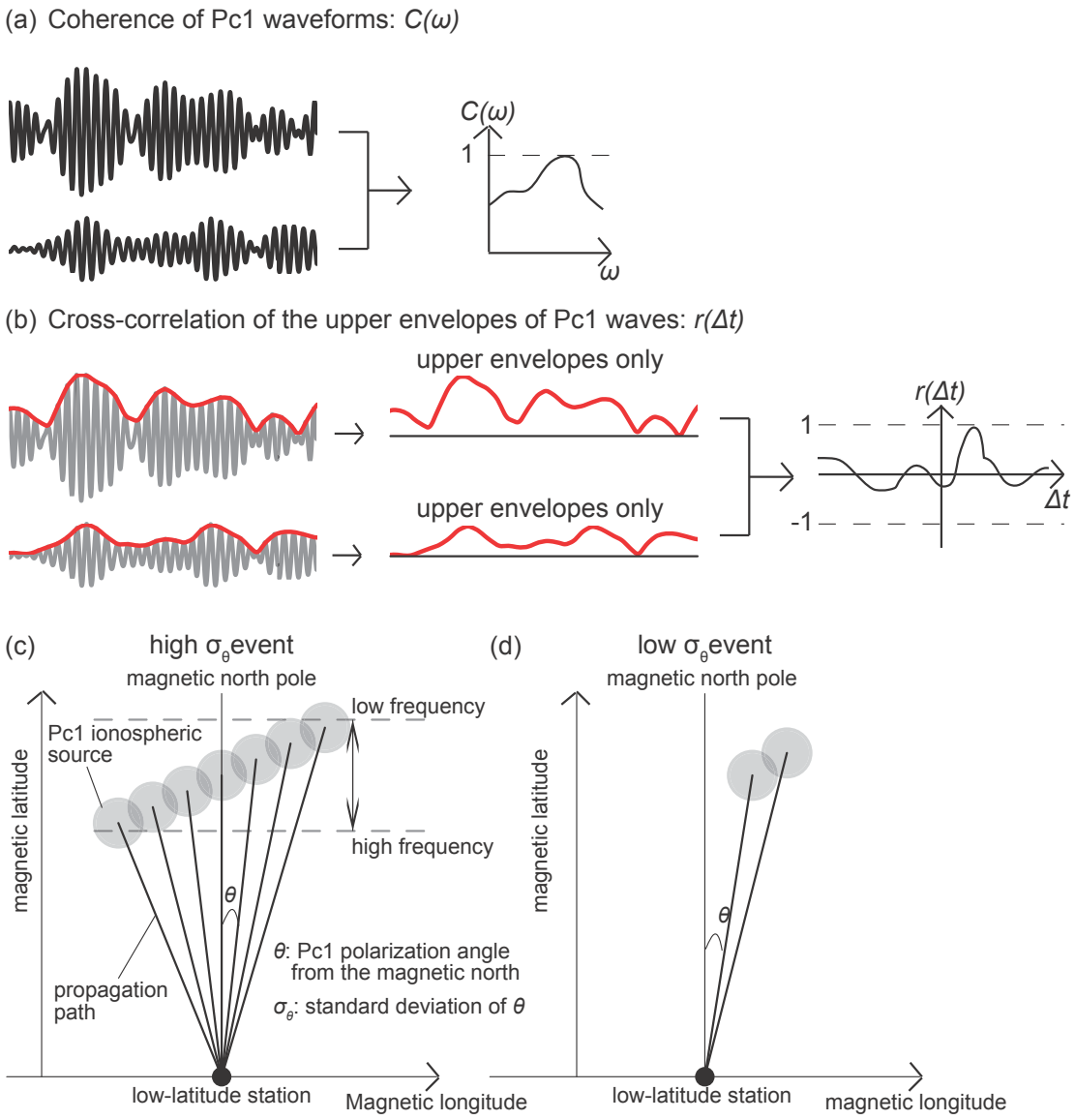

Figure 2.10 Schematic figures showing the meaning of (a) coherence of Pc1 waveforms $C(\omega)$, (b) cross-correlation of the upper envelopes of Pc1 waves $r(\theta t)$, and standard deviation of polarization angle σ_θ ((c): high σ_θ event, (d) low σ_θ event).

To define the similarity of Pc1 pearl structures between two different stations, we also calculated cross-correlation ($r(\Delta t)$) of the upper envelopes of Pc1 amplitudes, red solid curves shown in Figure 2.10b. For this calculation, in order to consider all possibility of propagation of Pc1 pulsations through the ionospheric duct from high to low latitudes, we applied the maximum propagation time delay between two stations based on the minimum ionospheric duct propagation speed. More detailed information for choosing the limitation of the time delay between two stations is written in Section 2.2.5.

To identify whether the ionospheric source extended over a range of longitudes, we also calculated the standard deviation of the polarization angle (σ_θ) for the high coherence Pc1 events only (Figures 2.10c and 2.10d). In each time window, we calculated the polarization angle (θ) as described by *Fowler et al.* [1997]. The angle (θ) is defined to be positive as measured westward from magnetic north. *Nomura et al.* [2011] found that the polarization angle has a dependence on Pc1 frequency. As Pc1 frequency is determined by local magnetic field intensity in the equatorial source region of the magnetosphere, an ionospheric source with a low (high) frequency of Pc1 pulsation would be located at higher (lower) latitudes. We assumed that a large (small) σ_θ would represent a spatially extended (localized) ionospheric source.

Chapter 3

Case studies and model calculation of Pc1 pearl structures

3.1 Introduction

In this chapter, we report two Pc1 pulsation events (case 1 and case 2) simultaneously observed at longitudinally and latitudinally separated ground stations to investigate generation mechanisms of Pc1 pearl structures. We used coherence analysis of waveforms to identify Pc1 pulsations coming from the same source region and observed simultaneously at the three stations. We then investigated the similarity of Pc1 pearl structures between two stations using cross-correlation analysis of the upper envelopes of the Pc1 pearl structures. In case 1, the Pc1 pearl structures are slightly different between stations, whereas in case 2, they are similar between all. Our model found that a spatially distributed ionospheric source can create different waveforms at different stations. This research is the first case study comparing the similarity of Pc1 pearl structures at very distant ground stations due to wave beating during ionospheric duct propagation. This research provides evidence of beating in the ionosphere as a possible generation mechanisms of Pc1 pearl structures. Note that the results of this chapter have been reported by *Jun et al.* [2014].

3.2 Observations

We present two Pc1 pulsation events to investigate Pc1 pearl structures using multi-point induction magnetometers deployed by the Institute for Space-Earth Environmental Research, Nagoya University, at Athabasca (ATH) in Canada, Magadan (MGD) in Russia, and Moshiri (MOS) in Japan. The distance between ATH and MGD is about 5,317 km, while MGD and

MOS are separated by about 1,880 km. We use data giving the H, D, and Z geomagnetic field components with a sampling rate of 64 Hz and a GPS clock accuracy of about 1 μs. The magnetometer sensors have nearly identical sensitivities and provide phase differences for H, D, and Z components in the Pc1 frequency range (0.2 to 5.0 Hz). Magnetometer data, originally in volts, were converted to physical units (nT) by considering the frequency-dependent sensitivity of the system. The sensor sensitivity was measured by a 2 m calibration coil, as described in Section 2.1.2. Additional details of these induction magnetometers are given by *Shiokawa et al.* [2010].

3.3 Results

3.3.1 Case 1: April 8, 2010

Figure 3.1 shows the dynamic spectra of H and D components of the magnetic field variations, polarization angle, coherence between different stations, and cross-correlation of Pc1 amplitude envelopes (red lines in Figure 3.2) for a clear Pc1 geomagnetic pulsation event observed simultaneously at ATH, MGD, and MOS at 1000 to 1200 UT on April 8, 2010. We chose the cross-correlation between the ATH H component and the MGD D component, since they show the highest correlation between ATH and MGD. During this event, geomagnetic activity was slightly elevated (Kp = 1 to 2), with auroral electrojet (AE) indices of approximately 300 to 500 nT. The local time at ATH was 0000 to 0200 LT, and the local time at MGD and MOS was 0600 to 0800 LT. In Figures 3.1a-f, Pc1 pulsations can be clearly identified at the three stations at frequencies of 0.4 to 1.2 Hz. The intensity of power spectral density (PSD) at MOS is weaker than at the other two stations, probably because of attenuation due to ionospheric duct propagation to lower latitudes [e.g., *Kawamura et al.*, 1981]. We can see that the Pc1 pulsations are observed during three separated time intervals,1012-1033, 1041-1053, and 1055-1149 UT at all stations. At ATH, the first and second Pc1 bursts can be clearly seen in Figures 3.1a,b, but the third Pc1 burst is much weaker than the others. Pc1 pulsations are clearly identifiable at MGD and MOS for all three intervals.

The polarization angles at ATH, MGD, and MOS are shown in Figures 3.1g-i. For ATH (Figure 3.1g), it increased from approximately -50° (dark blue) to -20°(light blue) for 0.6 to 1 Hz. At MGD (Figure 3.1h), the polarization angle varies from approximately -90° (black) to -50° (dark blue) in the same frequency range as ATH. The frequency dependence at MOS (Figure 3.1i) shows a decrease of the polarization angle from approximately 30° (green) to -50° (dark blue). According to *Nomura et al.* [2011], this polarization angle dependence on

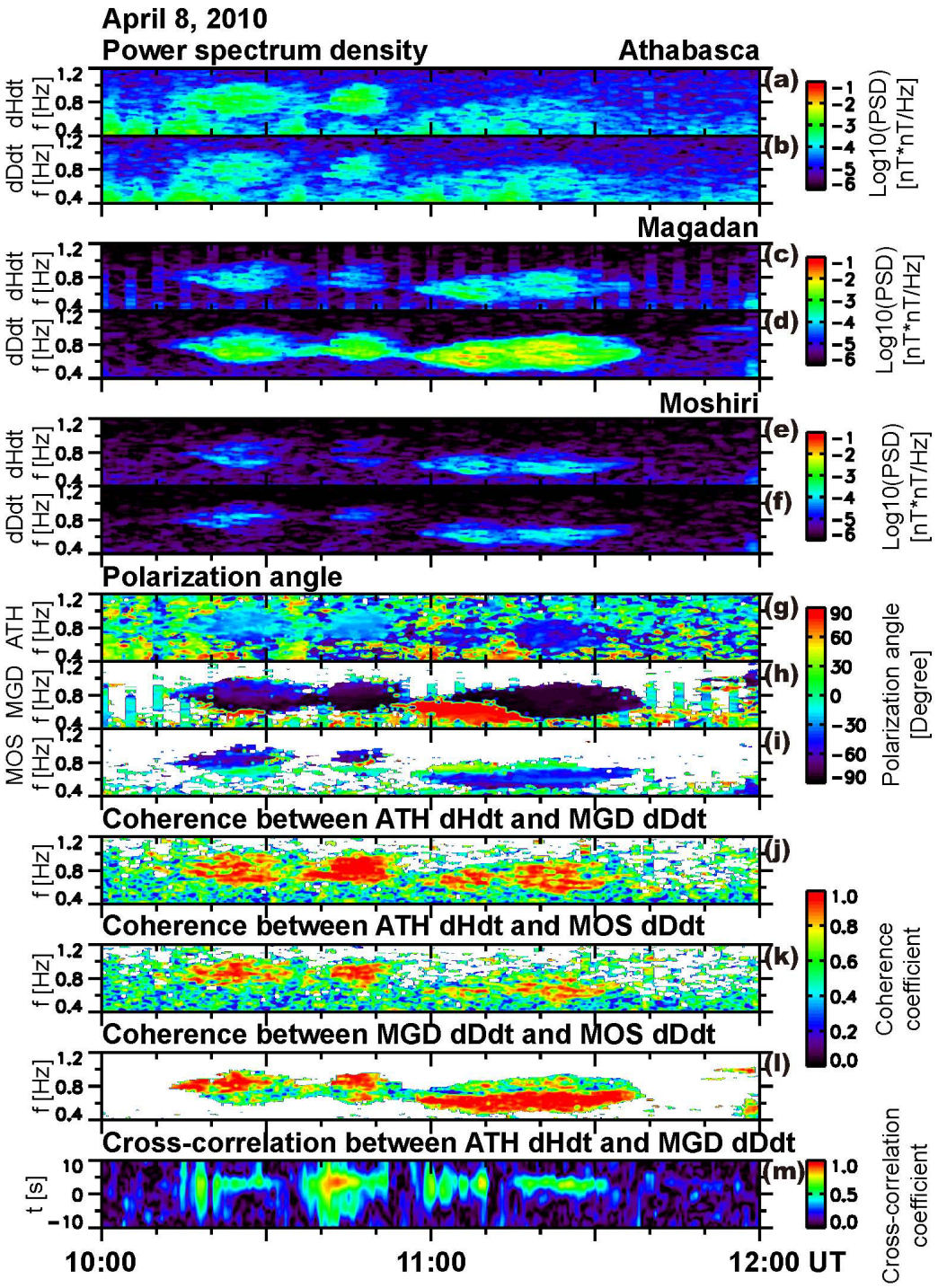

Figure 3.1 Spectral parameters of Pc1 pulsations in case 1.The figures show power spectrum densities of the (a) H and (b) D components of the magnetic field at ATH, (c) H and (d) D components at MGD, and (e) H and (f) D components at MOS; polarization angle at (g) ATH, (h) MGD, and(i) MOS; coherence between (j) ATH H and MGD D, (k) ATH H and MOS D, and (l) MGD D and MOS D components; and (m) cross-correlation of the upper envelopes of Pc1 pearl structures between ATH H and MGD D components observed at 1000 to 1200 UT on April 8, 2010 at frequencies of 0.4 to 1.2 Hz.

frequency indicates that the Pc1 pulsation observed at the three stations at 1000 to 1200 UT has a spatially distributed ionospheric source at high latitudes.

To distinguish whether the Pc1 pulsations propagated from the same ionospheric source, we show the coherence of Pc1 waveforms between each pair of stations in Figure 3.1j-l. High coherence of Pc1 waveforms was observed between two stations, indicating that the Pc1 pulsations observed at the three stations propagated from the same origin in the ionosphere.

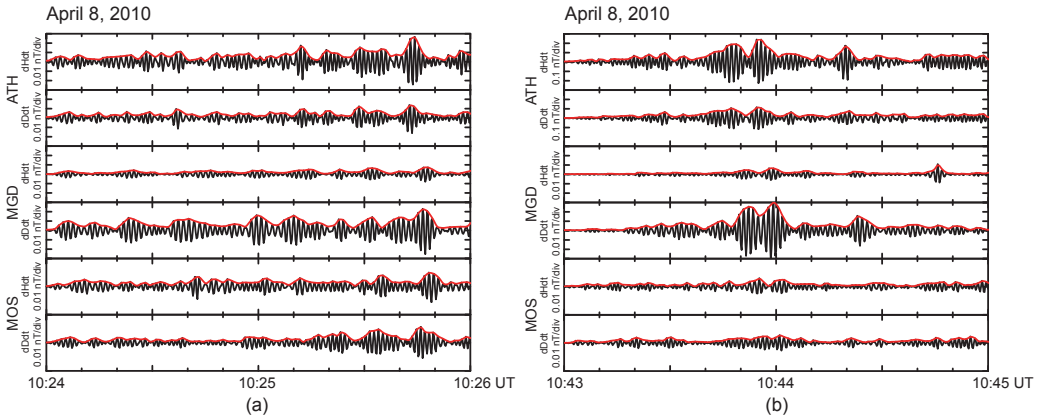

Figure 3.2 Time-series analysis of Pc1 pulsations in case 1.From top to bottom, the figures show band-pass filtered (0.5 to 1.2 Hz) Pc1 waveforms of the magnetic field of the H and D components observed at ATH, MGD, and MOS at (a) 1024-1026 and (b) 1043-1045 UT on April 8, 2010. Red solid lines indicate upper envelopes of Pc1 pearl structures.

Figure 3.2a,b shows the waveforms of the H and D components of Pc1 pulsations at ATH, MGD, and MOS on April 8, 2010, at 1024-1026 and 1043-1045 UT, respectively. To remove noise at other frequencies, we show the time series of Pc1 pulsations obtained using the MHL band-pass filter described in Section 2.2.4 at frequencies of 0.5 to 1.2 Hz. The amplitude modulation of the pulsations varies with a repetition period of approximately 10 s in both time intervals. The time difference between ATH and MGD (MGD and MOS) is approximately 4 s (0 s), which was confirmed by lag correlation studies (see below). The repetition periods of pearl structure changes in time during this event at all stations, and the structures observed at ATH, MGD, and MOS, are generally similar but differ in their details.

Figure 3.3 shows the PSD of the H and D components of magnetic field variations on April 8, 2010, at ATH and MGD, respectively, and the coherence of Pc1 waveforms between these two components at 1024:00-1026:08 (Figure 3.3a-c) and 1043:00-1045:08 UT (Figure 3.3d-f) with a resolution of 0.0078 Hz. Here, time intervals correspond to those shown in Figure 3.2a,b. In Figure 3.3a,b and Figure 3.3d,e, we can see a continuous high-PSD band at frequencies of 0.6-1.0 and 0.7-1.0 Hz, respectively. The coherence between the H

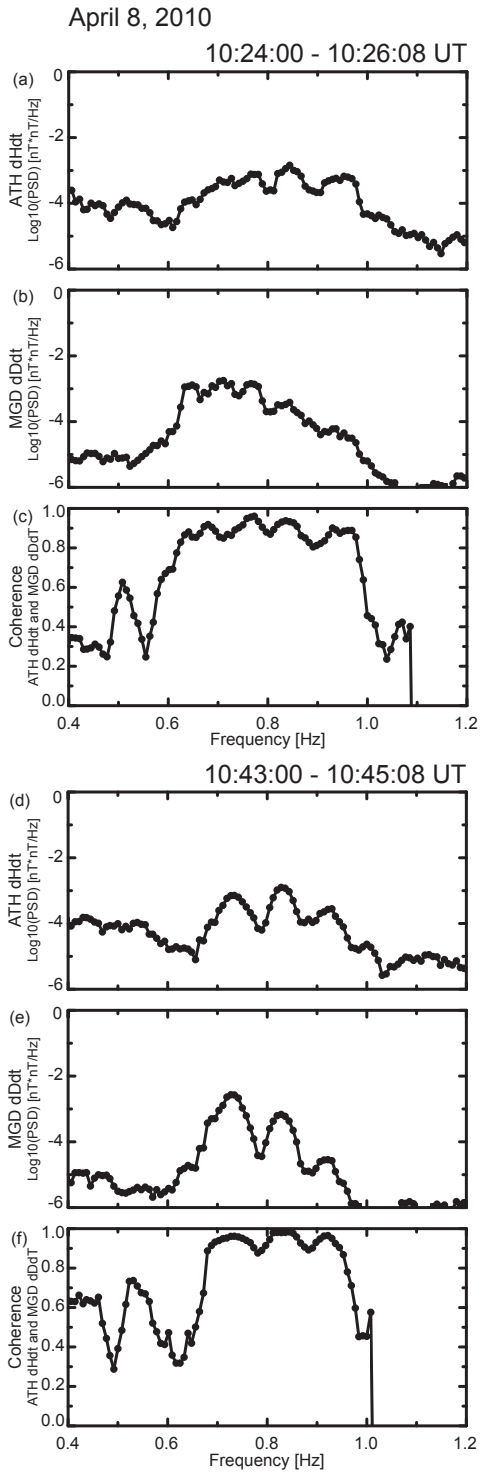

Figure 3.3 The PSD and coherence of Pc1 waveforms of the H and D components in case 1.The upper three panels show the power spectrum densities of (a) the H component of the magnetic field at ATH and (b) the D component of the magnetic field at MGD, as well as (c) coherence of Pc1 waveforms between the H component at ATH and the D component at MGD, as observed at 1024:00 to 102608 UT on April 8, 2010 at frequencies of 0.4 to 1.2 Hz. The lower three panels show the same quantities as observed at 1043:00 to 1045:08 UT on April 8, 2010.

component at ATH and the D component at MGD is close to one in the latter frequency range.

We investigated the cross-correlation between the H component at ATH and the D component at MGD using the upper envelope of Pc1 pearl structures in the time domain. We used only these components because they have the highest PSD intensity compared with the other components and the background intensity. Figure 3.4a,b shows the cross-correlation between the H component at ATH and D component at MGD obtained for the upper envelope of the Pc1 pearl structure at 1024:00-1026:08 and 1043:00-1045:08 UT, respectively, on April 8, 2010. In Figure 3.4a, we can see that the correlation is greater than 0.5 with a time difference of approximately 3 s. In contrast, in Figure 3.4b the cross-correlation between ATH and MGD is close to 0.9, indicating that the upper envelope of the Pc1 pearl structures is generally similar, with a time difference of approximately 3 s. In Figure 3.1m, the cross-correlation between the H component at ATH and the D component at MGD is greater than 0.5 throughout the event. For the second Pc1 burst in particular, the coherence and correlation are extremely high ($r > 0.8$). For the first and third Pc1 burst time intervals, however, the correlation decreases to 0.5, despite the waveform coherence being clearly close to one.

3.3.2 Case 2: April 11, 2010

Figure 3.5 shows the dynamic spectra of the H and D components of magnetic field variations, polarization angle, coherence between different stations, and cross-correlation of Pc1 amplitude envelopes (red lines in Figure 3.6) between the ATH H component and the MGD D component, for a clear Pc1 geomagnetic pulsation event observed simultaneously at ATH, MGD, and MOS at 1100 to 1300 UT on April 11, 2010. Geomagnetic activity was relatively high during this event, with Kp = 3 to 4. The average AE index during the 1100 to 1300 UT interval was approximately 104 nT. The local time at ATH was 0100-0300 and 0700-0900 LT at MGD and MOS. In Figure 3.5a-d, Pc1 pulsations were clearly identified at ATH and MGD at frequencies of 0.2 to 0.8 Hz. However, the Pc1 pulsations observed at MOS were much weaker than those seen at the other two stations (Figure 3.5e,f). At 1130 to 1220 UT at ATH, we can see three frequency bands of Pc1 pulsations at 0.38-0.48, 0.5-0.6, and 0.61-0.73 Hz. At MGD, the two frequency bands of Pc1 pulsations at 0.4-0.47 and 0.52-0.6 Hz can be seen in the D component of magnetic field variation (Figure 3.5d).

Figure 3.5g-i shows the polarization angles at ATH, MGD, and MOS. From 0.3 Hz to 0.7 Hz, the polarization angle at ATH (Figure 3.5g) is nearly constant, with values around 0° (light green). In Figure 3.5h, the polarization angle at MGD barely varies, and remains near −60° (dark blue) at frequencies of 0.3 to 0.6 Hz. The frequency dependence at MOS is not

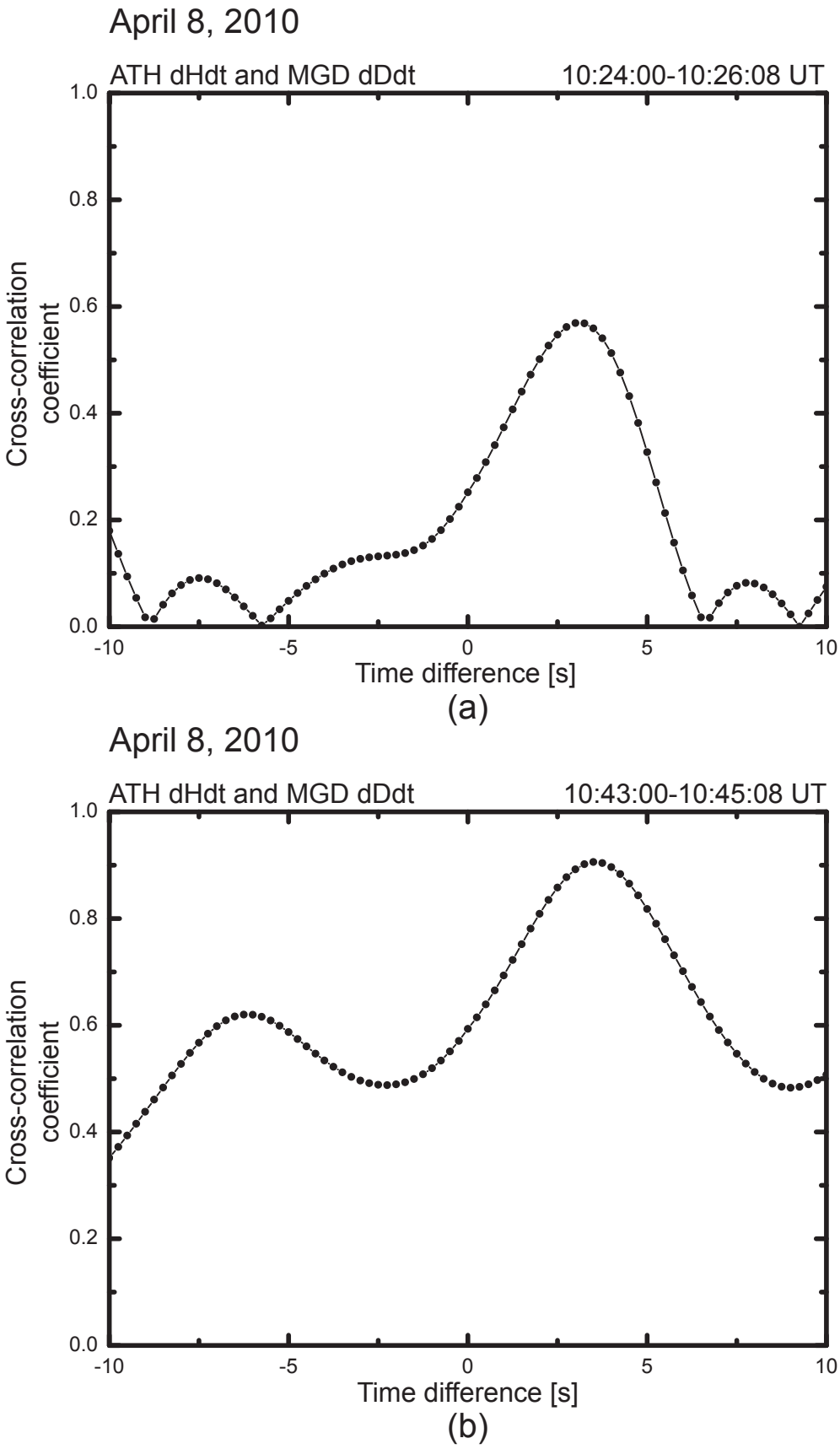

Figure 3.4 Cross-correlation analysis in case 1. Cross-correlation between the H component at ATH and the D component at MGD, obtained using the upper envelope of Pc1 pearl structures at (a) 1024:00-1026:08 and (b) 1043:00-1045:08 UT on April 8, 2010.

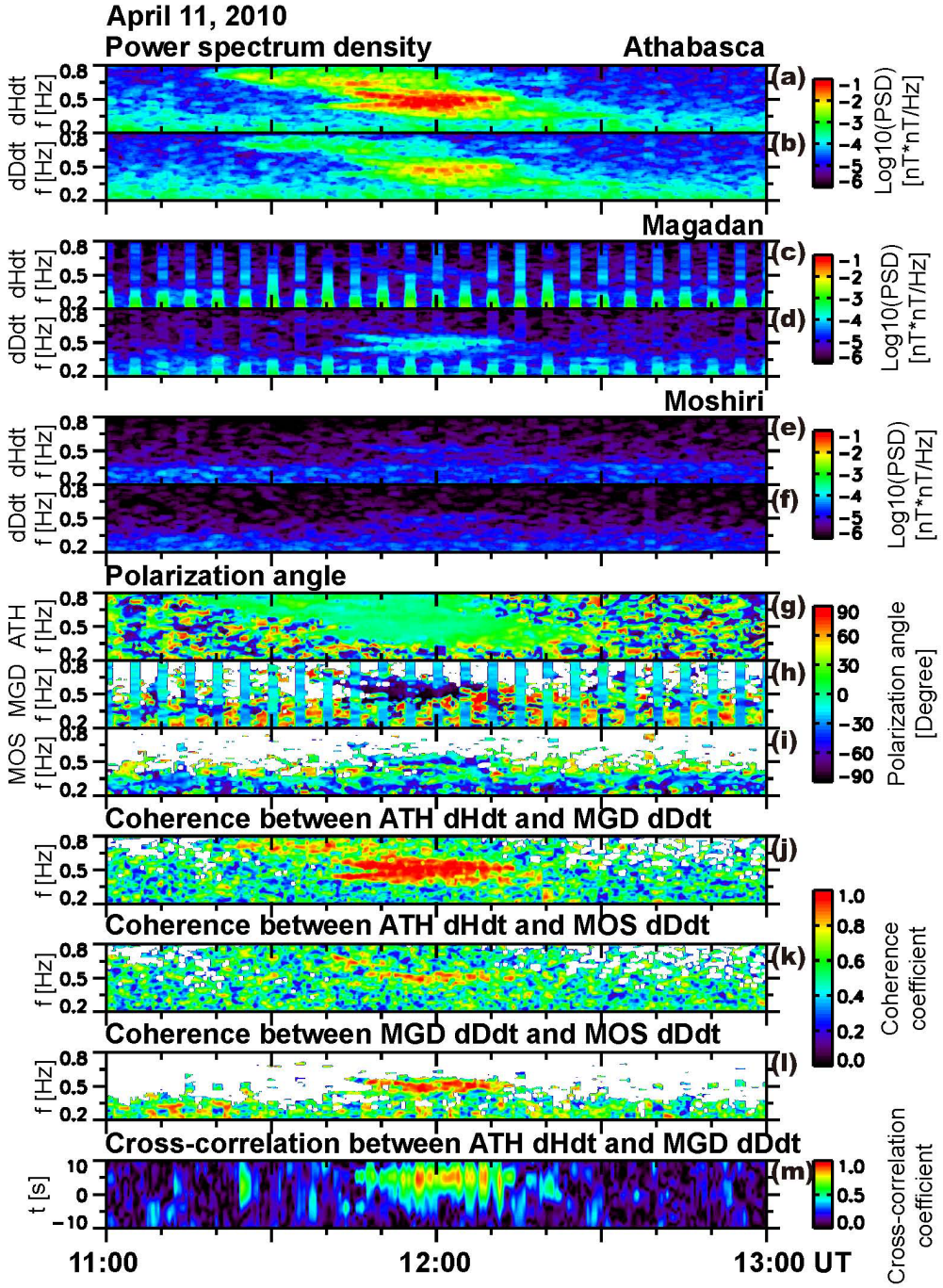

Figure 3.5 Spectral information of Pc1 pulsations in case 2. Power spectrum density of (a) H and (b) D components of magnetic field at ATH, (c) H and (d) D components of magnetic field at MGD, and (e) H and (f) D components of magnetic field at MOS; (g) polarization angle at ATH, (h) MGD, and (i) MOS; coherence between (j) ATH H and MGD D, (k) ATH H and MOS D, and (l) MGD D and MOS D components; (m) cross-correlation of the upper envelopes of Pc1 pearl structures between ATH H and MGD D components observed at 1100 to 1300 UT on April 11, 2010, for frequencies of 0.2 to 0.8 Hz. Vertical stripes seen approximately every 5 s in the PSD at MGD are due to artificial noise.

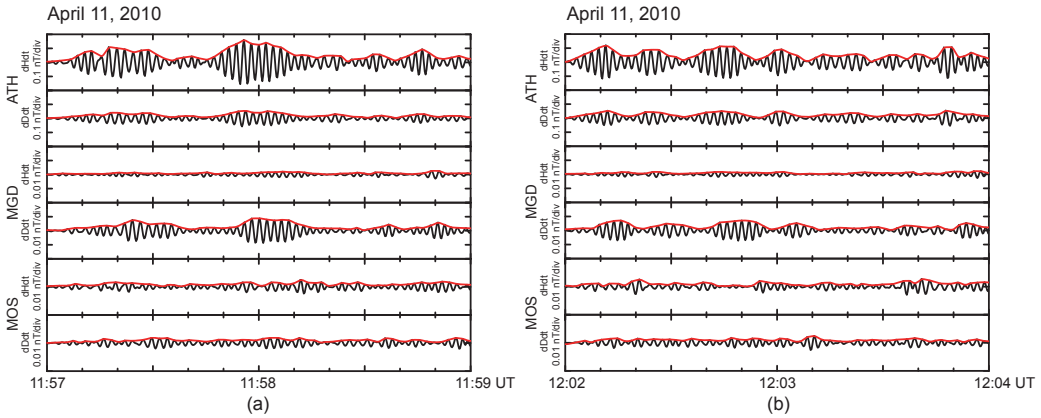

Figure 3.6 Time series analysis of Pc1 pulsations in case 2. From top to bottom, the figures show band-pass filtered (0.3 to 0.7 Hz) Pc1 waveforms of the magnetic field of H and D components observed at ATH, MGD, and MOS at (a) 1157-1159 and (b) 1202-1204 UT on April 11, 2010. Red solid lines indicate upper envelopes of Pc1 pearl structures.

clear, as seen in Figure 3.5i, because the intensity of the Pc1 pulsations is very weak. The constant polarization angle observed at ATH and MGD suggests, independent of frequency, that Pc1 pulsations have a localized ionospheric source at high latitudes [*Nomura et al.*, 2011].

To distinguish whether the observed Pc1 pulsations propagated from the same ionospheric source, we show the coherence of Pc1 waveforms between the different stations in Figure 3.5j-l. The coherence between two stations is close to one for all frequencies, though the Pc1 pulsation at MOS was weak for frequencies near 0.5 Hz. This indicates that the Pc1 pulsations observed at the three stations propagated from the same origin.

Figure 3.6a,b shows the waveforms of the H and D components of Pc1 pulsations observed at ATH, MGD, and MOS on April 11, 2010, at 1157-1159 and 1202-1204 UT, respectively. We show the time series of Pc1 pulsations obtained using a MHL band-pass filter from 0.3 to 0.7 Hz to remove noise at other frequencies. Even if the amplitude modulation of Pc1 pulsations at MOS was weak in both time intervals, we can clearly see Pc1 pearl structures at all three stations. The repetition periods of Pc1 pearl structures vary from 10 to 40 s. We also note that there is a time difference of a few seconds in the pearl structures between ATH and MGD. The Pc1 pearl structures observed at ATH and MGD are similar in the time series of magnetic field variation, even though these two stations are separated by a distance of approximately 5,000 km.

Figure 3.7 shows the PSD of the H and D component magnetic field variations at ATH and MGD, respectively, and the coherence between these two components at 1157:00 to 1159:08 (Figure 3.7a-c) and 1202:00 to 1204:08 UT (Figure 3.7d-f) on April 11, 2010, with

a frequency resolution of 0.0078 Hz. The time intervals in Figure 3.7a,b correspond to those in Figure 3.6a,b, respectively. In Figure 3.7a,b and Figure 3.7d,e, we can see a continuous high-PSD band at frequencies of 0.4 to 0.6 Hz in both time intervals. The coherence between the H component at ATH and the D component at MGD is close to one at frequencies of 0.4 to 0.6 Hz.

Figure 3.8a,b shows the cross-correlation between the upper envelopes of ATH H and MGD D components of Pc1 pearl structure at 1157:00-1159:08 and 1202:00-1204:08 UT, respectively, on April 11, 2010, in the same format as Figure 3.4. In Figure 3.8a,b, we can see that the correlation is greater than 0.8 with a time difference of approximately 4 s during both time intervals. As shown in Figure 3.5m, we performed this cross-correlation analysis of Pc1 envelopes for the whole time interval. The cross-correlation of Pc1 envelopes between the H component at ATH and the D component at MGD is greater than 0.8 throughout this Pc1 event, which also has high coherence ($r > 0.8$).

3.4 Discussion

Comparing the two case studies, we found that Pc1 pearl structures observed at widely separated ground stations can be generally similar. However, case 1 shows that detailed pearl structures are different in some time intervals, even if the coherence of Pc1 waveforms between the two stations is close to one. The polarization angle varied depending on frequency for case 1, suggesting a spatially distributed ionospheric source. On the other hand, case 2 shows that the coherence of Pc1 waveforms and cross-correlation of Pc1 envelopes can both be high ($r > 0.8$). In this second case, the polarization angle was nearly constant for frequencies from 0.4 to 0.6 Hz. Below, we discuss mechanisms that may have contributed to these differences.

3.4.1 Possible generation mechanisms of Pc1 pearl structures in the magnetosphere

One of the possible generation mechanisms is based on the bouncing wave packets (BWP model) [e.g., *Guglielmi et al.*, 1996; *Mursula et al.*, 1999]. This model explains Pc1 pearl structures as being caused by bouncing of Pc1 waves along the geomagnetic field line between the Northern and Southern Hemispheres. According to the BWP model, the repetition period of Pc1 pearl structures should be related to the length of the magnetic field line, as well as to the Alfvén velocity in the magnetosphere. According to this model, the expected repetition period of Pc1 pearl structures is several tens of seconds, depending on the radial

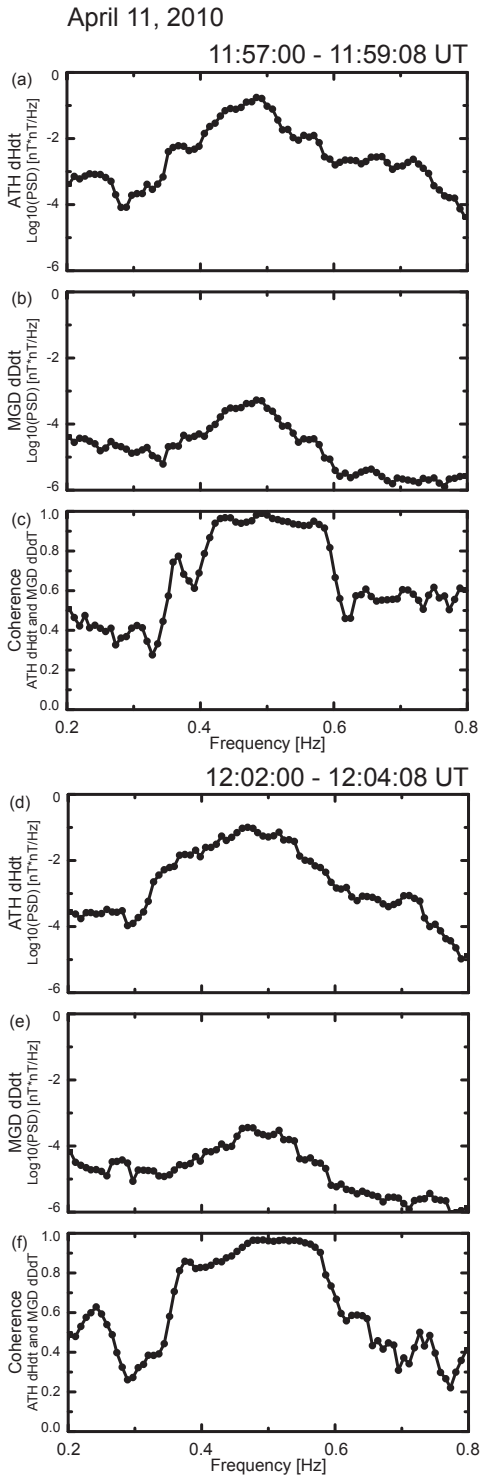

Figure 3.7 The PSD and coherence of Pc1 waveforms of the H and D components in case 2.The upper three panels show the power spectrum densities of (a) the H component of the magnetic field at ATH, (b) the D component of the magnetic field at MGD, and (c) coherence of Pc1 waveforms between the H component at ATH and the D component at MGD, observed at 1157:00 to 1159:08 UT on April 11, 2010, for frequencies of 0.2 to 0.8 Hz. The lower three panels (d-f) show the same quantities observed at 1202:00 to 1204:08 UT on April 11, 2010.

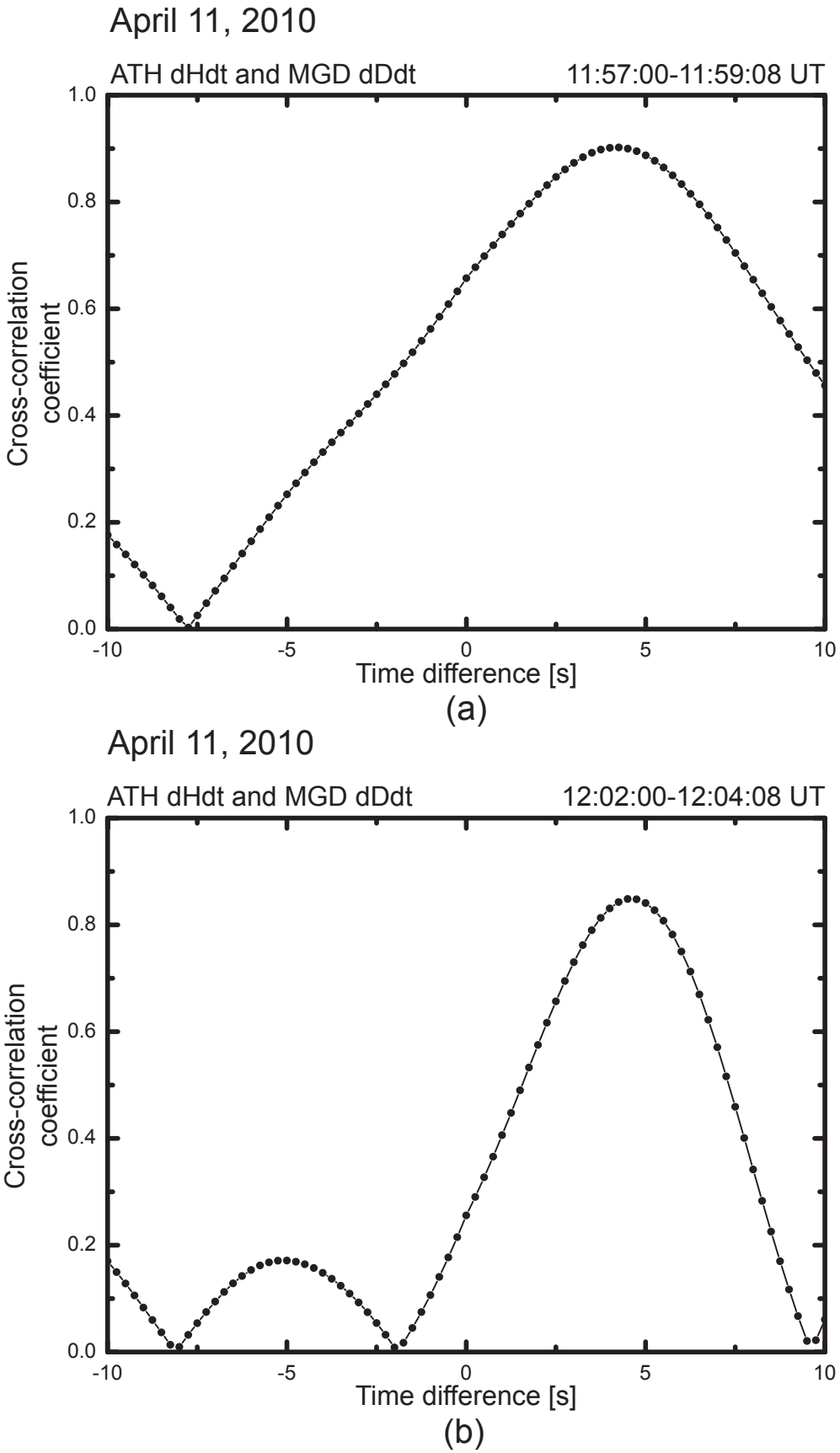

Figure 3.8 Cross-correlation analysis in case 2.Cross correlation between the H component at ATH and D component at MGD obtained for the upper envelope of Pc1 pearl structures at (a) 1157:00-1159:08 and (b) 1202:00-1204:08 UT on April 11, 2010.

distance of the generation region of electromagnetic ion cyclotron (EMIC) waves located near the magnetic equator. However, some studies have reconsidered the BWP model, because they found that observations did not match its predicted results. For example, the BWP model is based on comparison of ground and satellite data, yet *Perraut* [1982] found that the repetition period of Pc1 pearl structures seen at ground stations did not clearly match space-based observations. In addition, *Erlandson et al.* [1990] measured the Poynting flux of EMIC waves using the Viking satellite to investigate Pc1 pulsations near the plasmapause and found that the energy flux of Pc1 pearl structures was mainly downward, along magnetic field lines. Moreover, *Paulson et al.* [2014] measured the average wave power over 0.6 to 0.8 Hz Pc1 waves observed at the Hornsund station on the ground and the Van Allen Probes in space. They found that both repetition periods of an average wave power were approximately 130 s. They suggested that the similar repetition periods on the ground and in space contradict the BWP model, because if the BWP model is correct, the repetition period of average wave power in space would have to be half that observed on the ground. In Figures 3.2 and 3.6, the repetition period of Pc1 pearl structures at the three stations was approximately 10 s, which is much shorter than the expected repetition period from the BWP model.

Mursula et al. [2001] and *Mursula* [2007] attempted to explain Pc1 pearl structures as the result of modulation of EMIC waves by long-period ultra-long-frequency waves (such as Pc4 to Pc5 pulsations). The repetition periods of Pc1 pearl structures found in this study, approximately 10 s in case 1 and 10-40 s in case 2, are shorter than the period of Pc4 to Pc5 pulsations. Such generation mechanisms of Pc1 pearl structures in the magnetosphere do not explain the different wave structures at different stations that we observed, even in the case of Pc1 pulsations that propagated from the same source. If Pc1 waves with different frequencies are mixed in the magnetosphere, these waves should have similar waveforms, even if they are detected at different stations. As we observed in case 1, the detailed Pc1 pearl structures were slightly different at the three stations. In Figure 3.1m, the cross-correlation of Pc1 envelopes at ATH and MGD is less than 0.5 in the time interval of the first and third Pc1 bursts, although the coherence of Pc1 waveforms is close to one.

3.4.2 Comparison of observations and model calculations of Pc1 pearl structures

Some studies have considered that Pc1 pearl structures can be caused by beating in the ionosphere. This is a consequence of amplitude modulation of Pc1 waves caused by the superposition of waves at slightly different frequencies during their propagation through the ionospheric duct [*Pope*, 1964]. *Nomura et al.* [2011] found that some Pc1 events observed

at low latitudes have a polarization angle that is frequency dependent. This indicates that these Pc1 pulsations have a spatially distributed source region in the ionosphere that can cause beating in the ionosphere to create Pc1 pearl structures. In case 1, Figure 3.1g-i show that Pc1 pulsations at three stations can show variations in polarization angle depending on frequency, and thus we suggest that these waves have a spatially distributed source in the ionosphere. Figure 3.2a,b shows that the Pc1 pearl structures varied with a repetition period of 10 s, suggesting that these structures may also be caused by beating in the ionosphere. Moreover, their amplitude envelopes are slightly different at the three stations. In contrast, the polarization angle in case 2 does not show clear dependence on frequency (Figures 3.5g-i), indicating that these waves have a localized ionospheric source. Figure 3.6a,b shows that the Pc1 pearl structures at the three stations are similar, with a repetition period of approximately 10 s.

To understand the different features of Pc1 pearl structures between the two case studies, we performed two model calculations of Pc1 pearl structures under differing conditions, as shown in Figure 3.9. We generated simple sinusoidal waves at frequencies of 0.6 to 1.0 Hz, and assumed that they propagated through the ionospheric duct with an Alfvén velocity of 500 km/s, as estimated by *Fraser* [1975a]. We considered the time difference and polarization angle variation due to the relative location of these wave sources and the observation points. We did not consider the mode conversion effect or polarization sense of Pc1 waves during their propagation through the ionospheric duct. During duct propagation, we consider an attenuation effect that causes the amplitude of Pc1 waves to decrease by 25% per 1,000 km distance from the source region to each station. Subsequently, we checked the pearl structures under two conditions. First, model 1 assumes that Pc1 waves are generated in a north-south extended source region (orange line in Figure 3.9a) with frequencies that vary by latitude, from 0.6 (high latitude) to 1.0 Hz (low latitude). This would correspond to a pearl structure caused by beating during duct propagation in the ionosphere, from their source points to the observation points. Model 2 assumes that Pc1 waves with different frequencies are mixed at a point source in the ionosphere (orange point in Figure 3.9b), corresponding to pearl structures created in the magnetosphere.

Figures 3.9a-c and 3.9d-f show the results of models 1 and 2, respectively. For model 1, the source region is distributed from north to south with a length of 1,000 km. The waveforms of Pc1 waves in Figure 3.9b,c show that Pc1 pearl structures are slightly different at different stations, particularly for a station located at 90˚ (black dot in Figure 3.9a and black lines in Figure 3.9b,c), corresponding to a perpendicular direction from the source distribution. Additionally, the time difference between two stations with the same distance from the source region varies because of the changing angle between the stations from the south. In the case

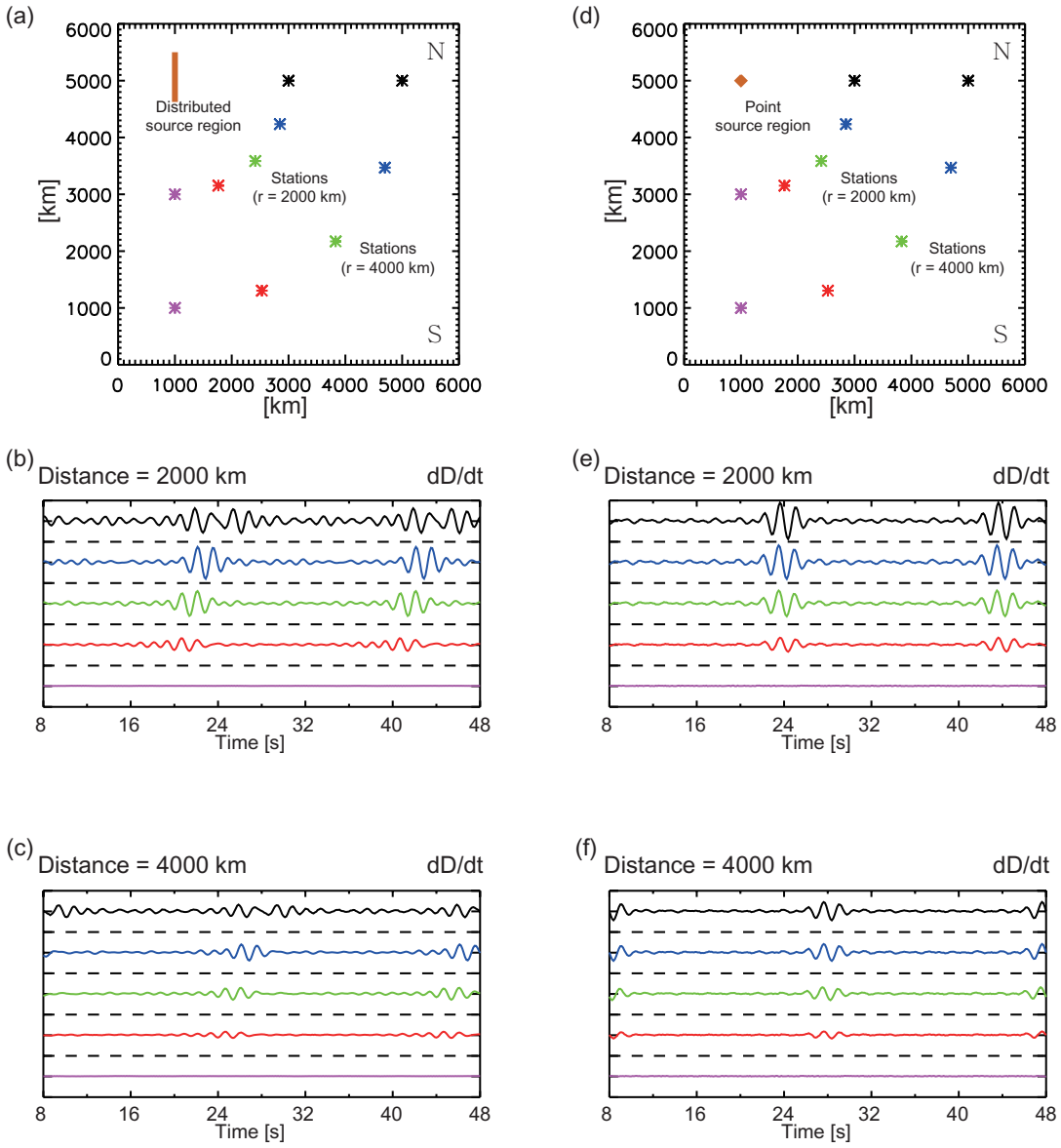

Figure 3.9 Simple model calculations for comparison between distributed and point sources. Location of stations and source region for(a) a distributed source region (model 1) and (d) a point source region (model 2). The D-component waveforms of the source waves with frequencies of 0.6 to 1.0 Hz and distances from the source region to stations of (b) 2,000 and (c) 4,000 km for model 1 and (e) 2,000 and (f) 4,000 km for model 2. Colors indicate angles of stations from the south.

of model 2, as shown in Figure 3.9d-f, Pc1 waves coming from a point ionospheric source have identical waveforms at different stations. The time difference between two stations at the same distance from a source region is close to zero. If the Pc1 waves propagated from a spatially distributed source region in the ionosphere, the different Pc1 pearl structures would be observed at different stations due to beating processes in the ionosphere, even if the waves are coming from the same ionospheric source region. In Case 1 of our observations (Figure 3.2), we found that Pc1 pearl structures were slightly different in some time intervals, with high coherence of Pc1 waveforms. We also found that variation of the polarization angle at the three stations depended on frequency. In Case 2 in Figure 3.6, however, the Pc1 pearl structures were similar, and the polarization angle was independent of frequency. As shown in the model calculations of Pc1 waves, we suggest that the observed Case 1 could be caused by beating processes in the ionosphere, while the Pc1 pearl structures in Case 2 could be created by magnetospheric effects.

We cannot exclude the possible effects of dispersive propagation occurring with ducted Pc1 waves,which could also contribute to the formation of Pc1 pearl structures in the ionosphere. Because the group velocity of dispersive waves differs from the phase speed, it can cause modulation of the wave amplitude in a wave packet. The high-latitude transmission and reflection properties of the ionosphere in the Pc1 frequency range are related to the wavenumber ω and the wave vector κ [*Greifinger*, 1972]. As shown by model calculations by *Fujita* [1987, 1988], the group velocity of Pc1 pulsations as a function of frequency increases near the lower cutoff frequency. If the observed Pc1 waves have a broad bandwidth, the amplitude modulation of Pc1 waves could be caused by dispersive propagation through the ionospheric duct. From our observations, Pc1 pearl structures can have either different (Case 1) or similar (Case 2) shapes at different stations. The bandwidth of case 1 (approximately 0.5 Hz) was wider than that of Case 2 (approximately0.2 Hz), suggesting that dispersive propagation contributes more to the creation of Pc1 pearl structures in the first case. In this study, however, we cannot quantify the contribution of this effect to the creation of Pc1 pearl structures in the ionosphere.

3.5 Conclusions

From January 1, 2009, to December 31, 2011, we investigated pearl structures of Pc1 geomagnetic pulsations observed by induction magnetometers at three mid- to low-latitude ground stations (ATH, MGD, and MOS). We selected two Pc1 pulsation events observed simultaneously at the three stations, Case 1 on April 8, 2010, and Case 2 on April 11, 2010. The results of this study can be summarized as follows

1. In Case 1, even though the coherence of Pc1 waveforms was high at different stations, the Pc1 pearl structures were slightly different at different stations in some time intervals. The polarization angle varied depending on frequency, indicating that the Pc1 pulsations propagated from a spatially distributed ionospheric source.

2. In Case 2, the Pc1 pearl structures were similar at different stations and had high waveform coherence. The polarization angle was nearly constant, indicating that the source region of Pc1 pulsation was positioned in a localized region in the high-latitude ionosphere.

3. Pc1 pearl structures with a repetition period of around 10 s in Case 1 and 10-40 s in Case 2 were observed at the three stations. These periods were shorter than BWP model predictions.

4. From the model calculation of Pc1 pearl structures, the pearl structures propagating from an ionospheric point source should have identical waveforms at different stations. The pearl structures generated by beating in the ionosphere with a spatially distributed source can be different at different stations.

From these results, we suggest that beating processes in the ionosphere with a spatially distributed ionospheric source can cause pearl structures during ionospheric duct propagation from high to low latitudes, with long distances from the source to the observation stations. In Case 2, however, we cannot reliably interpret the Pc1 pearl structures with a constant polarization angle using the beating process in the ionosphere. Therefore, we cannot exclude the possibility that mechanisms in the magnetosphere also contribute to the generation of Pc1 pearl structures. To understand and quantify the contribution of beating in the ionosphere to the creation of Pc1 pearl structures, we will investigate their statistical characteristics in the next chapter.

Chapter 4

Statistical study of Pc1 pearl structures observed on the ground

4.1 Introduction

Despite many previous studies having investigated the formation of Pc1 pearl structures, no dominant mechanism for their generation has been found. This is the first statistical report on the similarity of Pc1 pearl structures simultaneously observed at multi-point ground-based induction magnetometers, covering a six-year period from 2008 to 2013, half of a solar cycle from minimum to maximum. We selected Pc1 events with high coherence of Pc1 waveforms (> 0.7), indicating that the Pc1 pulsations observed at different stations came from the same source region, and study temporal characteristics and dependences of Pc1 pearl structures at longitudinally and latitudinally separated ground stations. If magnetospheric effects are dominant in the creation of Pc1 pearl structures, these structures should not change their shape during ionospheric duct propagation. However, if ionospheric effects are dominant, the structures may have different shapes when they are observed at different ground stations. In this chapter, we report that even though they came from the same source, more than half of the events had low similarity ($r < 0.7$) of Pc1 pearl structures. We conclude that the ionospheric beating effect during duct propagation could be the dominant process in Pc1 pearl generation.

4.2 Observations

In this statistical analysis of Pc1 pearl structures in the ionosphere, we used longitudinally and latitudinally distributed induction magnetometers installed by the Institute for Space-

Earth Environmental Research, Nagoya University, at Athabasca (ATH, 54.7 ˚N, 246.7 ˚E, L=4.3) in Canada, Magadan (MGD, 60.1 ˚N, 150.7 ˚E, L=2.6) in Russia, and Moshiri (MOS, 44.4 ˚N, 142.3 ˚E, L=1.5) in Japan as used in Chapter 3. The stations are separated by 5,317 km for ATH and MGD and 1,880 km for MGD and MOS. We take into account the three components (H, D, and Z) of the geomagnetic field provided by all three magnetometers. The detail information and the method of calibration of the induction magnetometers are written in Section 2.1.2 and provided by *Shiokawa et al.* [2010]. In this study, we used the H and D geomagnetic components obtained by induction magnetometers. Power spectrum density (PSD) is calculated for each component every 15 s with a time window of 64 s (4096 data points). The final frequency resolution is 0.0156 Hz.

4.2.1 Event selection

For this statistical study, we selected Pc1 pulsations observed simultaneously at two stations during a 6-year period, from January 1, 2008, to December 31, 2013, at the longitudinally (ATH and MGD) and latitudinally (MGD and MOS) separated stations. To select Pc1 pulsations observed simultaneously at the two stations, we used four selection criteria. First, the Pc1 pulsations must have a wave power higher than 10^{-7} nT^2/Hz in the dynamic spectra by visual inspection, in order to distinguish Pc1 pulsations from the background noise. Second, we take into account only high-coherence (> 0.7) waveforms to consider Pc1 waves came from the same source region. Third, to identify clear characteristics of each Pc1 event, we used only the timing with the highest integrated Pc1 power at both stations (within the Pc1 frequency range). Then we used the averaged values of σ_θ, central frequency, bandwidth, auroral electrojet (AE) index, pearl similarity $r(\Delta t)$, and repetition period of Pc1 pearl structures within ± 2 min of the selected timing, in order to obtain a representative value of these parameters of each event.

Using these criteria, we selected 84 simultaneous Pc1 events at the longitudinally separated stations and 370 events at the latitudinally separated stations from the full 6-year dataset. More than 86% of the 84 events for ATH-MGD gave the highest cross correlation r with time differences Δt less than 20s, corresponding to a propagation velocity higher than 265 km/s. More than 94% of the 370 events for MGD-MOS gave the highest cross correlation r with time differences Δt less than 6s, corresponding to a propagation velocity higher than 313 km/s.

4.2.2 Example of event selection: October 7, 2013

We illustrate our event selection using an event observed on October 7, 2013, between 11 and 13 UT at ATH and MGD. The dynamic spectra for H and D magnetic field components, the polarization angle, as well as the integrated wave power within the Pc1 frequency range is shown in Figure 4.1 for ATH (Figures 4.1a- 4.1d) and MGD (Figures 4.1e- 4.1h). The local time was 3 to 5 LT at ATH and 20 to 22 LT at MGD. During this time interval, AE index varied from 49 to 171 nT, indicating a weak substorm interval. In this time interval, we can see well-defined Pc1 pulsations observed at both stations. In Figures 4.1a-b and 4.1e-f, several Pc1 pulsations are shown clearly at both stations within the frequency range of 0.4 to 1 Hz. Pc1 pulsations observed at ATH can be separated into four time intervals with different frequency ranges: 0.8 to 1 Hz at 1100-1117 UT, 0.8 to 1 Hz at 1130-1200 UT, 0.5 to 0.7 Hz at 1140-1150 UT and finally 0.5 to 0.7 Hz at 1200-1250 UT. For MGD, Pc1 pulsations are observed at 1200-1240 UT within a frequency range of 0.5 to 0.7 Hz. The first three Pc1 bursts can be clearly seen at ATH as shown in Figures 4.1a-b, but they are not simultaneously detected at MGD. As shown in Figure 4.1i, $C(\omega)$ between the H component magnetic field variations at ATH and the D component at MGD is close to 0 during these three time intervals. Thus, we exclude those intervals from our final event list.

From the above considerations, we focus on the Pc1 event observed simultaneously at both stations at 1200-1240 UT within frequency range of 0.5 to 0.7 Hz with high $C(\omega)$ ($>$ 0.7). In Figures 4.1c and 4.1g, the angles θ at ATH and MGD are shown, respectively. For ATH (Figure 4.1c), it suddenly changed from approximately -20° (bright blue) to $+20^\circ$ (green) at 1220 UT. For MGD (Figure 4.1g), the polarization angle was almost constant, with values around -60° (dark blue) with same frequency range as ATH at 1200-1240 UT. In this time interval, $C(\omega)$ between ATH dD and MGD dH (Figure 4.1i) is close to one, suggesting that the observed Pc1 pulsations at both stations came from the same source region.

To investigate the similarity of Pc1 pearl structures at the two stations and its dependence on wave properties (i.e., central frequency, bandwidth, and standard deviation of polarization angle), we selected the time with the highest integrated Pc1 power at both stations. Figure 4.2 shows the averaged PSD of ATH dH and MGD dD, the polarization angle at ATH and MGD, and the coherence of Pc1 waveforms between the two stations at 1219-1221 UT on October 7, 2013 (resolution of 0.0156 Hz). At ATH (Figure 4.2a), a continuous high-PSD band existed at frequencies of 0.5 to 0.75 Hz. At MGD (Figure 4.2b), however, we see a narrow low-PSD band at frequencies of 0.58 to 0.63 Hz above 10^{-7} nT^2/Hz shown by the vertical dashed lines. $C(\omega)$ between the two stations is close to one in the latter frequency range. We also see a slight dependence of polarization angle on frequency at the two stations. In Figures 4.2c and 4.2d, the polarization angle varied from -11.5° to -8.11° at ATH and from

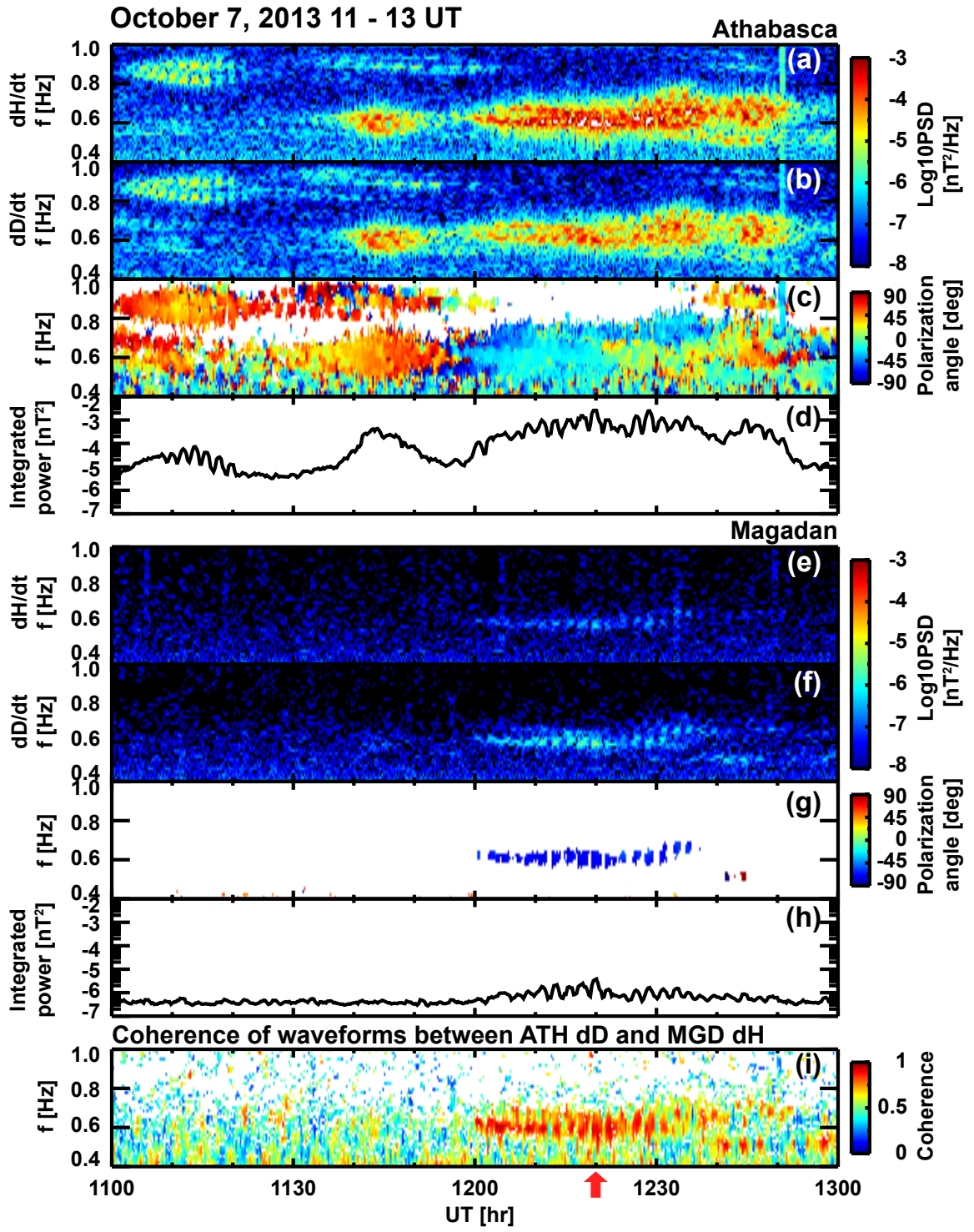

Figure 4.1 Dynamic spectrum densities of the (a) H and (b) D components of the magnetic field at ATH; (e) H and (f) D components of the magnetic field at MGD; (c) polarization angle at ATH, and (g) at MGD; (d) the integrated wave power at ATH and (h) at MGD; (i) coherence of waveforms between ATH D and MGD H observed for 1100-1300 UT on October 7, 2013, in a frequency range of 0.4-1 Hz. The vertical arrows indicate the times 1219-1221 UT for which the power PSD and the waveforms of the magnetic field are shown in Figures 4.3 and 4.4, respectively.

-62.8° to -75.8° at MGD in the frequency range of 0.58 to 0.63 Hz. Using these values, we calculated σ_θ in order to investigate the distribution of the ionospheric source regions. In this event, σ_θ at ATH and MGD are 1.77° and 16.89°, respectively.

To investigate the similarity of Pc1 pearl structures in the ionosphere, we calculated $r(\Delta t)$ between ATH and MGD. Figure 4.3 shows the waveforms of the H component of Pc1 pulsations at ATH and the D components at MGD on October 7, 2013, at 1218-1222 UT. To separate noise from the other frequencies, a band-pass filter is applied for frequencies between 0.55 and 0.63 Hz. This frequency range has the highest coherence of waveforms between the two stations. We see a clear modulation of Pc1 amplitudes, red solid curves in Figure 4.3a and 4.3b, with repetition periods of 25.3-44.7 s at ATH and 10.8-42.3 s at MGD. The average repetition periods at ATH and MGD are 34.6 s and 23.6 s, respectively. These modulations are the Pc1 pearl structures. In Figure 4.3c, the maximum cross-correlation coefficient between these envelopes is close to one ($r \sim 0.94$) with a time difference of approximately 4.3 s, indicating that ATH observed Pc1 amplitude modulations 4.3 s earlier than MGD.

4.3 Statistical analysis

Using 84 Pc1 events observed simultaneously at the longitudinally separated stations (ATH and MGD) and 370 events at the latitudinally separated stations (MGD and MOS), we investigated statistical characteristics of the Pc1 pearl structures in the ionosphere. In this section, we show the distribution of similarity of Pc1 pearl structures, temporal variations of Pc1 occurrence and similarity of Pc1 pearl structures, as well as their dependence on geomagnetic conditions and wave properties.

4.3.1 Distribution of similarity of Pc1 pearl structures

Figure 4.4 shows the distribution of the similarity of Pc1 pearl structures at the longitudinally (ATH and MGD) and latitudinally (MGD and MOS) separated stations. We found that pearl similarity r has peaks at ~ 0.2 at the longitudinally separated stations (ATH and MGD, Figure 4.4a), and at ~ 0.8 the latitudinally separated stations (MGD and MOS, Figure 4.4b). *Jun et al.,* [2014] reported that Pc1 pearl structures caused by beating processes in the ionosphere have slightly different shapes in model calculations of Pc1 pearl structures. Note that more than half of the events in both pairs (69 events at the longitudinally separated stations and 178 at the latitudinal stations) have similarities of less than 0.7. For the latitudinally separated stations, we detected simultaneous Pc1 events approximately four times more often

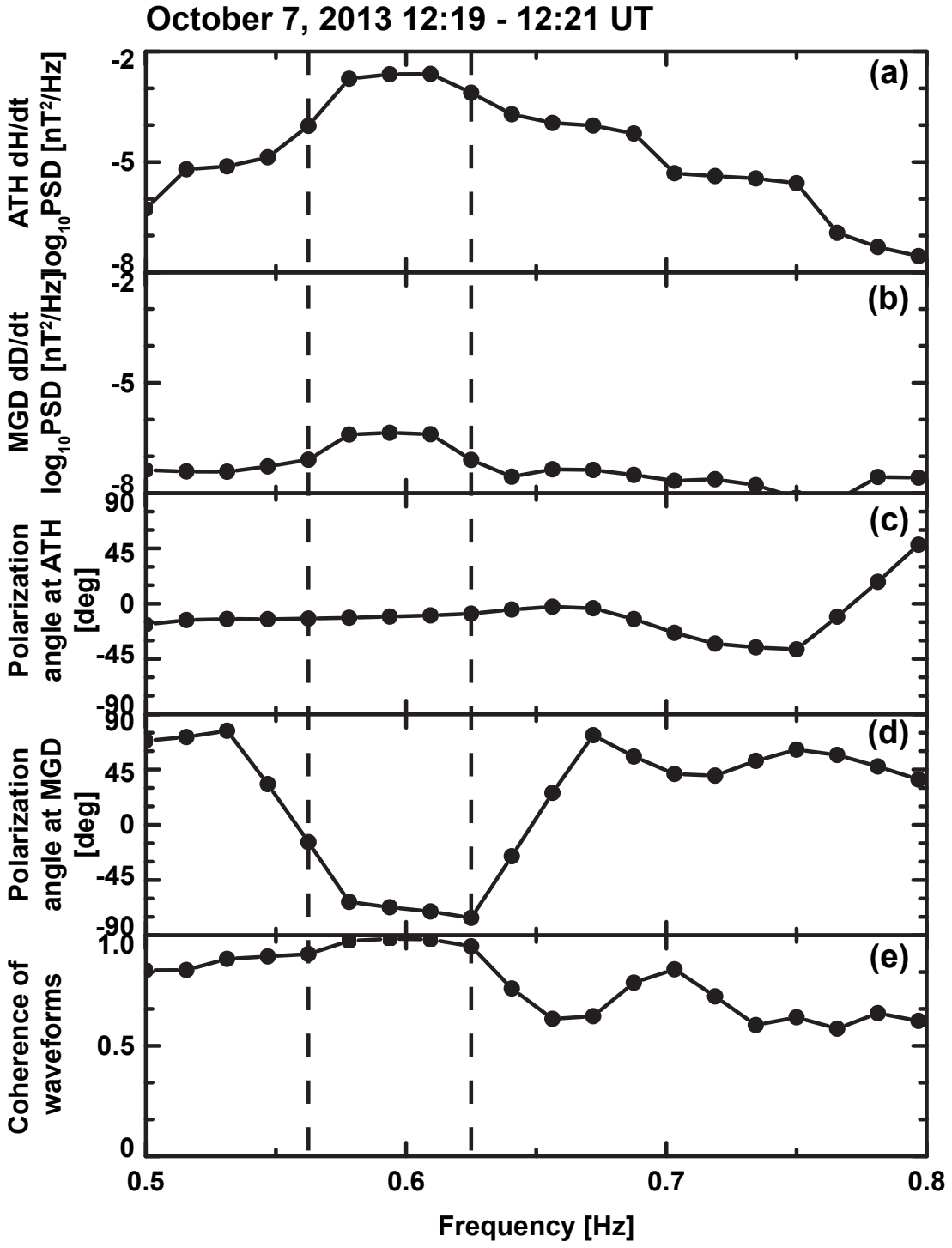

Figure 4.2 Power spectrum density of (a) the H component of the magnetic field at ATH and (b) the D component of the magnetic field at MGD, as well as (c) the coherence of Pc1 waveforms between the H component at ATH and D component at MGD, observed for 1219-1221 UT on October 7, 2013, in a frequency range of 0.5-0.8 Hz. The vertical dashed lines indicate the selected frequency range of 0.55 to 0.63 Hz, which satisfied our selection criteria.

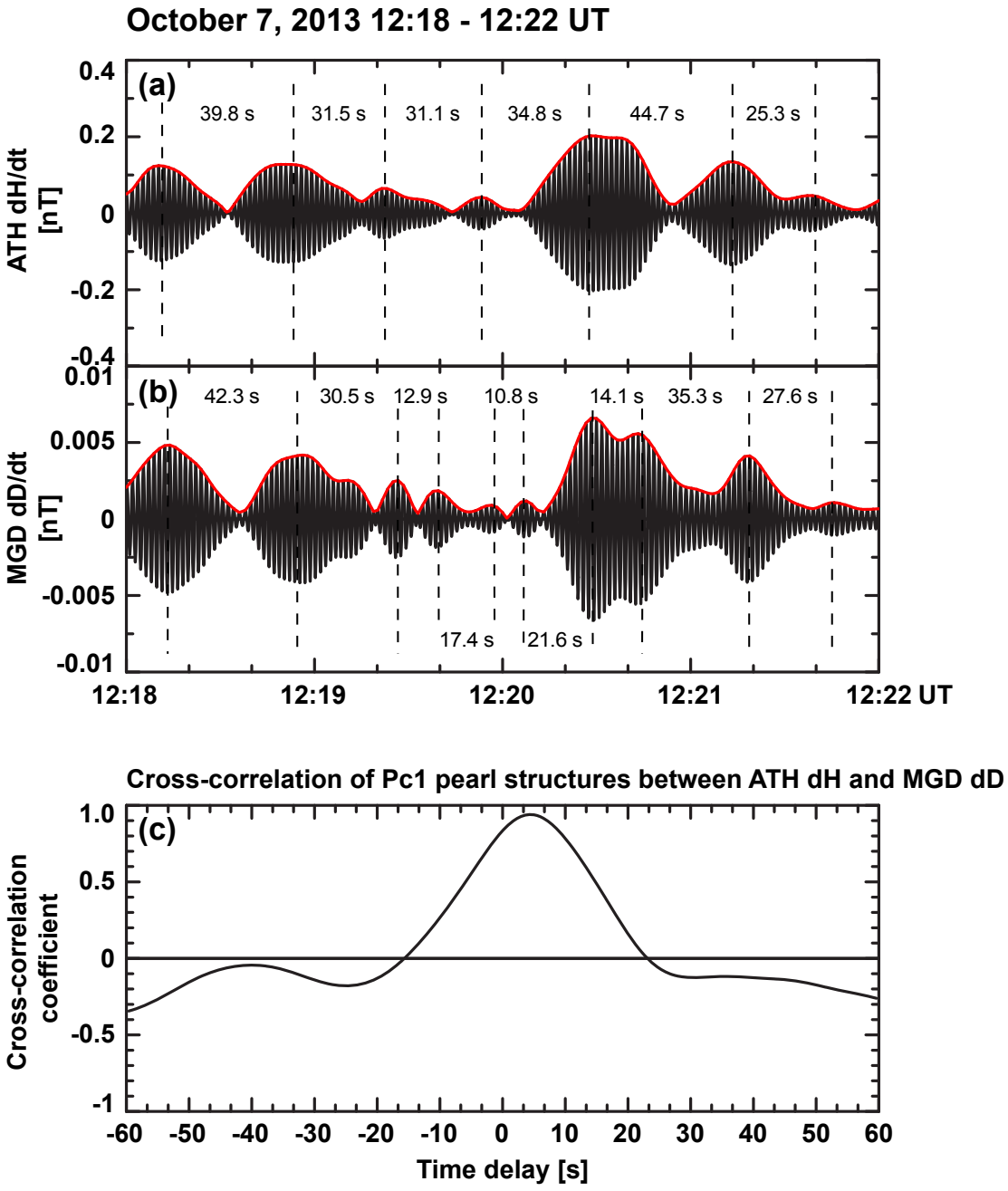

Figure 4.3 Band-pass filtered (0.55-0.63 Hz) Pc1 waveform of the magnetic field at (a) ATH (D component) and (b) MGD (H components) for 1218-1222 UT on April 8, 2010. Red solid lines indicate the upper envelope of the Pc1 pearl structures. (c) cross correlation between ATH D and MGD H components, obtained using the upper envelope of the Pc1 pearl structures

than at the longitudinally separated stations. This difference of Pc1 occurrence may be related to attenuation effects during ionospheric duct propagation [*Althouse and Davis*, 1978].

4.3.2 Temporal variations of similarity of Pc1 pearl structures in the ionosphere

Figure 4.5 shows the UT dependence of the occurrence of Pc1 pulsations observed at two stations and the similarity of Pc1 pearl structures in the ionosphere. The occurrence rate is calculated as the duration of the Pc1 event divided by the total observation time. In Figures 4.5a and 4.5d, Pc1 pulsations observed at ATH have a peak occurrence in the morning sector. On the other hand, for MGD and MOS the peak is in the daytime. The occurrence rates of Pc1 pulsations at ATH and MGD are consistent with previous statistical studies on the ground [e.g., *Fraser, 1968*; *Kawamura et al., 1981*; *Kuwashima et al., 1981*]. These studies suggest that the occurrence rate of Pc1 pulsations observed at high latitudes (low latitudes) has a maximum during the daytime and up to 1 hr after magnetic local noon (during the nighttime and up to 1 hr before sunrise) probably due to the ionospheric electron density profile in the F-region. However, the peak occurrence rate for MOS, located in the afternoon, differs from that found in previous studies.

Figure 4.5b shows that the occurrence rate of Pc1 pulsations observed simultaneously at the longitudinally separated stations has a clear peak around 15 UT, when ATH is on the dawn side and MGD is at midnight. For the latitudinally separated stations (Figure 4.5e), the peak of occurrence rate is located around 20 UT when both stations are on the dawn side. This result suggests that Pc1 pulsations can propagate with less attenuation to different stations in the nighttime because the plasma density in the F-region of the ionosphere is lower at these times. In Figure 4.5c, the similarity of Pc1 pearl structures at the longitudinally separated stations shows that high similarity events ($r > 0.7$) are concentrated between 6 and 15 UT when it is nighttime at both stations and, in particular, ATH is in the dawn sector and MGD in the midnight sector. However, in the case of latitudinally separated stations, as shown in Figure 4.5f, the similarity of Pc1 pearl structures is independent of UT.

Figure 4.6 shows the seasonal variations of the occurrence rate of Pc1 pulsations and the similarity of Pc1 pearl structures for the longitudinally and latitudinally separated stations. In both cases, we see that the highest occurrence rate of Pc1 pulsations at ATH, MGD, and MOS takes place near the equinoxes (peaks of occurrence in March and October), as shown in Figures 4.6a and 4.6b. The seasonal variations of Pc1 occurrence observed simultaneously at both stations are similar to those at each station. This result is consistent with those at

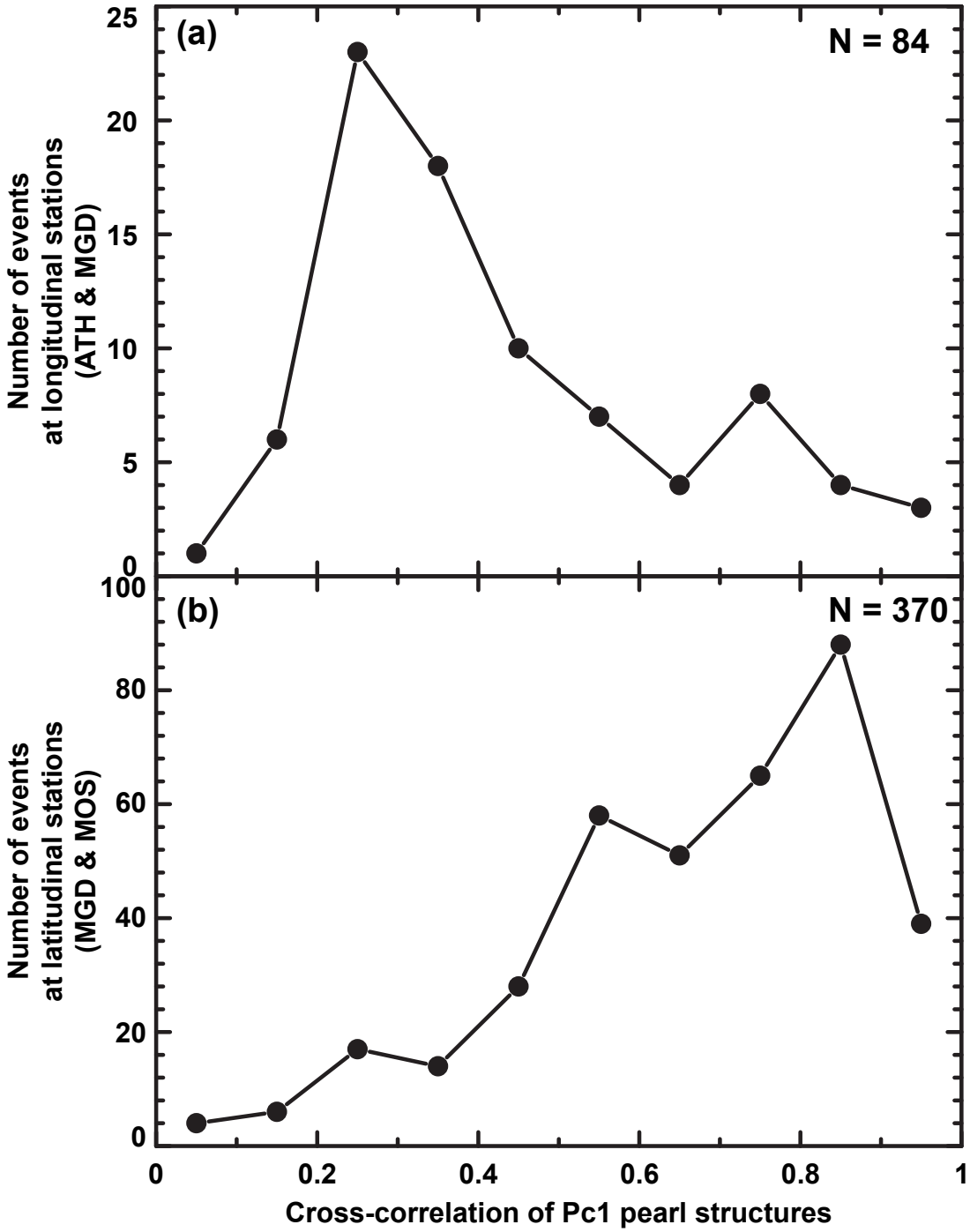

Figure 4.4 Distribution of similarity of Pc1 pearl structures observed at (a) longitudinally (ATH and MGD) and (b) latitudinally (MGD and MOS) separated stations.

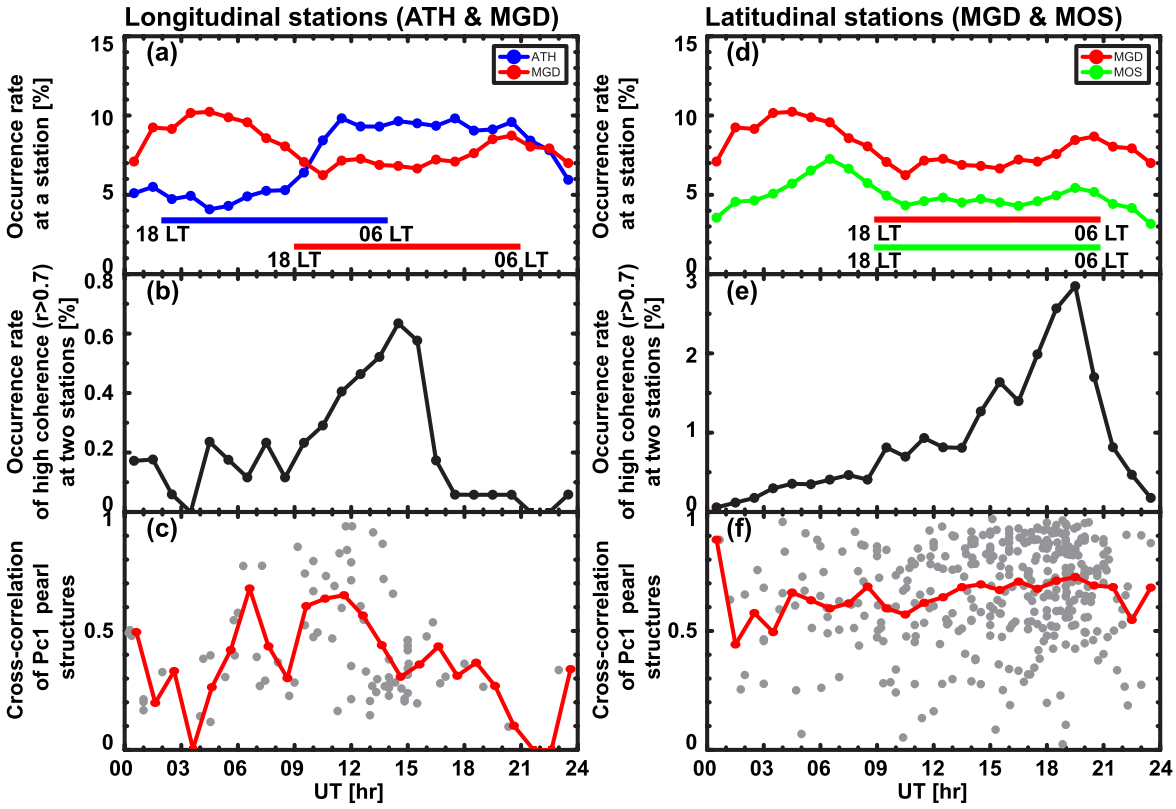

Figure 4.5 Universal time variations of the Pc1 occurrence rate observed at each station, at the two stations, and the cross correlation coefficient of Pc1 pearl structures for (a)-(c) longitudinally (ATH and MGD) and (d)-(f) latitudinally (MGD and MOS) separated stations. The horizontal colored bars in (a) and (d) indicate local night time at ATH (blue), MGD (red), and MOS (green). The solid red dots and lines in (c) and (f) indicate mean values of Pc1 pearl similarity ($r(\Delta t)$) at each 1-hour bin.

high latitudes reported by *Fraser* [1968] and *Kuwashima et al.* [1981]. They reported that seasonal variations of Pc1 occurrence reach a maximum at equinoxes at high latitudes and in the winter at low latitudes due to ionospheric plasma density variations depending on the season, causing different attenuations of Pc1 waves during ionospheric duct propagation. As shown in Figures 4.6c and 4.6f, the similarity of Pc1 pearl structures in both cases is highly scattered and shows no seasonal dependence.

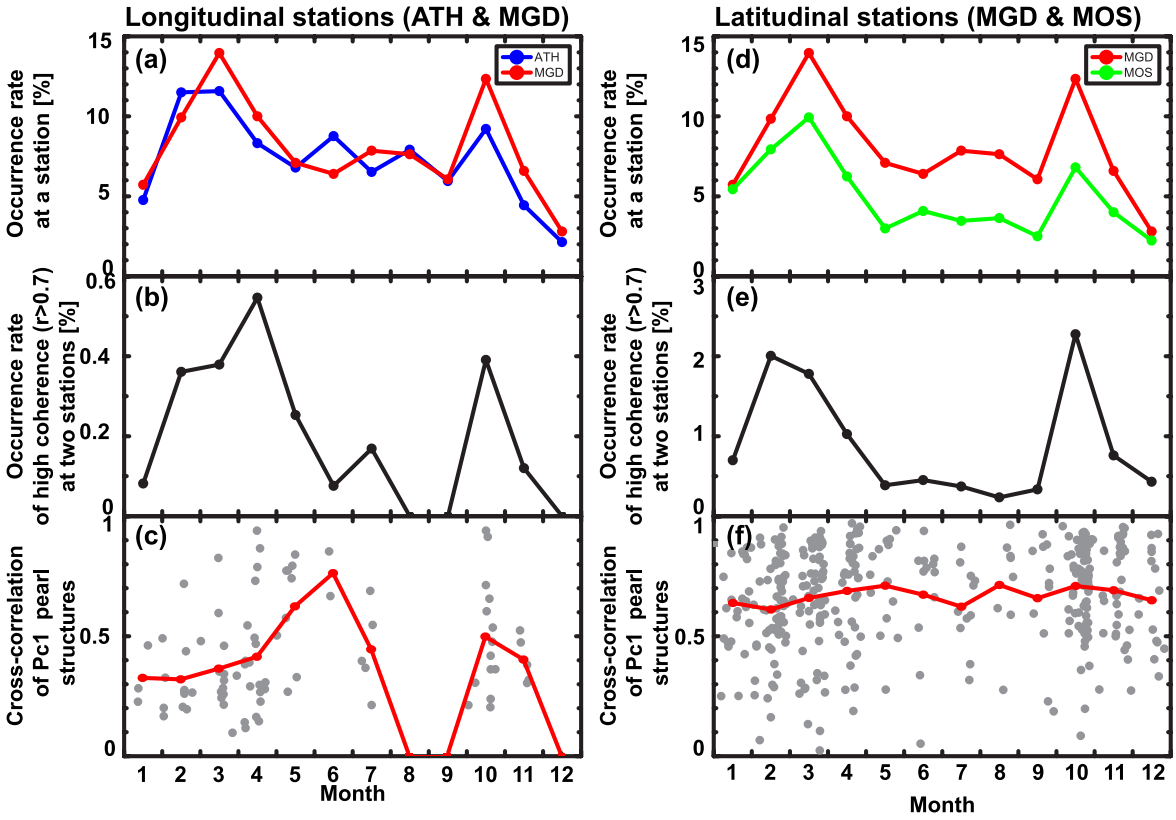

Figure 4.6 Seasonal variations of the Pc1 occurrence rate observed at each station, at the two stations, and the cross correlation coefficient of Pc1 pearl structures for (a)-(c) longitudinally (ATH and MGD) and (d)-(f) latitudinally (MGD and MOS) separated stations, respectively. The solid red dots and lines in (c) and (f) indicate mean values of Pc1 pearl similarity ($r(\Delta t)$) at each 1-month bin.

The annual variations of Pc1 occurrence and similarity of Pc1 pearl structures for the longitudinally and latitudinally separated stations are shown in Figure 4.7, together with monthly average sunspot number in Figure 4.7a. The sunspot numbers varied from minimum to maximum from 2008 to 2013. We observed fewer Pc1 events at these stations during the solar minimum than during the solar maximum, as shown in Figure 4.7b. The Pc1 occurrence at MGD (red line in Figure 4.7b) and MOS (green line in Figure 4.7b) seems to suddenly increase with increasing sunspot numbers until 2012 and then to decreases slightly in 2013.

This result differs from those of previous studies [*Fraser-Smith*, 1970; *Kawamura et al.*, 1985; *Park et al.*, 2013], where it was reported that Pc1 occurrence has a negative correlation with sunspot number variations. As our ground observation covers only half of the solar cycle, we cannot investigate Pc1 activity over the variation of a full cycle; therefore, this subject will be investigated in future works. The annual variations of Pc1 occurrence at each station (Figure 4.8b) and longitudinally and latitudinally separated stations (Figure 4.7c) show clear seasonal variations. The similarity of Pc1 pearl structures in both pairs (Figures 4.7d and 4.7e) seems to be independent of year and sunspot variation.

4.3.3 Dependence of the similarity of Pc1 pearl structures on geomagnetic conditions and wave properties

The relationships between the similarity of Pc1 pearl structures in the ionosphere and geomagnetic conditions and other wave properties are shown in Figure 4.8. Figures 4.8a-4.8d show the results for the longitudinally separated stations, and Figures 4.8e-4.8f show the results for the latitudinally separated stations. We calculated correlation coefficients R for these plots as noted in the top left of each panel. We investigated dependence of four parameters on the similarity of Pc1 pearl structures. σ_θ represents the ionospheric source distribution, as shown in Figures 2.10c and 2.10d. The central frequency and bandwidth of Pc1 pulsations represent latitudes of the ionospheric source. If Pc1 waves are generated at the equatorial region of the magnetosphere and propagate along the magnetic field lines, their frequencies depend on the magnetic field intensity at the equatorial region. We consider that higher (lower) frequencies of Pc1 pulsations are related to the magnetic field at lower (higher) latitudes. The average AE index represents the total current intensity in the auroral ionosphere and thus the level of disturbance of ionospheric conditions.

σ_θ in both pairs (Figure 4.8a and 4.8e) tends to have weak negative correlation with the similarity of Pc1 pearl structures. However, the coefficients (-0.19 for the longitudinally (Figure 4.8a) and -0.2 for the latitudinally (Figure 4.8b) separated stations) are small. We also found no relationships ($R \sim 0$) between the similarity of Pc1 pearl structures and wave properties (i.e., central frequency in Figures 4.8b and 4.8f and bandwidth in Figures 4.8d and 4.8f). In Figures 4.8c and 4.8e, the average AE index and the similarity of Pc1 pearl structures show weak positive and negative correlations for the longitudinally and latitudinally separated stations, respectively.

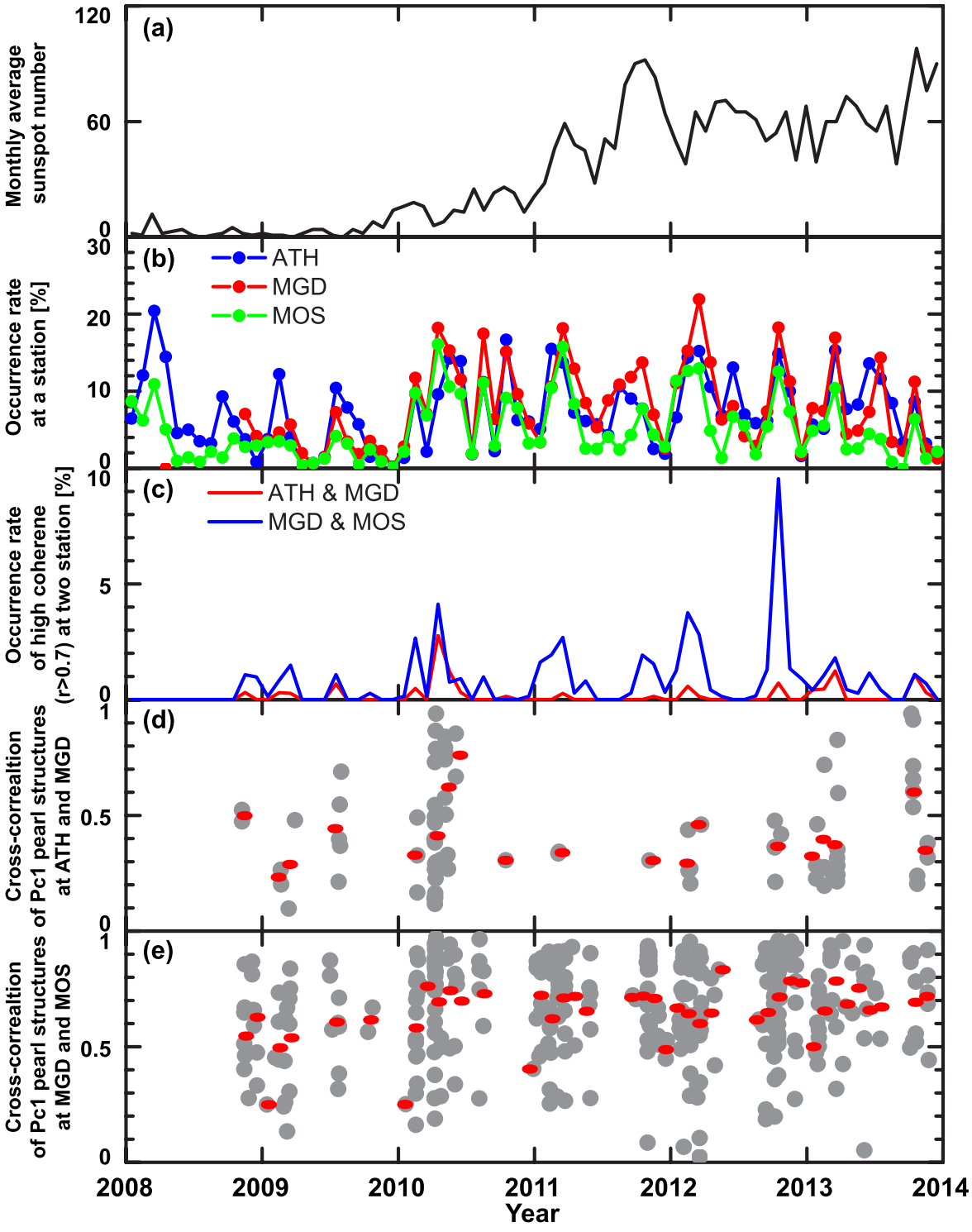

Figure 4.7 Annual variations of (a) monthly averaged sunspot number, the Pc1 occurrence rate observed (b) at ATH (blue line), MGD (red line) and MOS (green line), and (c) simultaneously at ATH and MGD (red line) and MGD and MOS (blue line), and cross correlation coefficients of Pc1 pearl structures for (d) longitudinally separated (ATH and MGD) and (e) latitudinally separated (MGD and MOS) stations, from January 1, 2008, to December 31, 2013. The solid red dots in (d) and (e) indicate mean values of Pc1 pearl similarity ($r(\Delta t)$) at each 1-month bin.

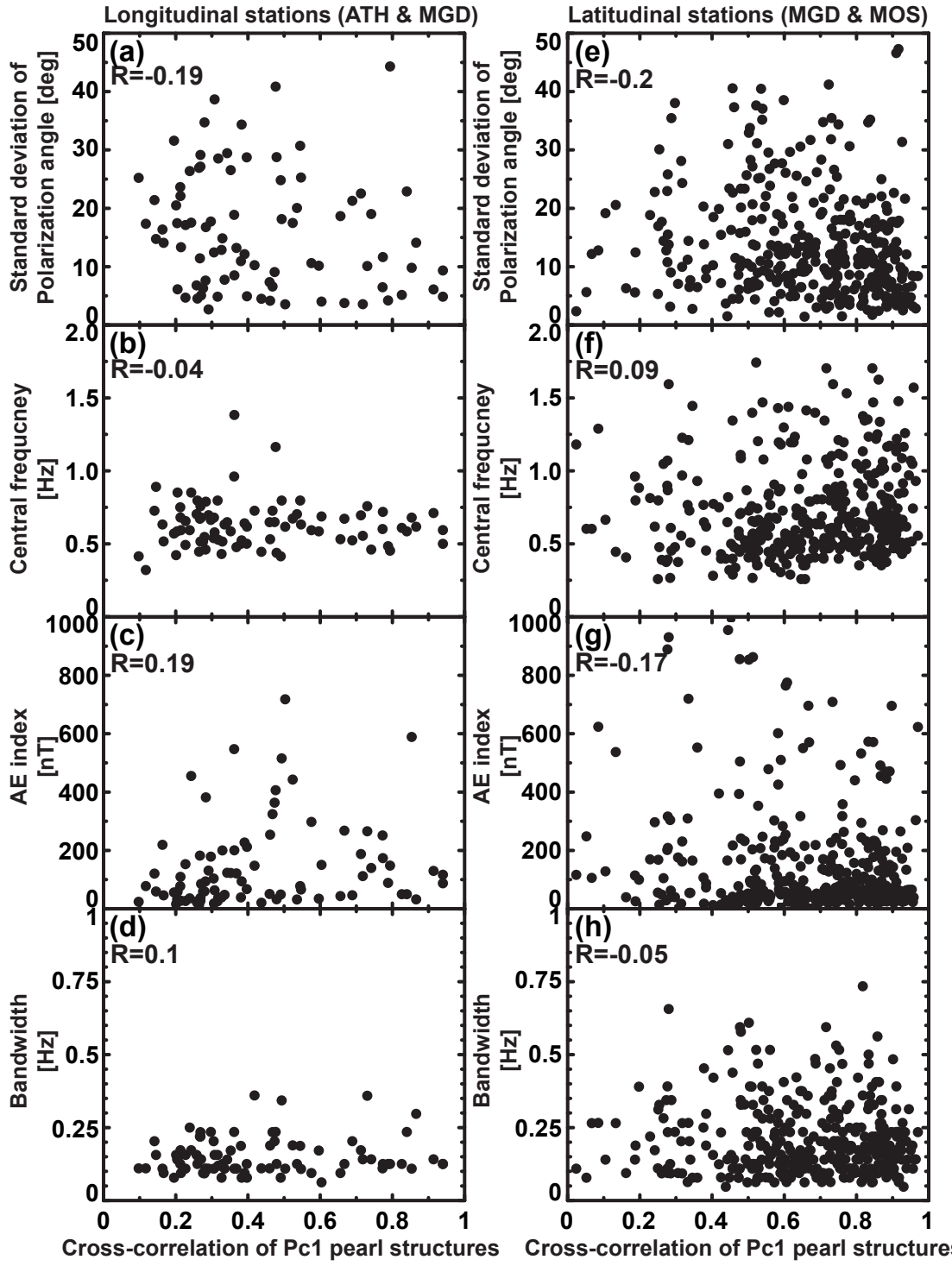

Figure 4.8 Dependence of the cross correlation coefficient of Pc1 pearl structures on the standard deviation of Pc1 polarization angle, Pc1 central frequency, AE index, and Pc1 bandwidth, for (a)-(d) longitudinally (ATH and MGD) and (e)-(h) latitudinally (MGD and MOS) separated stations.

4.3.4 Dependence of the Pc1 pearl periods on Pc1 bandwidth

If the Pc1 pearl structure is caused by the beating of Pc1 waves with slightly different frequencies during their duct propagation in the ionosphere, the repetition period of the pearl structure should have a relation to the frequency difference, i.e., bandwidth of the Pc1 waves. Namely, we can estimate the possible repetition period $T_{est} = 1/f_{beating}$ of Pc1 pearl structures using the observed Pc1 bandwidth, as described by the simple beating equation ($f_{beating} = f_{upper} - f_{lower}$), where f_{upper} and f_{lower} are upper and lower frequencies of the observed Pc1 band. Figure 4.9 shows the relationship between observed and estimated repetition periods of Pc1 pearl structures at the three stations. We used all the 84 Pc1 events at ATH and MGD and 370 at MGD and MOS. We define the observed repetition periods of Pc1 pearl structures by calculating the time intervals between amplitude peaks of the pearl structures, as shown in the example in Figures 4.3a and 4.3b, and calculated the average repetition period T_{obs} for each event by averaging all the repetition periods during the $\pm$ 2-min intervals of the event.

In Figure 4.9, we found that averaged repetition periods of Pc1 pearl structures have a clear positive correlation ($R = 0.89$) with the estimated values. We also note that they are always scattered below the estimated repetition period from the Pc1 bandwidth. Since we took the frequencies of the upper and lower boundary of the Pc1 bandwidth to estimate T_{est}, we expect the actual beating period T_{obs} should be always larger than the dashed line in Figure 4.9. Thus the two facts that there is a clear positive correlation between T_{obs} and T_{est} and that the T_{obs} is always larger than T_{est}, strongly support the idea that the beating of Pc1 waves in their bandwidth creates the Pc1 pearl structures.

4.4 Discussion

We investigated the statistical characteristics of Pc1 pearl structures in the ionosphere using multi-point ground stations, with the aim of understanding possible mechanisms for the generation of Pc1 pearl structures in the ionosphere.

We found that more than half of Pc1 events observed at the longitudinally and latitudinally separated stations had low similarity ($r < 0.7$) for the Pc1 pearl structures in Figure 4.4. If Pc1 pearl structures are mainly generated in the ionosphere, they should show different pearl structures at different stations, despite coming from the same source region. If magnetospheric effects cause Pc1 pearl structures, they should have a similar shape at different stations. Thus, the low similarity of Pc1 pearl structures at different stations suggests that ionospheric effects could be the dominant generation mechanism for Pc1 pearl structures in the ionosphere. The positive correlation between observed and estimated Pc1 repetition pe-

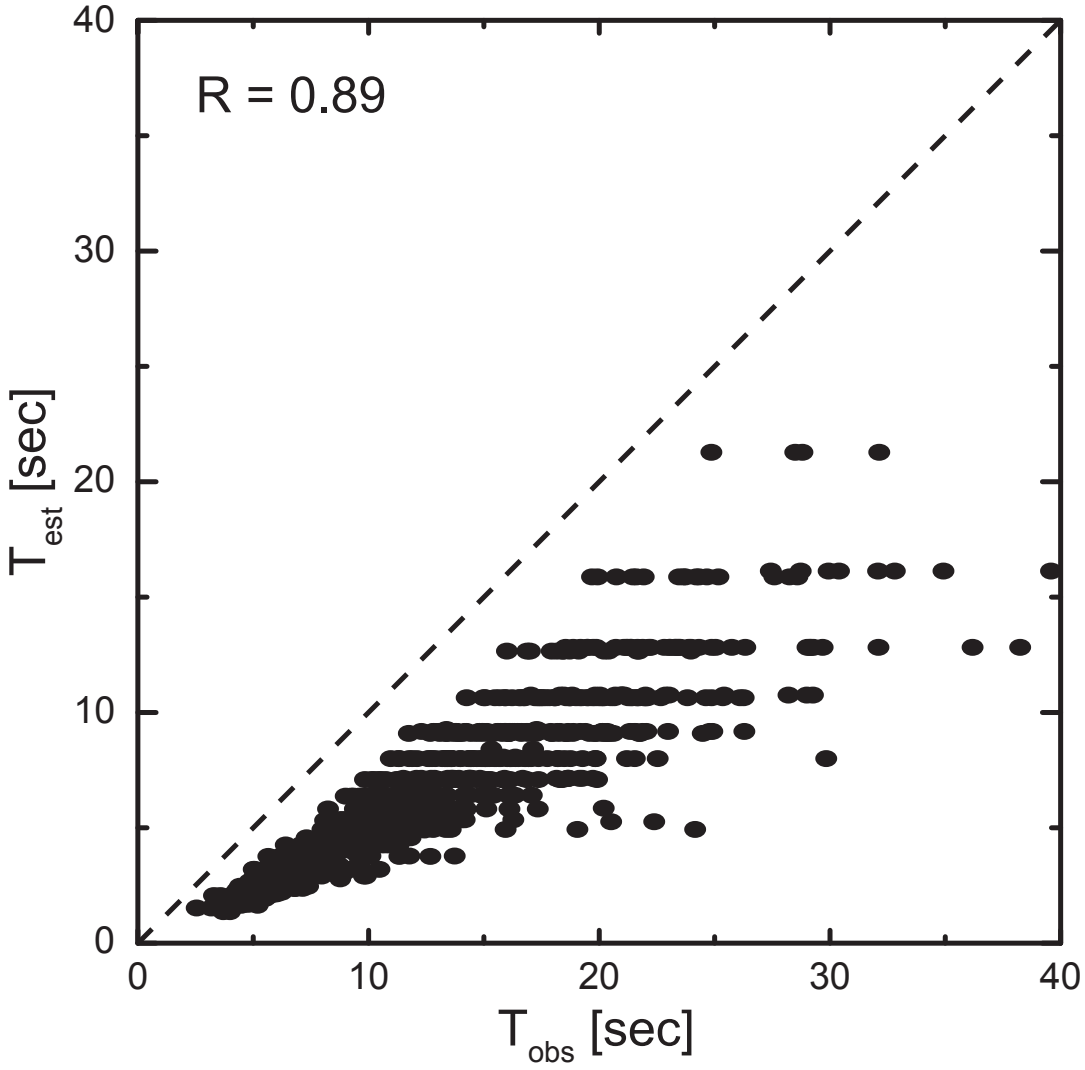

Figure 4.9 Scatterplot of observed repetition periods of Pc1 pearl structures versa the estimated beating periods at the three stations. The dashed line indicates the line of equality. *R* indicates the correlation coefficient between two values.

riods in Figure 4.9 suggests that the beating of different frequency waves in the ionospheric duct creates the Pc1 pearl structures.

When Pc1 pulsations propagate a longer distance through the ionospheric duct, they become more attenuated. Thus, stations located farther from the source region would observe weaker Pc1 pulsations. In that sense, we may not be able to exclude the possibility that local background noise becomes dominant for these waves, causing the low similarity r of Pc1 pearl structures. In this study, however, we selected Pc1 events with wave power higher than 10^{-7} nT^2/Hz, which is the threshold for which the observed pearl structures can be clearly distinguished from background noise. To identify whether the influence of background noise contributes to the low similarity of Pc1 pearl structures at different stations, we investigated the dependence of the similarity r of Pc1 pearl structures on Pc1 power at each station in pairs. The correlation coefficients between the pearl similarity and Pc1 wave power are 0.47 at ATH and 0.08 at MGD for the longitudinally separated stations, and 0.14 at MGD and 0.15 at MOS for the latitudinally separated stations. These results indicate that the similarity r of Pc1 pearl structures has a weak positive correlation with Pc1 wave power at only ATH for the longitudinally separated stations. We conclude that background noise does not have much affect on the similarity r of Pc1 pearl structures.

We investigated the temporal variations of the similarity of Pc1 pearl structures (Figures 4.5- 4.7). For UT variation in Figure 4.5, high similarity events at the longitudinally separated stations are detected only when both stations are located in the night sector. This result suggests that Pc1 pearl structures caused by magnetospheric effects are frequently observed in the nighttime of the magnetosphere. If this is the case, then latitudinally separated stations should also observe high similarity events of Pc1 pearl structures in the nighttime. However, for the latitudinally separated stations, the similarity of Pc1 pearl structures is highly scattered at all UT. We also could not find any seasonal and annual variations in the similarity of Pc1 pearl structures as shown in Figures 4.6 and 4.7. The formation of Pc1 pearl structures seems to be independent of ionospheric conditions.

We note that the similarity of Pc1 pearl structures has a weak negative correlation with the standard deviation of the polarization angle in both cases. Although it is small, this negative correlation supports the idea that Pc1 waves coming from a spatially distributed source can generate different Pc1 pearl structures at different observation points by beating processes in the ionosphere. *Nomura et al.* [2011] suggested that Pc1 polarization angle has dependence on frequency. *Sakaguchi et al.* [2008] reported that the isolated proton auroral spots, indicators of Pc1 ionospheric sources, were intermittently distributed over a 4-hr MLT period in the pre-midnight sector equatorward of the substorm auroral activity at auroral latitudes. *Jun et al.* [2014] noted that Pc1 pulsations having a polarization angle dependence on

Pc1 frequency have differently shaped Pc1 pearl structures at different stations. These observations indicate that, if Pc1 pulsations come from distributed ionospheric source regions, they could have different Pc1 pearl structures at different observation points due to different propagation time delays from the source regions to the ground stations.

Although the negative correlation between σ_θ and the pearl similarity r support the idea that Pc1 waves coming from a spatially distributed source cause beating and thus Pc1 pearl structure, the absolute value of the correlation is small ($\sim$0.2). This may be because of the effect of relative location of the ground station to the ionospheric source region. If the ionospheric source region is too close to the stations, the polarization angle θ shows complex patterns, as a mixture of direct incident Alfvén waves and ducting compressional waves. Thus, near the ionospheric source region, the minor (not major) axis of polarization angle can point to the source region [*Fujita and Tamao*, 1988; *Nomura et al.*, 2012]. This effect would contribute to reduce the correlation between σ_θ and the similarity r.

In our study, other parameters (i.e., central frequency, bandwidth, and AE index) did not have any correlation with the similarity of Pc1 pearl structures. We supposed that lower frequency Pc1 pulsations may have longer propagation time than that of higher frequency because they come from higher latitudes, resulting that lower frequency waves may be more attenuated during the ionospheric duct propagation. Thus, if the central frequency has a positive correlation with the Pc1 pearl similarity, Pc1 pearl similarity may be related to the attenuation effect. Our result shows, however, that Pc1 pearl similarity has no clear correlation with the central frequency and bandwidth. For the AE dependence in Figures 10c and 10e, if attenuation effect is controlled by the ionospheric condition represented by AE index, the similarity of Pc1 pearl structures should have a negative correlation with AE index. Our result shows, however, that there is no clear relationship between Pc1 pearl generation and AE index.

4.5 Conclusion

Between 2008 and 2013, we investigated the statistical characteristics of Pc1 pearl structures observed by induction magnetometers at three ground stations (ATH, MGD, and MOS) located at mid-to-low latitudes. We selected 84 Pc1 events simultaneously observed at longitudinally separated stations and 370 events at latitudinally separated stations. The results can be summarized as follows:

1. The cross-correlation coefficients $r(\Delta t)$ for pearl structure similarities have a peak of occurrence at around 0.2 for the longitudinally separated stations (ATH and MGD), and at around 0.8 for the latitudinally separated stations (MGD and MOS). More than

half of the events in both pairs (69 events at the longitudinally separated stations and 178 at the latitudinally separated stations) have a similarity of pearl structures less than 0.7, suggesting that ionospheric effects could be the dominant generation mechanism for Pc1 pearl structures in the ionosphere.

2. Highly similar Pc1 pearl structures ($r > 0.7$) at the longitudinally separated stations are concentrated between 6 and 15 UT, when it is nighttime at both stations. We found no seasonal or annual dependence in the similarity of Pc1 pearl structures.

3. Pc1 occurrences at all stations peak in the daytime during equinox periods. However, Pc1 pulsations simultaneously observed at two stations in both pairs are frequently detected in the dawn sector, indicating that the dawn sector and equinox period provide favorable conditions for propagation of Pc1 pulsations through the ionospheric duct.

4. The similarity of Pc1 pearl structures tends to have weak negative correlation with the standard deviation of the polarization angle ($R \sim 0.2$) for both longitudinally and latitudinally separated stations. However, we found that the similarity of Pc1 pearl structures is less correlated with central frequency and bandwidth at longitudinally and latitudinally separated stations. If we consider the AE index, in both cases the correlation coefficient between AE and Pc1 similarity has the same absolute value, but is positive for the longitudinal case and negative for latitudinally separated stations. We thus found no relation between the similarity of Pc1 pearl structures and other parameters (central frequency, bandwidth, and AE index).

5. There is a clear positive correlation between the observed Pc1 repetition periods and the periods estimated from the Pc1 bandwidth by considering beating. The observed repetition period is always larger than the estimated period.

From these results, we conclude that ionospheric effects, particularly the beating of different frequency waves, could be the dominant mechanism for Pc1 pearl structures in the ionosphere. We also suggest that the different shapes of Pc1 pearl structures at different points could be mainly by beating in the ionosphere with a spatially extended ionospheric source during ionospheric duct propagation. Highly similar events of Pc1 pearl structures were also observed at both longitudinally and latitudinally separated stations. Thus, we should also consider that magnetospheric processes, such as electromagnetic ion cyclotron waves modulated by long-period ULF waves, could contribute to the generation of Pc1 pearl structures. To understand and quantify these contributions to the creation of Pc1 pearl structures in the ionosphere and in the magnetosphere, in future studies we would like to in-

vestigate the statistical propagation characteristics of Pc1 pearl structures using combined ground-satellite observations.

Chapter 5

Conclusion and future works

We investigated possible generation mechanisms of Pc1 pearl structures in the ionosphere using multi-point ground induction magnetometers. From the analysis of the magnetic field data obtained at the three stations at Athabasca (ATH), Magadan (MGD), and Moshiri (MOS), in Chapter 3 we compared two Pc1 events simultaneously observed at the three stations. Case 1 on April 8, 2010, showed that Pc1 pearl structures observed at two stations have difference shape with polarization angle dependence on Pc1 frequency. In contrast, case 2 on April 11, 2010, showed similar Pc1 pearl structures at two stations with constant polarization angle in the Pc1 frequency range. In addition, Pc1 pearl structures with a repetition period of approximately 10 s in Case 1, and approximately 10 to 40 s in Case 2, were observed at three stations. These periods are shorter than those expected from the bouncing wave-packets model, which is one candidate magnetospheric effect for the formation of Pc1 pearl structures.

Using two simple model calculations under different conditions, we also investigated the possibility of beating processes in the ionosphere as a potential generation mechanism of the Pc1 pearl structures. The first model assumed that Pc1 waves propagate from a latitudinally distributed source with different frequencies at different latitudes to the observation point, representing beating processes in the ionosphere. The second model assumed that Pc1 waves with different frequencies are mixed at a point source and propagates to the observation points, indicating that Pc1 pearl structures are caused by magnetospheric effects. The first model showed slightly different waveforms at different observation points, but the second model showed identical waveforms among the observation points. The result of the first model is related with case 1, which showed different Pc1 pearl structures with dependence of polarization angle on frequency at the three stations.

From these results, we suggest that beating processes in the ionosphere with a spatially distributed ionospheric source can cause pearl structures during the ionospheric duct prop-

agation from high-to-low latitudes, with long distances from the source to the stations. In case 2, however, we cannot reliably interpret the Pc1 pearl structures with a constant polarization angle as using the beating process in the ionosphere. Thus, we cannot exclude the possibility that mechanisms in the magnetosphere also contribute to the generation of Pc1 pearl structures.

To quantify the contribution of beating in the ionosphere to the creation of Pc1 pearl structures in the ionosphere, we investigated the statistical characteristics of Pc1 pearl structures observed from 2008 to 2013 by longitudinally and latitudinally separated induction magnetometer stations (ATH, MGD, and MOS), located at mid-to-low latitudes. In this stage, we identified the dominant generation mechanism of Pc1 pearl structures in the ionosphere. We selected 84 Pc1 events simultaneously observed at longitudinally separated stations and 370 events at latitudinally separated stations.

We found that the cross-correlation coefficients $r(\Delta t)$ for pearl structure similarities have a peak occurrence at ~ 0.2 for the longitudinally separated stations (ATH and MGD), and at ~ 0.8 for the latitudinally separated stations (MGD and MOS). More than half of the events in both pairs (69 events at the longitudinally separated stations and 178 at the latitudinally separated stations) had a pearl structure similarity of less than 0.7, suggesting that ionospheric effects could be the dominant generation mechanism for Pc1 pearl structures in the ionosphere.

In temporal characteristics of Pc1 pearl structures, highly similar Pc1 pearl structures ($r > 0.7$) at the longitudinally separated stations are concentrated between 6 and 15 UT, when it is nighttime at both stations. We found no seasonal or annual dependence in the similarity of Pc1 pearl structures. We further found that Pc1 occurrences at all stations have a peak in the daytime during equinox periods. However, Pc1 pulsations observed simultaneously at two stations in both pairs are frequently detected in the dawn sector. According to *Kuwashima et al.* [1981], Pc1 occurrence has a tendency to have an anti-correlation with electron density in the ionosphere. During the ionospheric duct propagation, Pc1 waves have attenuation effect by absorptions. The attenuation effect would increase with the increase of the electron density in the ionosphere. Thus, this result indicates that the dawn sector and equinox period, which is low attenuation effect by the small electron density, provide favorable conditions for propagation of Pc1 pulsations through the ionospheric duct.

We also investigated the relations between the similarity of Pc1 pearl structures and geomagnetic and polarization parameters. The similarity of Pc1 pearl structures tends to have a weak negative correlation with the standard deviation of the polarization angle ($R \sim 0.2$) at both longitudinally and latitudinally separated stations. However, we found that the similarity of Pc1 pearl structures is less correlated with central frequency and bandwidth. If we

consider the auroral electrojet (AE) index, in both cases the correlation coefficient between AE and Pc1 similarity has the same absolute value, but is positive for the longitudinal case and negative for latitudinal one. We thus found no relation between the similarity of Pc1 pearl structures and other investigated parameters (central frequency, bandwidth, and AE index).

We also found a clear positive correlation between the observed Pc1 repetition periods with the periods estimated from the Pc1 bandwidth by considering beating. The observed repetition period is always larger than the estimated period. This result suggests that beating processes in the ionosphere cause Pc1 pearl structures.

From these results, we conclude that ionospheric effects, particularly the beating of different frequency waves, could be the dominant mechanism for Pc1 pearl structures in the ionosphere. We also suggest that the different shapes of Pc1 pearl structures at different points could be mainly due to beating in the ionosphere with a spatially extended ionospheric source during ionospheric duct propagation. Highly similar Pc1 pearl structures were also observed at both longitudinally and latitudinally separated stations. We should thus also consider that magnetospheric processes, such as electromagnetic ion cyclotron (EMIC) waves modulated by long-period ultra low-frequency (ULF) waves, could contribute to the generation of Pc1 pearl structures.

Future works

We found that more than half of Pc1 events have low similarity of Pc1 pearl structure between two stations. We also reported that the standard deviation of Pc1 polarization angle has a negative correlation with the similarity of Pc1 pearl structures. These results suggest that ionospheric effects, such as beating processes in the ionosphere with spatially distributed Pc1 ionospheric source, are the dominant mechanism for the formation of Pc1 pearl structures in the ionosphere. However, we cannot exclude the possibility that their generation could also be caused by magnetospheric effects, such as EMIC rising-tone emissions, long-period ULF wave modulation, or superposition of EMIC waves within the coherent length in the magnetosphere. We have not been able to identify other possibilities of ionospheric effects.

To identify the dominant generation mechanism of Pc1 pearl structures, we would like to investigate the similarity of Pc1 pearl structures using conjugated events simultaneously observed on the ground and in space. If Pc1 pearl structures are mainly caused by magnetospheric effects, Pc1 pearl generation could be related to EMIC wave generation. For example, in the case of long-period ULF wave modulation, the magnetic field intensity near the EMIC generation region will vary due to magnetospheric compressional-mode waves (such as Pc3-5 pulsations), causing EMIC amplitude modulation. If, however, we consider

ionospheric effects such as beating processes in the ionosphere, Pc1 pearl structures could be caused by Pc1 waves mixing without energy transfer between the waves and particles in the ionosphere. The Van Allen Probes (RBSP-A and -B) give us a perfect opportunity to identify Pc1 pearl generation. These satellites were launched in August 2012, and follow similar orbits encompassing both the inner and outer radiation belts [*Kessel et al.*, 2013]. These satellites can measure high-energy particles in the radiation belts, as well as the ambient magnetic and electric fields. For this study, we will select conjugated EMIC/Pc1 events between the ground and space. From 2012 to 2015, during the solar maximum, we could also investigate the generation and propagation characteristics of Pc1 pearl structures under active magnetospheric conditions. This work will provide an opportunity to better understand EMIC/Pc1 wave generation.

Another idea is to investigate the propagation characteristics of EMIC waves from the magnetosphere into the ionosphere. In theory, EMIC waves are perfectly trapped between the northern and southern reflection regions at high latitudes in the magnetosphere. Thus, these waves should not propagate into the ionosphere. However, as ground observations clearly show, we can observe Pc1 pulsations frequently from high-to-low latitudes. We will select conjugate EMIC/Pc1 events between ground and space, considering that the footprints of the satellites are up to 1,000 km from the ground stations. We could also investigate the particle distributions at high latitudes using the Polar Orbiting Environmental Satellite to determine the quantity of heavy ions in this region. These observations provide important information toward understanding EMIC wave propagation in the ionosphere.

A final possibility is investigating the relation between isolated pulsating proton aurora and Pc1 amplitude variations. During our research trip to Canada on November 11, 2015, we observed an isolated pulsating proton aurora at ATH with a repetition period of approximately 20-30 s. In this interval, strong Pc1 pulsations were also observed at ATH. We found that Pc1 amplitude modulations during this event had a similar repetition period consistent with that of the isolated pulsating proton aurora. EMIC waves interact with energetic ions in the magnetosphere during their propagation along the magnetic field lines, causing pitch angle scattering of these ions and making them precipitate into the ionosphere. We can simultaneously observe Pc1 pulsations and isolated proton aurora at subauroral latitudes. By measuring the total intensity of isolated pulsating proton auroras during the event, we could compare the repetition periods of aurora and Pc1 amplitude modulations. This would give sufficient information to understand the energy transfer between energetic particles and EMIC wave packets during their bouncing motion along the magnetic field lines, as well as the resonance conditions of EMIC waves with protons at high latitudes.

References

Althouse, E. L., and J. R. Davis (1978), Five-station observations of Pc 1 micropulsation propagation, *Journal of Geophysical Research: Space Physics*, *83*, 132-144.

Altman, C., and E. Fijalkow (1980), The horizontal propagation of Pc1 pulsations in the ionosphere, *Planetary and Space Science*, *28*, 61-68.

Anderson, B., R. Denton, G. Ho, D. Hamilton, S. Fuselier, and R. Strangeway (1996), Observational test of local proton cyclotron instability in the earth's magnetosphere, *Journal of Geophysical Research: Space Physics*, *101*, 21527-21543.

Campbell, W. H. (1967), Low attenuation of hydromagnetic waves in the ionosphere and implied characteristics in the magnetosphere for Pc 1 events, *Journal of Geophysical Research: Space Physics*, *72*, 3429-3445.

Erlandson, R., L. Zanetti, T. Potemra, L. Block, and G. Holmgren (1990), Viking magnetic and electric field observations of Pc 1 waves at high latitudes, *Journal of Geophysical Research: Space Physics*, *95*, 5941-5955.

Fowler, R., B. Kotick, and R. Elliott (1967), Polarization analysis of natural and artificially induced geomagnetic micropulsations, *Journal of Geophysical Research: Space Physics*, *72*, 2871-2883.

Fraser, B. (1968), Temporal variations in Pc1 geomagnetic micropulsations, *Planetary and Space Science*, *16*, 111-124.

Fraser, B. (1975a), Ionospheric duct propagation and Pc 1 pulsation sources, *Journal of Geophysical Research: Space Physics*, *80*, 2790-2796.

Fraser, B. (1975b), Polarization of Pc 1 pulsations at high and middle latitudes, *Journal of Geophysical Research: Space Physics*, *80*, 2797-2807.

Fraser-Smith, A. (1970), Some statistics on Pc 1 geomagnetic micropulsation occurrence at middle latitudes: Inverse relation with sunspot cycle and semi-annual period, *Journal of Geophysical Research: Space Physics*, *75*, 4735-4745.

Fujita, S. (1987), Duct propagation of a short-period hydromagnetic wave based on the international reference ionosphere model, *Planetary and Space Science*, *35*, 91-103.

Fujita, S. (1988), Duct propagation of hydromagnetic waves in the upper ionosphere 2. Dispersion characteristics and loss mechanism, *Journal of Geophysical Research: Space Physics*, *93*, 14674-14682.

Fukunishi, H., T. Toya, K. Koike, M. Kuwashima, and M. Kawamura (1981), Classification of hydromagnetic emissions based on frequency-time spectra, *Journal of Geophysical Research: Space Physics*, *86*, 9029-9039.

Greifinger, C., and P. S. Greifinger (1968), Theory of hydromagnetic propagation in the ionospheric waveguide, *Journal of Geophysical Research: Space Physics*, *73*, 7473-7490.

Greifinger, P. (1972), Ionospheric propagation of oblique hydromagnetic plane waves at micropulsation frequencies, *Journal of Geophysical Research: Space Physics*, *77*, 2377-2391.

Guglielmi, A., F. Feygin, K. Mursula, J. Kangas, T. Pikkarainen, and A. Kalisher (1996), Fluctuations of the repetition period of Pc1 pearl pulsations, *Geophysical Research Letters*, *23*, 1041-1044.

Hino, M. (1977), Spectral analysis, *Asakura*, *Tokyo*, 19778.

Horne, R. B., and R. M. Thorne (1993), On the preferred source location for the convective amplification of ion cyclotron waves, *Journal of Geophysical Research: Space Physics*, *98*, 9233-9247.

Hu, Y., and R. Denton (2009), Two-dimensional hybrid code simulation of electromagnetic ion cyclotron waves in a dipole magnetic field, *Journal of Geophysical Research: Space Physics*, *114*, A12217.

Jacobs, J., and T. Watanabe (1964), Micropulsation whistlers, *Journal of Atmospheric and Terrestrial Physics*, *26*, 825-826.

Jun, C.-W., K. Shiokawa, M. Connors, I. Schofield, I. Poddelsky, and B. Shevtsov (2014), Study of Pc1 pearl structures observed at multi-point ground stations in Russia, Japan, and Canada, *Earth, Planets and Space*, *66*, 1-14.

Kawamura, M., M. Kuwashima, and T. Toya (1981), Comparative study of magnetic Pc1 pulsations between low latitudes and high latitudes: Source region and propagation mechanism of the waves deduced from the characteristics of the pulsations at middle and low latitudes, *Memoirs of National Institute of Polar Research. Special issue*, *18*, 83-100.

Kawamura, M., M. Kuwashima, and T. Toya (1982), Comparative study of magnetic Pc 1 pulsations observed at low and high latitudes: Source region and generation mechanism of periodic hydromagnetic emissions, *Memoirs of National Institute of Polar Research. Special issue*, *22*, 3-16.

Kim, H., M. Lessard, M. Engebretson, and H. Lühr (2010), Ducting characteristics of Pc 1 waves at high latitudes on the ground and in space, *Journal of Geophysical Research: Space Physics*, *115*, A09310.

Kim, H., M. Lessard, M. Engebretson, and M. Young (2011), Statistical study of Pc1-2 wave propagation characteristics in the high-latitude ionospheric waveguide, *Journal of Geophysical Research: Space Physics*, *116*, A07227.

Kuwashima, M., T. Toya, M. Kawamura, T. Hirasawa, H. Fukunishi, and M. Ayukawa (1981), Comparative study of magnetic Pc1 pulsations between low latitudes and high latitudes: Statistical study, *Memoirs of National Institute of Polar Research. Special issue*, *18*, 101-117.

Lysak, R. (2004), Magnetosphere-ionosphere coupling by Alfvén waves at midlatitudes, *Journal of Geophysical Research: Space Physics*, *109*, A07201.

Manchester, R. (1966), Propagation of Pc 1 micropulsations from high to low latitudes, *Journal of Geophysical Research: Space Physics*, *71*, 3749-3754.

Manchester, R. (1970), Propagation of hydromagnetic emissions in the ionospheric duct, *Planetary and Space Science*, *18*, 299-307.

Miyoshi, Y., K. Sakaguchi, K. Shiokawa, D. Evans, J. Albert, M. Connors, and V. Jordanova (2008), Precipitation of radiation belt electrons by EMIC waves, observed from ground and space, *Geophysical Research Letters*, *35*, L3101.

Mursula, K., J. Kangas, R. Kerttula, T. Pikkarainen, A. Guglielmi, O. Pokhotelov, and A. Potapov (1999), New constraints on theories of Pc1 pearl formation, *Journal of Geophysical Research: Space Physics*, *104*, 12399-12406.

Mursula, K., R. Rasinkangas, T. Bösinger, R. Erlandson, and P.-A. Lindqvist (1997), Non-bouncing Pc 1 wave bursts, *Journal of Geophysical Research: Space Physics*, *102*, 17611-17624.

Mursula, K., T. Bräysy, K. Niskala, and C. Russell (2001), Pc1 pearls revisited: Structured electromagnetic ion cyclotron waves on Polar satellite and on ground, *Journal of Geophysical Research: Space Physics*, *106*, 29543-29553.

Mursula, K. (2007), Satellite observations of Pc 1 pearl waves: The changing paradigm, *Journal of Atmospheric and Solar-Terrestrial Physics*, *69*, 1623-1634.

Nakamura, S., Y. Omura, S. Machida, M. Shoji, M. Nosé, and V. Angelopoulos (2014), Electromagnetic ion cyclotron rising tone emissions observed by THEMIS probes outside the plasmapause, *Journal of Geophysical Research: Space Physics*, *119*, 1874-1886.

Nomura, R., K. Shiokawa, V. Pilipenko, and B. Shevtsov (2011), Frequency-dependent polarization characteristics of Pc1 geomagnetic pulsations observed by multipoint ground stations at low latitudes, *Journal of Geophysical Research: Space Physics*, *116*, A01204.

Nomura, R., K. Shiokawa, K. Sakaguchi, Y. Otsuka, and M. Connors (2012), Polarization of Pc1/EMIC waves and related proton auroras observed at subauroral latitudes, *Journal of Geophysical Research: Space Physics*, *117*, A02318.

Omura, Y., J. Pickett, B. Grison, O. Santolik, I. Dandouras, M. Engebretson, P. M. Décréau, and A. Masson (2010), Theory and observation of electromagnetic ion cyclotron triggered emissions in the magnetosphere, *Journal of Geophysical Research: Space Physics*, *115*, A07234.

Park, J., H. Lühr, and J. Rauberg (2013), Global characteristics of Pc1 magnetic pulsations during solar cycle 23 deduced from CHAMP data, *Annales Geophysicae*, *31*, 1507-1520.

Parks, G. K. (2004), Physics of space plasmas: an introduction, *Westview Press*, Colorado, USA

Paulson, K., C. Smith, M. Lessard, M. Engebretson, R. Torbert, and C. Kletzing (2014), In situ observations of Pc1 pearl pulsations by the Van Allen Probes, *Geophysical Research Letters*, *41*, 1823-1829.

Perraut, S. (1982), Wave-particle interactions in the ULF range: GEOS-1 and-2 results, *Planetary and Space Science*, *30*, 1219-1227.

Pope, J. H. (1964), An explanation for the apparent polarization of some geomagnetic micropulsations (pearls), *Journal of Geophysical Research: Space Physics*, *69*, 399-405.

Rasinkangas, R., and K. Mursula (1998), Modulation of magnetospheric EMIC waves by Pc 3 pulsations of upstream origin, *Geophysical Research Letters*, *25*, 869-872.

Sakaguchi, K., K. Shiokawa, A. Ieda, Y. Miyoshi, Y. Otsuka, T. Ogawa, M. Connors, E. F. Donovan, and F. Rich (2007), Simultaneous ground and satellite observations of an isolated proton arc at subauroral latitudes, *Journal of Geophysical Research: Space Physics*, *112*, A04202.

Sakaguchi, K., K. Shiokawa, Y. Miyoshi, Y. Otsuka, T. Ogawa, K. Asamura, and M. Connors (2008), Simultaneous appearance of isolated auroral arcs and Pc 1 geomagnetic pulsations at subauroral latitudes, *Journal of Geophysical Research: Space Physics*, *113*, A05201.

Sakaguchi, K., Y. Miyoshi, E. Spanswick, E. Donovan, I. Mann, V. Jordanova, K. Shiokawa, M. Connors, and J. Green (2012), Visualization of ion cyclotron wave and particle interactions in the inner magnetosphere via THEMIS-ASI observations, *Journal of Geophysical Research: Space Physics*, *117*, A10204.

Shiokawa, K., R. Nomura, K. Sakaguchi, Y. Otsuka, Y. Hamaguchi, M. Satoh, Y. Katoh, Y. Yamamoto, B. Shevtsov, S. Smirnov, et al. (2010), The STEL induction magnetometer network for observation of high-frequency geomagnetic pulsations, *Earth Planets and Space*, *62*, 517-524.

Shoji, M., and Y. Omura (2013), Triggering process of electromagnetic ion cyclotron rising tone emissions in the inner magnetosphere, *Journal of Geophysical Research: Space Physics*, *118*, 5553-5561.

Tepley, L., and R. Landshoff (1966), Waveguide theory for ionospheric propagation of hydromagnetic emissions, *Journal of Geophysical Research: Space Physics*, *71*, 1499-1504.

Thorne, R. M. (2010), Radiation belt dynamics: The importance of wave-particle interactions, *Geophysical Research Letters*, *37*, L22107.

Troitskaya, V., and A. Gul'Elmi (1967), Geomagnetic micropulsations and diagnostics of the magnetosphere, *Space Science Reviews*, *7*, 689-768.

Usanova, M., I. Mann, I. Rae, Z. Kale, V. Angelopoulos, J. Bonnell, K.-H. Glassmeier, H. Auster, and H. Singer (2008), Multipoint observations of magnetospheric compression-related EMIC Pc1 waves by THEMIS and CARISMA, *Geophysical Research Letters*, *35*, L17S25.

Waters, C., R. Lysak, and M. Sciffer (2013), On the coupling of fast and shear Alfvén wave modes by the ionospheric hall conductance, *Earth Planets Space*, *65*, 385-396.

Yahnina, T., A. Yahnin, J. Kangas, and J. Manninen (2000), Proton precipitation related to Pc1 pulsations, *Geophysical Research Letters*, *27*, 3575-3578.